Quantum parametric double Raman oscillators with co- and counterpropagating fields: Relative intensity squeezing and spatial photon correlations

C. H. Raymond Ooi [1,2] and Konstantin Dorfman [3,4,5]

[1]*Department of Physics, University of Malaya, 50603 Kuala Lumpur, Malaysia*

[2]*Institute for Quantum Science and Engineering (IQSE) and Department of Physics and Astronomy, Texas A&M University, College Station, Texas 77843-4242, USA*

[3]*State Key Laboratory of Precision Spectroscopy, East China Normal University, Shanghai 200062, China*

[4]*Collaborative Innovation Center of Extreme Optics, Shanxi University, Taiyuan, Shanxi 030006, China*

[5]*Himalayan Institute for Advanced Study, Unit of Gopinath Seva Foundation, MIG 38, Avas Vikas, Rishikesh, Uttarakhand 249201, India*

(Received 29 October 2021; revised 14 May 2022; accepted 26 September 2022; published 7 November 2022; corrected 23 November 2022)

We present a comprehensive study of co- and counterpropagating Stokes and anti-Stokes quantum fields in double Raman four-wave mixing parametric oscillators using full quantum Heisenberg-Langevin framework with noise operators. General analytical solutions of the fields operators at any point in the Raman medium are obtained for four cases: two possible copropagating (forward) and two counterpropagating (backward) Stokes and anti-Stokes. We analyze the symmetrical properties of the complex linear and nonlinear susceptibilities spectra of the quantum fields, nonclassicality of two-photon correlation functions, spatial variations of the quantum fields, and the two-mode relative intensity squeezing. We compare the results of forward and backward cases for several limiting double Raman schemes. We find interesting resonant effects of medium length, laser detunings and laser field strengths (Rabi frequencies) for backward-propagating geometries. Analysis of the solutions provide insights on the resonant conditions while computation over multiple variables enables us to identify the values of laser detuning, field strength, and propagation length that give enhanced nonclassical intensity squeezing and persistent correlations. The present work sets the crucial foundations for optimization of the nonclassicality of photons in double Raman systems and would be useful for quantum information storage, quantum nonlinear optics, and quantum spectroscopy.

DOI: 10.1103/PhysRevA.106.053705

I. INTRODUCTION

Nonclassical photon pairs from double Raman scheme in backward geometry, with counterpropagating quantum (and laser) fields, have been shown to exhibit amplified reflection, phase conjugation and oscillations without a cavity [1–3]), phase transformation to self oscillations [4], perfect squeezing and spectral line narrowing [5]. Frequency-tunable mirrorless parametric oscillation was recently demonstrated in the THz domain [6] with high efficiency.

The scheme is promising for quantum nonlinear optics [7] at low light level, even with cold atoms [8,9], where a few photons is sufficient for establishing sustained oscillations [10]. It is of interest for storing quantum information in the coherence between the ground states, such as long-live atomic dark state.

The double Raman scheme has been widely adopted for quantum memory where more efficient storage and retrieval of single-photon information has been demonstrated using counterpropagating laser geometry [11]. In atomic gases, the spectral broadening due to Doppler frequency shift of moving atoms determines the efficiency of a high-speed quantum memory [12]. Counterpropagating pump and control lasers used for backward retrieval of signal field managed to achieve higher retrieval efficiency in atomic quantum memory [13] without the need for cavity [14]. It was shown that 100% retrieval efficiency is possible, despite the presence of Doppler shift, by using the laser direction to control the bandwidth of quantum memory [15]. Coherent manipulation technique [16] can also completely freeze motion-induced dephasing by engineering the spin-wave momentum with negligible noise and zeroing the spin-wave momentum.

The copropagating geometry has been widely studied due to high degree of phase matching. For instance, in recent experiments four-wave mixing with a single control laser in hot Rb vapor has also produced multiple quantum correlated beams using cascading four-wave mixing (FWM) [17] and intensity-difference squeezing in two-mode phase-sensitive amplifier [18]. In quantum regime counterpropagating geometry provides highly efficient nonlinear interactions in photonic (periodically poled) structure [19] to generate narrow bandwidth entangled photons [20] useful for quantum repeaters [21]. At the low light perturbative regime the nearly degenerate four-wave mixing with counterpropagating laser enables phase conjugation process [22] that produces time reversible retrieval of stored quantum information. The increasing research outcome involving counterpropagating optical setups shows that this scheme deserves careful and integrated theoretical study.

Spectroscopic techniques to investigate properties of matter with quantum light have recently been developed based on FWM where noise-free spectroscopy [23] and quantum

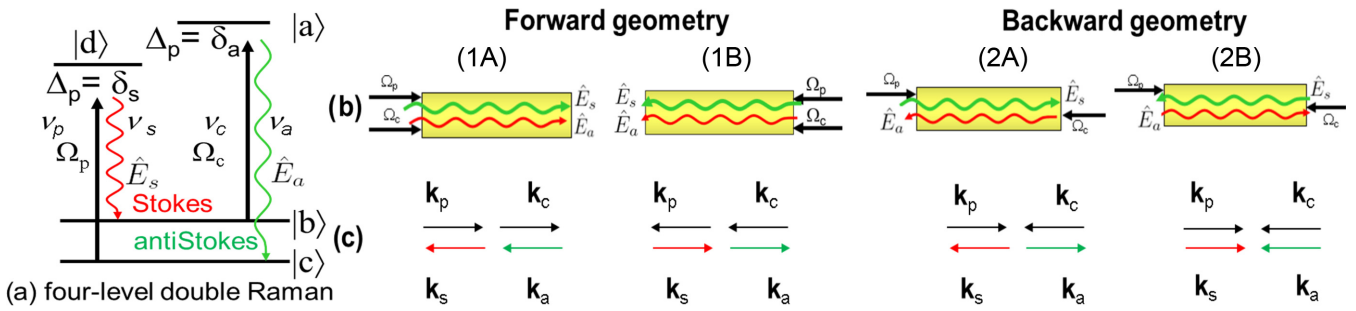

FIG. 1. (a) Double Raman scheme, (b) two-possible copropagating and two-possible counterpropagating schemes for Stokes and anti-Stokes photons in 1D medium with length L. (c) Possible phase-matched wave vector directions for the pump and control lasers.

memory using seeded squeezed light [24] were demonstrated. Vacuum squeezing through self-rotation [25] with the generation of pulsed and continuous-wave squeezed light [26] makes use of spatial dependent phase and quadratures of the complex elliptically polarized electric field of the photons in the controlled quantum medium and single-pass interactions without cavity or mirror. The implicit criteria for squeezing is where the creation or annihilation operator at the output is dependent on both the creation and annihilation operators of the input (vacuum).

It is possible to obtain $\chi^{(3)}$ using classical intensity gain spectra given by quantum measurement via the relative intensity squeezing spectra [27]. We verify the validity of our model through an experimental study in Rb vapor [23] which showed that external noise degrades the resolution of classical measurements, while quantum signals remain intact. Using squeezed light source, noise spectra of quantum detection provide high-precision measurements beyond the shot-noise limit, which is especially crucial in the case of weakly absorbing materials.

Our present work provides a comprehensive theoretical basis useful for those experimental works. The improved model is impactful as it is capable of predicting new experimental measurements in recently obtained experimental results, such as the investigation of squeezing and quantum light spectroscopy [28]. Here, we consider the backward-propagating quantum parametric oscillators medium with length L composed of four-level double Raman system [Fig. 1(a)], valid for arbitrary pump and control laser fields using the Heisenberg-Langevin framework with noise operators. The inclusion of quantum noise is crucial in small signal regime because the amplification comes from a constant supply of excited atoms undergoing spontaneous emissions. We obtain general nontrivial solutions for Stokes and anti-Stokes quantum fields at any point in the medium for four cases (Fig. 1): two possible copropagating (forward geometry) and two for counterpropagating (backward geometry). The solutions for counterpropagating case in Ref. [29] were only for both ends of the medium. This enables us to compute photon correlations functions between any two spatial points and relative photon number or intensity squeezing S_{as} [30].

One important aspect or novelty in the present work is the development of full quantum approach for study of two-mode squeezing, especially the counterpropagating geometry. The second important result is on understanding the effect of propagation length as well as the laser parameters to optimize the two-mode squeezing. We also address the question: How are the nonclassical correlations affected by the medium or propagation length L, laser parameters and counterpropagating lasers (backward geometry)? We focus our analysis on the backward case, especially the regime around mirrorless amplification. We find intriguing features in the Cauchy-Schwarz correlation $g_{as}^{CS}(\tau)$ and the relative intensity squeezing. The results give important insights for optimizing the nonclassicality and controlling the noise of double Raman photon pairs for quantum information storage, quantum nonlinear optics, and spectroscopy.

In Sec. II, we obtain semi-analytical expressions for the Stokes and anti-Stokes fields in Fourier-transformed spaces by self-consistently solving the equations for the coherences with the field propagation equations. This gives the pair of coupled parametric equations for the quantum fields with coefficients expressed in microscopic quantities valid to all orders of laser fields. From the coherence operators, we obtain the linear and third-order susceptibilities (Sec. III). In Sec. IV the solutions of the Stokes and anti-Stokes operators for forward and backward cases are obtained after considering the different boundary conditions. In Sec. V, the expressions linking the correlations and intensity difference squeezing are presented. Simulated results are discussed in Sec. VI for varying propagating lengths and for different detunings that represent different Raman schemes. In Sec. VII, we highlight insightful observations and new effects in our results, make connections with quantum memory, and relevance to existing works, phase matching, Doppler effect, presence of hyperfine levels, laser phase locking, and proposal for experiment.

We have also provided mathematical details in the six Appendixes; all the Heisenberg-Langevin equations with noise operators in Appendix A, coefficients of the susceptibilities and parametric oscillator equations in Appendix B, roots of the parametric oscillator equations in Appendix C, differential equations of the spatial factors governing spatial propagation in Appendix D, derivation of correlations of boundary operators in Appendix E, and derivation of correlations of noise operators in Appendix F.

II. NONLINEAR THEORY FOUR-LEVEL DOUBLE COHERENT RAMAN MEDIUM

The Hamiltonian of the four-level system is given by $H_o + V(\{\mathbf{r}_j\}, t)$:

$$H_o = \sum_j \sum_{\varsigma=a,b,c,d} \hbar\omega_\varsigma |\varsigma^j\rangle\langle\varsigma^j| + \sum_{\mathbf{k},\lambda} \left(\hat{a}^\dagger_{\mathbf{k}\lambda}\hat{a}_{\mathbf{k}\lambda} + \frac{1}{2}\right)\hbar\nu_{\mathbf{k}\lambda}, \tag{1}$$

$$\begin{aligned} V(\{\mathbf{r}_j\}, t) = -\sum_j \Bigg[& \sum_{\mathbf{k}\lambda,\varsigma=b,c} \hbar g^j_{d\varsigma,\mathbf{k}\lambda}\hat{a}_{\mathbf{k}\lambda}|d^j\rangle\langle\varsigma^j|e^{i\mathbf{k}_\lambda\cdot\mathbf{r}_j} \\ & + \sum_{\mathbf{q}\lambda,\varsigma=b,c} \hbar g^j_{a\varsigma,\mathbf{q}\lambda}\hat{a}_{\mathbf{q}\lambda}|a^j\rangle\langle\varsigma^j|e^{i\mathbf{q}_\lambda\cdot\mathbf{r}_j} \\ & + \hbar\Omega_p(\mathbf{r}_j, t)|d^j\rangle\langle c^j|e^{i(\mathbf{k}_p\cdot\mathbf{r}_j - \nu_p t)} \\ & + \hbar g_s|d^j\rangle\langle b^j|\hat{E}_s(\mathbf{r}_j, t)e^{i\mathbf{k}_s\cdot\mathbf{r}_j} \\ & + \hbar\Omega_c(\mathbf{r}_j, t)|a^j\rangle\langle b^j|e^{i(\mathbf{k}_c\cdot\mathbf{r}_j - \nu_c t)} \\ & + \hbar g_a|a^j\rangle\langle c^j|\hat{E}_a(\mathbf{r}_j, t)e^{i\mathbf{k}_a\cdot\mathbf{r}_j} + \text{H.c.}\Bigg], \end{aligned} \tag{2}$$

where $\Delta_{a\varsigma,\mathbf{k}\lambda} = \nu_{\mathbf{k}\lambda} - \omega_{a\varsigma}$, $\Delta_{d\varsigma,\mathbf{k}\lambda} = \nu_{\mathbf{k}\lambda} - \omega_{d\varsigma}$, $\Delta_c = \nu_c - \omega_{ab}$, $\delta_a = \nu_a - \omega_{ac}$, $\Delta_p = \nu_p - \omega_{dc}$, $\delta_s = \nu_s - \omega_{db}$ are the photon-atomic frequency detunings. The subscripts p, s, c, a stand for pump, Stokes, control, and anti-Stokes fields, respectively. Initially, the Stokes and anti-Stokes photons are emitted into all directions. However, stimulated emissions and the geometry ensure that the Hamiltonian only has the particular mode along the z direction that satisfies a minimum phase mismatch. The first line contains the quantum vacuum's multimode photonic operators. The Stokes and anti-Stokes quantum fields, denoted by operators (with hat) $\hat{E}_s$ and $\hat{E}_a$ are composed of some of these modes.

The Rabi frequencies for the two laser fields E_p, E_c and two quantum fields $\hat{E}_s, \hat{E}_a$ that contain the spatially dependent phase $k_j z$ and absolute phase φ_j in the factor $e^{i(k_j z+\varphi_j)}$ are defined as

$$\Omega_p(z, t) = |\Omega_p|e^{i(\varphi_p)}, \quad \Omega_c(z, t) = |\Omega_c|e^{i(\varphi_c)}, \tag{3}$$

$$\hat{S}(z, t) = g_s\hat{E}_s e^{i(\varphi_s)}, \quad \hat{A}(z, t) = g_a\hat{E}_a e^{i(\varphi_a)}, \tag{4}$$

with the coupling constants $g_s = \wp_{ab}/\hbar$, $g_a = \wp_{ac}/\hbar$, $|\Omega_p| = \wp_{dc}E_p/\hbar$, $|\Omega_c| = \wp_{ab}E_c/\hbar$. The terms contain absorption and emission processes [the corresponding terms in Hermitian conjugates (H.c.) with *] while the spatial factor $e^{i|k_j|z}$ is for forward-propagating laser and $e^{-i|k_j|z}$ for backward.

The Hamiltonian leads to 16 coupled Heisenberg-Langevin (HL) equations for the atomic operators, as given in Appendix A and also Ref. [29], along with definitions of the complex decoherences $T_{\alpha\beta}$, effective decoherence rates $\gamma_{\alpha\beta}$, and noise operators $\hat{F}_{\alpha\beta}$, α, $\beta = a, b, c, d$. For derivation of HL equations, the readers can refer to Refs. [31] and [32].

The spatial-temporal dynamics of the quantized fields, denoted as Stokes and anti-Stokes operators, are governed by the Maxwell's propagation equation in the slowly varying envelope approximation (SVEA) coupled to the atomic operators $\hat{p}_{bd}$, $\hat{p}_{ac}$ through

$$\left(\frac{1}{c}\frac{\partial}{\partial t} + \varsigma_s\frac{\partial}{\partial z}\right)\hat{E}_s(z, t) = i\kappa_s e^{-ik_s z}\hat{p}_{bd}(z, t), \tag{5}$$

$$\left(\frac{1}{c}\frac{\partial}{\partial t} + \varsigma_a\frac{\partial}{\partial z}\right)\hat{E}^\dagger_a(z, t) = -i\kappa^*_a e^{ik_a z}\hat{p}_{ac}(z, t), \tag{6}$$

where $\kappa_f = \frac{1}{2}N\wp_{\alpha\beta}c\mu_o\omega_{\alpha\beta}$, N is number density, and $f = s, a$; $\alpha\beta = db, ca$. This can also be derived from the Heisenberg equation with the commutation relation $[\hat{E}_s(\mathbf{r}, t), \hat{E}^\dagger_s(\mathbf{r}_j, t)] = (c^2\mu_o\hbar\omega_{db}/2)\delta^3(\mathbf{r} - \mathbf{r}_j) = (\hbar\omega_{db}/2\varepsilon_o)\delta^3(\mathbf{r} - \mathbf{r}_j)$ and $d\mathbf{r}/dt = \partial v_s/\partial k \to \partial z/\partial t = c$.

The rates for all broadening mechanisms such as spontaneous emissions (Γ_{dc}, Γ_{db}, Γ_{ab}, Γ_{ac}) and dephasing are contained in the decoherences $\gamma_{\alpha\beta}$. The wave vector and frequency mismatches are defined as (assuming one dimension, along z)

$$\Delta\mathbf{k} = \mathbf{k}_p + \mathbf{k}_c - \mathbf{k}_s - \mathbf{k}_a, \tag{7}$$

$$\Delta\nu = \nu_p + \nu_c - \nu_s - \nu_a, \tag{8}$$

$$\mathbf{k}_j = \hat{n}_j k_j = \hat{n}_j\sqrt{\varepsilon_j}\nu_j/c, \tag{9}$$

where $\varsigma_f = \pm 1$ is the sign of quantum fields unit vector $\hat{n}_f$, $\hat{n}_j = \pm\hat{z}$ ($j = p, s, c, a$) is the unit vector of the wave vector that determines the directions of the pump, control, Stokes and anti-Stokes photons, specifically in one dimension (1D) $\hat{n}_j = +\hat{z}$ for photons propagating along $+z$ and $\hat{n}_j = -\hat{z}$ for $-z$ directions, with corresponding dielectric function ε_j.

We adopt the linearization approximation for those terms containing the quantum fields (weak signals) $\hat{E}_s$ and $\hat{E}_a$ by assuming that the diagonal operators $\hat{\sigma}^{st}_{\alpha\alpha}$, and $\hat{p}^{st}_{ab}$, $\hat{p}^{st}_{cd}$ with their conjugates are at steady state, i.e.,

$$\hat{p}_{rs}(z, t)\hat{E}_f(z, t) \simeq \hat{E}_f(z, t)\tilde{\rho}^{st}_{sr}(z). \tag{10}$$

Note that the quantum fields terms would give rise to nonlinearity if $\hat{p}_{rs}$ were not approximated to be steady state.

Neglecting the terms with quantum fields in the equations for $\frac{d}{dt}\hat{p}_{ba}$ and $\frac{d}{dt}\hat{p}_{cd}$,

$$\frac{d}{dt}\hat{p}_{ba} \simeq -T^*_{ab}\hat{p}_{ba} + i\Omega_c e^{ik_c z}(\hat{\sigma}_{bb} - \hat{\sigma}_{aa}) + e^{i\nu_c t}\hat{F}^\dagger_{ab}, \tag{11}$$

$$\frac{d}{dt}\hat{p}_{cd} \simeq -T^*_{dc}\hat{p}_{cd} + i\Omega_p e^{ik_p z}(\hat{\sigma}_{cc} - \hat{\sigma}_{dd}) + e^{i\nu_p t}\hat{F}^\dagger_{dc}, \tag{12}$$

coupled to the equations for $\frac{d}{dt}\hat{\sigma}_{\alpha\alpha}$,

$$\frac{d}{dt}\hat{\sigma}_{aa} \simeq i\left(\Omega_c e^{ik_c z}\hat{p}_{ab} - \Omega^*_c e^{-ik_c z}\hat{p}_{ba}\right) - (\Gamma_{ab} + \Gamma_{ac})\hat{\sigma}_{aa} + \hat{F}_{aa}, \tag{13a}$$

$$\frac{d}{dt}\hat{\sigma}_{bb} \simeq i\left(\Omega^*_c e^{-ik_c z}\hat{p}_{ba} - \Omega_c e^{ik_c z}\hat{p}_{ab}\right) + \Gamma_{ab}\hat{\sigma}_{aa} + \Gamma_{db}\hat{\sigma}_{dd} + \hat{F}_{bb}, \tag{13b}$$

$$\frac{d}{dt}\hat{\sigma}_{cc} \simeq -i\left(\Omega_p e^{ik_p z}\hat{p}_{dc} - \Omega^*_p e^{-ik_p z}\hat{p}_{cd}\right) + \Gamma_{ac}\hat{\sigma}_{aa} + \Gamma_{dc}\hat{\sigma}_{dd} + \hat{F}_{cc}, \tag{13c}$$

$$\frac{d}{dt}\hat{\sigma}_{dd} \simeq i\left(\Omega_p e^{ik_p z}\hat{p}_{dc} - \Omega^*_p e^{-ik_p z}\hat{p}_{cd}\right) - (\Gamma_{db} + \Gamma_{dc})\hat{\sigma}_{dd} + \hat{F}_{dd}, \tag{13d}$$

form a closed set of equations of zeroth order in quantum fields. Exact analytical solutions for the steady-state operators population $\hat{\sigma}^{st}_{\alpha\alpha}$ and coherences $\hat{p}^{st}_{ba}$ and $\hat{p}^{st}_{cd}$ are obtained, for example,

$$T^*_{ab}\hat{p}_{ba} \simeq iR_c(\hat{\sigma}_{bb} - \hat{\sigma}_{aa}) + e^{i\nu_c t}\hat{F}^\dagger_{ab}, \tag{14a}$$

$$T^*_{dc}\hat{p}_{cd} \simeq iR_p(\hat{\sigma}_{cc} - \hat{\sigma}_{dd}) + e^{i\nu_p t}\hat{F}^\dagger_{dc}, \tag{14b}$$

and hence the expectations

$$\tilde{\rho}^{st}_{ab} = \langle \hat{p}^{st}_{ba} \rangle \simeq -i\frac{R_c}{T^*_{ab}} w^{aa}_{bb}, \tag{15}$$

$$\tilde{\rho}^{st}_{dc} = \langle \hat{p}^{st}_{cd} \rangle \simeq -i\frac{R_p}{T^*_{dc}} w^{dd}_{cc}, \tag{16}$$

where $R_{p,c} = \Omega_{p,c}e^{ik_{p,c}z}$ and $w^{\alpha\alpha}_{\beta\beta} = p_{\alpha\alpha} - p_{\beta\beta} = \langle \hat{\sigma}_{\alpha\alpha} - \hat{\sigma}_{\beta\beta} \rangle$ ($\alpha, \beta = a, b, c, d$) are the population inversions, $T_{ab} = i\Delta_c + \gamma_{ab}$, $T_{dc} = i\Delta_p + \gamma_{dc}$.

The four equations (from Appendix A) for $\frac{d}{dt}\hat{p}_{\alpha\beta}(t)$, $\alpha\beta = bd, ac, bc, ad$ that have been linearized are in closed form

$$\left(\frac{d}{dt} + T_{ad}\right)\hat{p}_{ad} = i\big(R_p\hat{p}_{ac}e^{-i\Delta\nu t} - R^*_c\hat{p}_{bd} + \hat{S}\langle \hat{p}^{st}_{ab} \rangle - \hat{A}^\dagger e^{-i\Delta\nu t}\langle \hat{p}^{st}_{cd} \rangle\big) + e^{-i\nu_{cs}t}\hat{F}_{ad}, \tag{17a}$$

$$\left(\frac{d}{dt} + T_{ac}\right)\hat{p}_{ac} = i\big[(p^{st}_{aa} - p^{st}_{cc})\hat{A}^\dagger - R^*_c\hat{p}_{bc} + e^{i\Delta\nu t}R^*_p\hat{p}_{ad}\big] + e^{-i\nu_a t}\hat{F}_{ac}, \tag{17b}$$

$$\left(\frac{d}{dt} + T_{bc}\right)\hat{p}_{bc} = -i\big(R_c\hat{p}_{ac} - e^{i\Delta\nu t}R^*_p\hat{p}_{bd}\big) - i\big(e^{i\Delta\nu t}\hat{S}\langle \hat{p}^{st}_{dc} \rangle - \hat{A}^\dagger\langle \hat{p}^{st}_{ba} \rangle\big) + e^{i\nu_{ca}t}\hat{F}_{bc}, \tag{17c}$$

$$\left(\frac{d}{dt} + T^*_{db}\right)\hat{p}_{bd} = i\big[R_p e^{-i\Delta\nu t}\hat{p}_{bc} - R_c\hat{p}_{ad} + \hat{S}(p^{st}_{bb} - p^{st}_{dd})\big] + e^{i\nu_s t}\hat{F}^\dagger_{db}, \tag{17d}$$

$$T_{ac} = i\delta_a + \gamma_{ac}, \tag{18a}$$

$$T_{ad} = i(\Delta_c - \delta_s) + \gamma_{ad}, \tag{18b}$$

$$T_{bc} = i(\delta_a - \Delta_c) + \gamma_{bc}, \tag{18c}$$

$$T^*_{db} = -i\delta_s + \gamma_{db}. \tag{18d}$$

Hence, we have a closed set of four HL equations involving $\hat{p}_{bd}, \hat{p}_{ac}; \hat{p}_{ad}, \hat{p}_{bc}$ coupled with the propagation equations for quantum fields. The solutions for $\hat{p}_{\alpha\beta}(\nu)$ can be obtained in terms of analytical expressions for steady-state density matrix elements of (a) diagonal operators $\hat{\sigma}^{st}_{\alpha\alpha}$ and (b) coherences driven by lasers $\hat{p}^{st}_{ab}$, $\hat{p}^{st}_{cd}$ after performing Fourier transform ($\mathcal{F}$ operation) and Laplace transform ($\mathcal{L}$ operation) defined by $\mathcal{X}(\nu) = \int X(t)e^{i\nu t}dt$, $\mathcal{Y}(q) = \int Y(z)e^{-qz}dz$ from time (t) and space (z) to frequency (ν) and wave vector (q) on the above four equations.

By performing Laplace-Fourier ($\mathcal{LF}$) transform to wave vector q and frequency ν domains, we obtain analytical solutions for $\hat{p}_{ad}(q + ik_{sq}, \nu)$, $\hat{p}_{bc}(q + ik_{sp}, \nu - \Delta\nu)$ including the coherences $\hat{p}_{bd}(q + ik_s, \nu)$ and $\hat{p}_{ac}(q - ik_a - i\Delta k, \nu - \Delta\nu)$ associated with the quantum fields $\hat{\mathcal{S}}(q, \nu) = \mathcal{LF}\{\hat{S}(z, t)\}$ and $\hat{\mathcal{A}}^\dagger(q', \nu') = \mathcal{LF}\{\hat{A}^\dagger(z, t)\}$.

Explicitly, the transformed Stokes field in wave vector–frequency domain is

$$\hat{\mathcal{S}}(q, \nu) = \frac{\hat{\mathcal{S}}(0, \nu)}{Q(\nu)} + \frac{ig_s\kappa_s}{Q(\nu)}\hat{p}_{bd}(q + ik_s, \nu) \tag{19}$$

$$= \frac{\hat{\mathcal{S}}(0, \nu)}{Q(\nu)} + \frac{ig_s\kappa_s}{Q(\nu)D_q} \times \left[\sum_{j=1}^{4}\mathcal{G}'_j\hat{\mathcal{F}}_j(q, \nu) + i\left(\mathcal{W}'_s + \frac{\kappa^*_a g^*_a}{Q_\varphi(\nu)}\mathcal{W}_{as}\right)\frac{\hat{\mathcal{S}}(0, \nu)}{Q(\nu)} - i\mathcal{W}'_a\frac{\hat{\mathcal{A}}^\dagger(0, \nu - \Delta\nu)}{Q_\varphi(\nu)}\right], \tag{20}$$

and similarly, the anti-Stokes field

$$\hat{\mathcal{A}}^\dagger(q', \nu') = \frac{\hat{\mathcal{A}}^\dagger(0, \nu')}{Q_\varphi(\nu)} + \frac{-ig^*_a\kappa^*_a}{Q_\varphi(\nu)D_q}\left[\sum_{j=1}^{4}\mathcal{G}_j\hat{\mathcal{F}}_j(q, \nu) - i\left[\mathcal{W}_a + \frac{\kappa_s g_s}{Q(\nu)}\mathcal{W}_{as}\right]\frac{\hat{\mathcal{A}}^\dagger(0, \nu')}{Q_\varphi(\nu)} + i\mathcal{W}_s\frac{\hat{\mathcal{S}}(0, \nu)}{Q(\nu)}\right], \tag{21}$$

where

$$Q(\nu) = \varsigma_s q - i\nu/c, \quad Q'(\nu) = \varsigma_a q - i\nu/c, \tag{22a}$$

$$Q_\varphi(\nu) = \varsigma_a(q - i\Delta k) - i(\nu - \Delta\nu)/c = Q'(\nu) + i\varphi, \tag{22b}$$

$$\varphi = \Delta\nu/c - \varsigma_a\Delta k, \tag{22c}$$

and $\nu' = \nu - \Delta\nu$, $q' = q - i\Delta k$. The summation indexes $j = 1, 2, 3, 4$ correspond to ac, ad, bc, bd. The coefficients $\mathcal{W}_{s,a}$, $\mathcal{W}'_{s,a}$, $\mathcal{W}_{as}$, $\mathcal{G}_j$, $\mathcal{G}'_j$ are given by Eqs. (B3), (B6), (B9), and (B10) in Appendix B.

We may consider four cases (as illustrated in Fig. 1): (1A) forward (Stokes and anti-Stokes are co-propagating), Stokes and anti-Stokes in $+z$ direction ($\hat{n}_s = \hat{n}_a = \hat{z}$); (1B) forward, Stokes and anti-Stokes in $-z$ direction ($\hat{n}_s = \hat{n}_a = -\hat{z}$); (2A) backward (Stokes and anti-Stokes are counterpropagating), Stokes in $+z$ and anti-Stokes in $-z$ directions; (2B) backward, Stokes in $-z$ and anti-Stokes in $+z$ directions. The cases A and B are different relative to the propagation directions of the pump and control lasers:

$$Q(\nu) = (-i\nu/c + q) = Q', \quad \varphi = \Delta\nu/c - \Delta k \text{ (Case 1A)}, \tag{23a}$$

$$Q(\nu) = (-i\nu/c - q) = Q', \quad \varphi = \Delta\nu/c + \Delta k \text{ (Case 1B)}, \tag{23b}$$

$$Q(\nu) = (-i\nu/c + q), \quad Q'(\nu) = (-i\nu/c - q) = -Q^*, \quad \varphi = \Delta\nu/c + \Delta k \text{ (Case 2A)}, \tag{23c}$$

$$Q(\nu) = (-i\nu/c - q), \quad Q'(\nu) = (-i\nu/c + q) = -Q^*, \quad \varphi = \Delta\nu/c - \Delta k \text{ (Case 2B)}. \tag{23d}$$

III. SUSCEPTIBILITIES IN q AND ν

The polarization $\hat{P}_{a,k}(q',\nu') = N\wp_k\hat{p}_{ac}$ associated with the anti-Stokes coherence $\hat{p}_{ac}$ (and density matrix element ρ_{ca}) is obtained generally as

$$\langle P_{a,k}(q',\nu')\rangle = \frac{N\wp_k}{D_q(q,\nu)}\left\{-i\left[\mathcal{W}_a + \frac{\kappa_s g_s}{Q(\nu)}\mathcal{W}_{as}\right]\frac{\hat{\mathcal{A}}^\dagger(0,\nu')}{Q_\varphi(\nu)} + i\mathcal{W}_s\frac{\hat{\mathcal{S}}(0,\nu)}{Q(\nu)}\right\} \tag{24}$$

$$= \varepsilon_0\sum_l \chi^{(1)}_{a,kl}E^*_{a,l}(0,\nu') + \varepsilon_0\sum_{lmn}\chi^{(3)}_{a,klmn}\hat{E}^*_{p,l}\hat{E}_{s,m}(0,\nu)\hat{E}^*_{c,n}, \tag{25}$$

where

$$D_q(q,\nu) = \mathcal{D}(\nu) + \frac{\kappa_s g_s}{Q(\nu)}\mathcal{W}'_s + \frac{\kappa^*_a g^*_a}{Q_\varphi(\nu)}\mathcal{W}_a + \frac{\kappa^*_a g^*_a}{Q_\varphi(\nu)}\frac{\kappa_s g_s}{Q(\nu)}\mathcal{W}_{as}, \tag{26}$$

$$\mathcal{D}(\nu) = (T^*_{db} - i\nu)(T_{ac} - i\nu')(T_{ad} - i\nu)(T_{bc} - i\nu') + I^2_{pc} + I_p\{(T_{ac} - i\nu')(T_{ad} - i\nu) + (T^*_{db} - i\nu)(T_{bc} - i\nu')\}$$
$$+ I_c\{(T_{ac} - i\nu')(T_{bc} - i\nu') + (T^*_{db} - i\nu)(T_{ad} - i\nu)\}, \tag{27}$$

and contains the linear $\chi^{(1)}_{a,kl}$ and nonlinear $\chi^{(3)}_{a,klmn}$ susceptibilities with temporal and spatial dispersions. Please note that, while the susceptibilities for the Stokes $\chi^{(1,3)}_s$ correspond to text [31], the susceptibilities for the anti-Stokes defined here $\chi_a(-\nu) = [\chi^{SZ}_a(\nu)]^*$ are the complex conjugates.

Replacing Eqs. (15) and (16) into Eq. (B3),

$$\mathcal{W}_s = \Omega^*_p\Omega^*_c\left\{-\frac{w^{aa}_{bb}}{T_{ab}}[I_{pc} + T^*_{bd}(\nu)T_{bc}(\nu')] + \frac{w^{dd}_{cc}}{T_{dc}}[I_{pc} - T^*_{bd}(\nu)T_{ad}(\nu)] - w^{dd}_{bb}[T_{bc}(\nu') + T_{ad}(\nu)]\right\}, \tag{28}$$

$$\mathcal{W}_a = I_p\frac{w^{dd}_{cc}}{T^*_{dc}}[I_{pc} + T^*_{bd}(\nu)T_{bc}(\nu')] - I_c\frac{w^{aa}_{bb}}{T^*_{ab}}[I_{pc} - T^*_{bd}(\nu)T_{ad}(\nu)] - w^{aa}_{cc}\{I_pT_{ad}(\nu) + I_cT_{bc}(\nu') + T^*_{bd}(\nu)T_{ad}(\nu)T_{bc}(\nu')\}, \tag{29}$$

leads to familiar expressions for the linear susceptibility $\chi^{(1)}_{kl}$ and third-order susceptibility $\chi^{(3)}_{klmn}$.

The term $\frac{\kappa_s g_s}{Q(\nu)}\mathcal{W}_{as}$ gives nonlinear dependence on the optical density in $\chi^{(1)}_{kl}$. Inserting the definitions of $\Omega_p = \sum_l g_{p,l}E_{p,l}e^{ik_pz}$, $\Omega_c = \sum_n g_{c,n}E_{c,n}e^{ik_cz}$, $\hat{\mathcal{A}}^\dagger(0,\nu') = \sum_l g^*_{a,l}\hat{E}^\dagger_{a,l}(0,\nu')e^{-ik_az}$, $\hat{\mathcal{S}}(0,\nu) = \sum_l g_{s,l}\hat{E}_{s,l}(0,\nu)e^{ik_sz}$ $(l = x,y,z)$ and $Q(\nu)$, $Q_\varphi(\nu)$, we may write analytical expressions for the susceptibilities (neglecting $\frac{\kappa_s g_s}{Q(\nu)}\mathcal{W}_{as}$) in terms of the parametric oscillator coefficients Eqs. (45) and (46) (in next section)

$$\chi^{(1)}_{a,kl}(q,\nu) \simeq -i\frac{\mathcal{W}_a}{\mathcal{D}(\nu)Q_\varphi(\nu)}\frac{N\wp_{ac,k}\wp^*_{a,l}}{\varepsilon_0\hbar} = -i\frac{\left(\mathcal{G}_a + \frac{i\nu'}{c}\right)}{Q_\varphi(\nu)(k_a/2)} \tag{30}$$

$$= \frac{iF_{kl}}{\mathcal{D}(\nu)Q_\varphi(\nu)}\begin{bmatrix} I_c\frac{w^{aa}_{bb}}{T^*_{ab}}[I_{pc} - T^*_{bd}(\nu)T_{ad}(\nu)] - I_p\frac{w^{dd}_{cc}}{T^*_{dc}}[I_{pc} + T^*_{bd}(\nu)T_{bc}(\nu')] \\ + w^{aa}_{cc}\{I_pT_{ad}(\nu) + I_cT_{bc}(\nu') + T^*_{bd}(\nu)T_{ad}(\nu)T_{bc}(\nu')\}\end{bmatrix}, \tag{31}$$

$$\chi^{(3)}_{a,klmn}(q,\nu) = \frac{N\wp_k i\mathcal{W}_s}{\varepsilon_0\mathcal{D}(\nu)\hat{E}^*_{p,l}\hat{E}_{s,m}(0,\nu)\hat{E}^*_{c,n}}\frac{\hat{\mathcal{S}}(0,\nu)}{Q(\nu)} = \frac{i\mathcal{W}_s}{\mathcal{D}(\nu)Q(\nu)}\frac{N\wp_k\sum_{lmn}\wp^*_{p,l}\wp_{s,m}\wp^*_{c,n}}{\Omega^*_p\Omega^*_c\varepsilon_0\hbar^3}$$

$$= -\frac{g_s}{g^*_a}\frac{i\mathcal{K}_a}{\frac{1}{2}k_aQ(\nu)\hat{E}^*_{p,l}\hat{E}^*_{c,n}} \tag{32}$$

$$= i\frac{F_{klmn}}{\mathcal{D}(\nu)Q(\nu)}\left\{-\frac{w^{aa}_{bb}}{T_{ab}}[I_{pc} + T^*_{bd}(\nu)T_{bc}(\nu')] + \frac{w^{dd}_{cc}}{T_{dc}}[I_{pc} - T^*_{bd}(\nu)T_{ad}(\nu)] - w^{dd}_{bb}[T_{bc}(\nu') + T_{ad}(\nu)]\right\}, \tag{33}$$

where $F_{kl} = N\wp_k\wp^*_{a,l}/(\varepsilon_0\hbar)$, $F_{klmn} = N\wp_k\wp^*_{p,l}\wp_{s,m}\wp^*_{c,n}/(\varepsilon_0\hbar^3)$.

The associated phases $e^{i(\Delta k + \frac{\nu-\Delta\nu}{c})z}$ and $e^{i(\frac{\nu}{c})z}$ from inverse transform are removed by the definition of susceptibilities in (z,ν). Equation (30) recovers the susceptibility for electromagnetic induced transparency (EIT) by setting $I_p = 0$,

$$\chi^{(1)}_{a,kl} = \frac{iF_{kl}}{\left(q - i\Delta k - i\frac{\nu-\Delta\nu}{c}\right)}\left[-I_c\frac{w^{aa}_{bb}}{T^*_{ab}}[I_c + T^*_{bd}(\nu)T_{ad}(\nu)] + \{I_c + T^*_{bd}(\nu)T_{ad}(\nu)\}T_{bc}(\nu')w^{aa}_{cc}\right] \tag{34}$$

$$\simeq \frac{iF_{kl}}{\left(q - i\Delta k - i\frac{\nu-\Delta\nu}{c}\right)}\left[\frac{T_{bc}(\nu')w^{aa}_{cc} - I_c\frac{w^{aa}_{bb}}{T^*_{ab}}}{T_{ac}(\nu')T_{bc}(\nu')}\right]\left(\frac{1 + \frac{I_c}{T^*_{db}(\nu)T_{ad}(\nu)}}{1 + I_c\left\{\frac{1}{T^*_{db}(\nu)T_{ad}(\nu)} + \frac{1}{T_{ac}(\nu')T_{bc}(\nu')}\right\}}\right), \tag{35}$$

$$]\mathcal{D}(\nu) \to \left(T^*_{db} - i\nu\right)(T_{ac} - i\nu')(T_{ad} - i\nu)(T_{bc} - i\nu') - I^2_c + I_c\{(T_{ac} - i\nu')(T_{bc} - i\nu') + (T^*_{db} - i\nu)(T_{ad} - i\nu)\}, \tag{36}$$

which reproduces the usual result without laser field,

$$\chi_{a,kl} \simeq i\frac{N\wp_k\wp^*_{a,l}w^{aa}_{cc}}{\varepsilon_0\hbar(-i\frac{\nu-\Delta\nu}{c}+q-i\Delta k)[T_{ac}-i(\nu-\Delta\nu)]}.$$

Keeping the pump and control fields to first order means setting $D \to (T^*_{db}-i\nu)(T_{ac}-i\nu')(T_{ad}-i\nu)(T_{bc}-i\nu')$ and $I_p,\ I_c \to 0$ in the numerator, we have the perturbative third-order susceptibility

$$\chi^{(3)}_{a,klmn} = iN\wp_k\sum_{lmn}\wp^*_{p,l}\wp_{3,m}\wp^*_{c,n}\frac{-\frac{w^{aa}_{bb}}{T_{ab}}T^*_{bd}(\nu)T_{bc}(\nu')-\frac{w^{dd}_{cc}}{T_{dc}}T^*_{bd}(\nu)T_{ad}(\nu)-w^{dd}_{bb}[T_{bc}(\nu')+T_{ad}(\nu)]}{\varepsilon_0\hbar^3\left(q-i\frac{\nu}{c}\right)(T^*_{db}-i\nu)(T_{ac}-i\nu')(T_{ad}-i\nu)(T_{bc}-i\nu')}. \tag{37}$$

IV. PARAMETRIC OPERATOR EQUATIONS FOR QUANTUM FIELDS

We can derive the coupled parametric differential equations by performing only Fourier transformation in time (as in previous section) on the four HL equations and two propagation equations or the quantum fields $\hat{\mathcal{S}}(z,\nu)=\mathcal{F}\{\hat{S}(z,t)\}$ and $\hat{\mathcal{A}}^\dagger(z,\nu)=\mathcal{F}\{\hat{A}^\dagger(z,t)\}$:

$$\left(\varsigma_s\frac{\partial}{\partial z}+\mathcal{G}_s\right)\hat{\mathcal{S}}(z,\nu)+\mathcal{K}_s\hat{\mathcal{A}}^\dagger(z,\nu)=\hat{\mathcal{F}}_s(z,\nu), \tag{38}$$

$$\left(\varsigma_a\frac{\partial}{\partial z}+\mathcal{G}_a\right)\hat{\mathcal{A}}^\dagger(z,\nu)+\mathcal{K}_a\hat{\mathcal{S}}(z,\nu)=\hat{\mathcal{F}}^\dagger_a(z,\nu), \tag{39}$$

with effective noise operators

$$\hat{\mathcal{F}}_s(z,\nu)=ig_s\kappa_s\sum_{i=1}^4\mathcal{C}'_i\hat{\mathcal{F}}_i(z,\nu), \tag{40}$$

$$\hat{\mathcal{F}}^\dagger_a(z,\nu)=-ig^*_a\kappa^*_a\sum_{i=1}^4\mathcal{C}_i\hat{\mathcal{F}}_i(z,\nu), \tag{41}$$

$$\hat{\mathcal{F}}_{ac}(z,\nu)=\mathcal{F}\{e^{i\Delta kz}e^{-i\Delta\nu t}e^{i(k_az-\nu_at)}\hat{F}_{ac}(z,t)\}, \tag{42a}$$

$$\hat{\mathcal{F}}_{ad}(z,\nu)=\mathcal{F}\{e^{i(k_{cs}z-\nu_{cs}t)}\hat{F}_{ad}(z,t)\}, \tag{42b}$$

$$\hat{\mathcal{F}}_{bc}(z,\nu)=\mathcal{F}\{e^{i\Delta kz}e^{-i\Delta\nu t}e^{-i(k_{ca}z-\nu_{ca}t)}\hat{F}_{bc}(z,t)\}, \tag{42c}$$

$$\hat{\mathcal{F}}_{bd}(z,\nu)=\mathcal{F}\{e^{-i(k_sz-\nu_st)}\hat{F}_{bd}(z,t)\}, \tag{42d}$$

where $\mathcal{C}'_i=\frac{\mathcal{N}'_i}{\mathcal{D}}$ and $\mathcal{C}_i=\frac{\mathcal{N}_i}{\mathcal{D}}$ and the frequency-dependent coefficients

$$\mathcal{G}_s=g_s\kappa_s\frac{\mathcal{W}'_s}{\mathcal{D}}-\frac{i\nu}{c}, \tag{43}$$

$$\mathcal{K}_s=-g_s\kappa_s\frac{\mathcal{W}'_a}{\mathcal{D}}, \tag{44}$$

$$\mathcal{G}_a=g^*_a\kappa^*_a\frac{\mathcal{W}_a}{\mathcal{D}}-\frac{i(\nu-\Delta\nu)}{c}, \tag{45}$$

$$\mathcal{K}_a=-g^*_a\kappa^*_a\frac{\mathcal{W}_s}{\mathcal{D}}. \tag{46}$$

For Raman-EIT (REIT) scheme, where the first (Stokes) Raman is far-detuned while the second (anti-Stokes) Raman is resonant, we find $\mathcal{K}_s\approx-\mathcal{K}_a$ while $|\mathcal{G}_s|\ll|\mathcal{K}_a|$.

A. Solutions of the parametric equations

The coupled parametric equations (38), (39) can be solved by Laplace transform method, giving the general solutions in terms of the fields $\hat{\mathcal{S}}_0$, $\hat{\mathcal{A}}^\dagger_0$ at $z=0$ and the convoluted noise operators

$$\begin{aligned}\hat{\mathcal{S}}(z)=&\left(\Xi_q(z)-\mathcal{G}_a\frac{\Xi(z)}{\varsigma_a}\right)\hat{\mathcal{S}}_0+\frac{\Xi(z)}{\varsigma_s}\mathcal{K}_s\hat{\mathcal{A}}^\dagger_0\\&+\int_0^z\left[\mathcal{K}_s\frac{\Xi(z-s)}{\varsigma_s}\frac{\hat{\mathcal{F}}^\dagger_a(s)}{\varsigma_a}\right.\\&\left.+\left\{\Xi_q(z-s)-\mathcal{G}_a\frac{\Xi(z-s)}{\varsigma_a}\right\}\frac{\hat{\mathcal{F}}_s(s)}{\varsigma_s}\right]ds,\end{aligned} \tag{47}$$

$$\begin{aligned}\hat{\mathcal{A}}^\dagger(z)=&\left(\Xi_q(z)-\mathcal{G}_s\frac{\Xi(z)}{\varsigma_s}\right)\hat{\mathcal{A}}^\dagger_0+\mathcal{K}_a\frac{\Xi(z)}{\varsigma_a}\hat{\mathcal{S}}_0\\&+\int_0^z\left[\left\{\Xi_q(z-s)-\mathcal{G}_s\frac{\Xi(z-s)}{\varsigma_s}\right\}\frac{\hat{\mathcal{F}}^\dagger_a(s)}{\varsigma_a}\right.\\&\left.+\mathcal{K}_a\frac{\Xi(z-s)}{\varsigma_a}\frac{\hat{\mathcal{F}}_s(s)}{\varsigma_s}\right]ds,\end{aligned} \tag{48}$$

with the spatially dependent factors

$$\begin{aligned}\Xi_q(z)&=\frac{q_+e^{-q_+z}-q_-e^{-q_-z}}{q_+-q_-}\\&=e^{-\alpha z}\frac{(\alpha+\beta)e^{-\beta z}-(\alpha-\beta)e^{\beta z}}{2\beta}\\&=e^{-\alpha z}\left(\cosh\beta z-\frac{\alpha}{\beta}\sinh\beta z\right),\end{aligned} \tag{49}$$

$$\begin{aligned}\Xi(z)&=\frac{e^{-q_+z}-e^{-q_-z}}{q_+-q_-}=e^{-\alpha z}\frac{e^{-\beta z}-e^{\beta z}}{2\beta}\\&=-e^{-\alpha z}\frac{\sinh\beta z}{\beta},\end{aligned} \tag{50}$$

where the two roots $q_\pm$ for any geometry are derived in Appendix C for finite Δk and for $\Delta k=0$,

$$q_\pm=\alpha\pm\beta, \tag{51a}$$

$$\alpha=\frac{1}{2}(\mathcal{G}_a/\varsigma_a+\mathcal{G}_s/\varsigma_s), \tag{51b}$$

$$\beta=\frac{1}{2}\sqrt{\alpha^2-\frac{4}{\varsigma_a\varsigma_s}(\mathcal{G}_a\mathcal{G}_s-\mathcal{K}_a\mathcal{K}_s)} \tag{51c}$$

$$= \sqrt{\left(\frac{\mathcal{G}_a/\varsigma_a - \mathcal{G}_s/\varsigma_s}{2}\right)^2 + \frac{\mathcal{K}_a\mathcal{K}_s}{\varsigma_a\varsigma_s}}. \tag{51d}$$

We take note of the properties

$$q_+ + q_- = (\mathcal{G}_a/\varsigma + \mathcal{G}_s/\varsigma_s), \tag{52}$$

$$q_+q_- = \frac{1}{\varsigma_a\varsigma_s}(\mathcal{G}_a\mathcal{G}_s - \mathcal{K}_a\mathcal{K}_s). \tag{53}$$

We found the following identities that are used to verify the correctness of the solutions:

$$\frac{\partial}{\partial z}\Xi(z) = -\Xi_q(z), \tag{54}$$

$$\frac{\partial}{\partial z}\Xi_q(z) = -\frac{\partial^2}{\partial z^2}\Xi(z). \tag{55}$$

It would be useful to define $\Pi_f^{\pm} = (\mathcal{G}_f\Xi \pm \Xi_q)$ and provide their mathematical relations in Appendix D.

B. Case 1A: Forward geometry, Stokes and anti-Stokes copropagating toward $+z$

For $\hat{n}_s = \hat{n}_a = +\hat{z}$ ($\varsigma_s = \varsigma_a = 1$) with input fields at $z = 0$, $\hat{\mathcal{S}}_0 = \hat{\mathcal{S}}(0), \hat{\mathcal{S}} = \hat{\mathcal{S}}(z), \hat{\mathcal{A}}_0^\dagger = \hat{\mathcal{A}}^\dagger(0), \hat{\mathcal{A}}^\dagger = \hat{\mathcal{A}}^\dagger(z)$ the solutions are straightforward:

$$\hat{\mathcal{S}}(z,\nu) = -\Pi_a^-(z)\hat{\mathcal{S}}(0) + \mathcal{K}_s\Xi(z)\hat{\mathcal{A}}^\dagger(0) + J_S(z), \tag{56}$$

$$\hat{\mathcal{A}}^\dagger(z,\nu) = -\Pi_s^-(z)\hat{\mathcal{A}}^\dagger(0) + \mathcal{K}_a\Xi(z)\hat{\mathcal{S}}(0) + J_A(z), \tag{57}$$

$$J_S(z) = \int_0^z [-\Pi_a^-(z-s)\hat{\mathcal{F}}_s(s) + \mathcal{K}_s\Xi(z-s)\hat{\mathcal{F}}_a^\dagger(s)]ds, \tag{58}$$

$$J_A(z) = \int_0^z [-\Pi_s^-(z-s)\hat{\mathcal{F}}_a^\dagger(s) + \mathcal{K}_a\Xi(z-s)\hat{\mathcal{F}}_s(s)]ds, \tag{59}$$

with the response functions to the noise sources $\bar{F}_s$ and $\bar{F}_a^\dagger$ that are spatially nonlocal. Here,

$$q_\pm = \tfrac{1}{2}(\mathcal{G}_a + \mathcal{G}_s) \pm \tfrac{1}{2}\sqrt{(\mathcal{G}_a + \mathcal{G}_s)^2 - 4(\mathcal{G}_a\mathcal{G}_s - \mathcal{K}_a\mathcal{K}_s)}. \tag{60}$$

If we define

$$\psi_s^s(x,\nu) = -\Pi_a^-(x), \quad \psi_a^s(x,\nu) = \mathcal{K}_s\Xi(x), \tag{61}$$

$$\psi_s^a(x,\nu) = \mathcal{K}_a\Xi(x), \quad \psi_a^a(x,\nu) = -\Pi_s^-(x), \tag{62}$$

the solutions can be rewritten using the same symbols as

$$\hat{\mathcal{S}}(z,\nu) = \psi_s^s(z,\nu)\hat{\mathcal{S}}(0,\nu) + \psi_a^s(z,\nu)\hat{\mathcal{A}}^\dagger(0,\nu) + \int_0^z \left[\psi_s^s(\xi,\nu)\hat{\mathcal{F}}_s(s,\nu) + \psi_a^s(\xi,\nu)\hat{\mathcal{F}}_a^\dagger(s,\nu)\right]ds, \tag{63}$$

$$\hat{\mathcal{A}}^\dagger(z,\nu) = \psi_a^a(z,\nu)\hat{\mathcal{A}}^\dagger(0,\nu) + \psi_s^a(z,\nu)\hat{\mathcal{S}}(0,\nu) + \int_0^z \left[\psi_s^a(\xi,\nu)\hat{\mathcal{F}}_s(s,\nu) + \psi_a^a(\xi,\nu)\hat{\mathcal{F}}_a^\dagger(s,\nu)\right]ds, \tag{64}$$

where $\xi = z - s$.

Here we obtain useful relations

$$\frac{\partial}{\partial z}\Pi_s^- = \mathcal{K}_s\mathcal{K}_a\Xi(z) - \mathcal{G}_a\Pi_s^-(z), \tag{65}$$

$$\frac{\partial}{\partial z}\Pi_a^- = \mathcal{K}_s\mathcal{K}_a\Xi(z) - \mathcal{G}_s\Pi_a^-(z), \tag{66}$$

using Eqs. (D4) and (D2) that enable us to verify the correctness of the obtained general solutions. The phase matching condition here is $\Delta k_{1A} = (k_p + k_c - k_s - k_a) = 0$ for 1D.

C. Case 1B: Forward geometry, Stokes and anti-Stokes copropagating toward $-z$

For $\hat{n}_s = \hat{n}_a = -\hat{z}$ ($\varsigma_s = \varsigma_a = -1$) with input fields at $z = L$, $\hat{\mathcal{S}}(L), \hat{\mathcal{A}}^\dagger(L)$ the solutions are straightforward:

$$\hat{\mathcal{S}}(z,\nu) = \Pi_a^+(z)\hat{\mathcal{S}}(0) - \mathcal{K}_s\Xi(z)\hat{\mathcal{A}}^\dagger(0) + J_S(z), \tag{67}$$

$$\hat{\mathcal{A}}^\dagger(z,\nu) = \Pi_s^+(z)\hat{\mathcal{A}}^\dagger(0) - \mathcal{K}_a\Xi(z)\hat{\mathcal{S}}(0) + J_A(z), \tag{68}$$

$$J_S(z) = \int_0^z [\mathcal{K}_s\Xi(z-s)\hat{\mathcal{F}}_a^\dagger(s) - \Pi_a^+(z-s)\hat{\mathcal{F}}_s(s)]ds, \tag{69}$$

$$J_A(z) = \int_0^z [\mathcal{K}_a\Xi(z-s)\hat{\mathcal{F}}_s(s) - \Pi_s^+(z-s)\hat{\mathcal{F}}_a^\dagger(s)]ds, \tag{70}$$

with the boundary fields

$$\hat{\mathcal{S}}(L) = \Pi_a^+(L)\hat{\mathcal{S}}(0) - \mathcal{K}_s\Xi(L)\hat{\mathcal{A}}^\dagger(0) + J_S(L), \tag{71}$$

$$\hat{\mathcal{A}}^\dagger(L) = \Pi_s^+(L)\hat{\mathcal{A}}^\dagger(0) - \mathcal{K}_a\Xi(L)\hat{\mathcal{S}}(0) + J_A(L). \tag{72}$$

Solving these simultaneously we have

$$\hat{\mathcal{S}}(0) = \frac{1}{Z(L)}[\Pi_s^+(L)\hat{\mathcal{S}}(L) + \mathcal{K}_s\Xi(L)\hat{\mathcal{A}}^\dagger(L) - \Pi_s^+(L)J_S(L) - \mathcal{K}_s\Xi(L)J_A(L)], \tag{73}$$

$$\hat{\mathcal{A}}^\dagger(0) = \frac{1}{Z(L)}[\Pi_a^+(L)\hat{\mathcal{A}}^\dagger(L) + \mathcal{K}_a\Xi(L)\hat{\mathcal{S}}(L) - \Pi_a^+(L)J_A(L) - \Xi(L)\mathcal{K}_aJ_S(L)], \tag{74}$$

where the denominator

$$Z(L) = \Pi_a^+(L)\Pi_s^+(L) - \Xi(L)^2\mathcal{K}_a\mathcal{K}_s \tag{75}$$

can be evaluated as

$$Z(L) = \Xi_q^2 + \Xi\Xi_q(\mathcal{G}_a + \mathcal{G}_s) + \Xi^2(\mathcal{G}_aG_s - \mathcal{K}_a\mathcal{K}_s) \tag{76}$$

$$= e^{-q_+L}e^{-q_-L} = e^{(\mathcal{G}_s+\mathcal{G}_a)L}, \tag{77}$$

$$q_\pm = -\frac{1}{2}(\mathcal{G}_s + \mathcal{G}_a) \pm \frac{1}{2}\sqrt{(\mathcal{G}_s + \mathcal{G}_a)^2 - 4(\mathcal{G}_a\mathcal{G}_s - \mathcal{K}_a\mathcal{K}_s)}. \tag{78}$$

The phase matching condition here is $\Delta k_{1B} = (-k_p - k_c + k_s + k_a) = 0$, which means the wave vectors of the lasers must be opposite to the Case 1A.

Replacing $\hat{\mathcal{S}}(0)$, $\hat{\mathcal{A}}^\dagger(0)$ from Eqs. (73) and (74), the solutions Eqs. (67) and (68) are finally expressed in terms of the boundary operators $\hat{\mathcal{S}}(L)$, $\hat{\mathcal{A}}^\dagger(L)$:

$$\hat{\mathcal{S}}(z,\nu) = \psi_s^s(z,L,\nu)\hat{\mathcal{S}}(L) + \psi_a^s(z,L,\nu)\hat{\mathcal{A}}^\dagger(L) - \psi_s^s(z,L,\nu)J_S(L) - \psi_a^s(z,L,\nu)J_A(L) + J_S(z), \tag{79}$$

$$\hat{\mathcal{A}}^\dagger(z,\nu) = \psi_s^a(z,L,\nu)\hat{\mathcal{S}}(L) + \psi_a^a(z,L,\nu)\hat{\mathcal{A}}^\dagger(L) - \psi_s^a(z,L,\nu)J_S(L) - \psi_a^a(z,L,\nu)J_A(L) + J_A(z), \tag{80}$$

$$\psi_s^s(z,L,\nu) = \frac{1}{Z(L)}\{\Pi_a^+(z)\Pi_s^+(L) - \mathcal{K}_a\mathcal{K}_s\Xi(z)\Xi(L)\}, \tag{81}$$

$$\psi_a^s(z,L,\nu) = \frac{\mathcal{K}_s}{Z(L)}\{\Pi_a^+(z)\Xi(L) - \Pi_a^+(L)\Xi(z)\}, \tag{82}$$

$$\psi_s^a(z,L,\nu) = \frac{\mathcal{K}_a}{Z(L)}\{\Pi_s^+(z)\Xi(L) - \Xi(z)\Pi_s^+(L)\}, \tag{83}$$

$$\psi_a^a(z,L,\nu) = \frac{1}{Z(L)}\{\Pi_s^+(z)\Pi_a^+(L) - \mathcal{K}_a\mathcal{K}_s\Xi(z)\Xi(L)\}. \tag{84}$$

D. Case 2A: Backward geometry, Stokes (anti-Stokes) propagating towards +z (−z)

Here, $\hat{n}_s = +\hat{z}$ and $\hat{n}_a = -\hat{z}$ ($\varsigma_s = 1$, $\varsigma_a = -1$) with the fields must be expressed in terms of the fields at boundaries $\hat{\mathcal{S}}(0)$ and $\hat{\mathcal{A}}^\dagger(L)$. The solution of the Stokes and anti-Stokes fields are

$$\hat{\mathcal{S}}(z,\nu) = \Pi_a^+(z)\hat{\mathcal{S}}(0) + \mathcal{K}_s\Xi(z)\hat{\mathcal{A}}^\dagger(0) + J_S(z), \tag{85}$$

$$\hat{\mathcal{A}}^\dagger(z,\nu) = -\Pi_s^-(z)\hat{\mathcal{A}}^\dagger(0) - \mathcal{K}_a\Xi(z)\hat{\mathcal{S}}(0) + J_A(z), \tag{86}$$

$$J_S(z) = \int_0^z [\Pi_a^+(z-s)\hat{\mathcal{F}}_s(s) - \mathcal{K}_s\Xi(z-s)\hat{\mathcal{F}}_a^\dagger(s)]ds, \tag{87}$$

$$J_A(z) = \int_0^z [\Pi_s^-(z-s)\hat{\mathcal{F}}_a^\dagger(s) - \mathcal{K}_a\Xi(z-s)\hat{\mathcal{F}}_s(s)]ds. \tag{88}$$

Using Eqs. (85) and (86) we obtain $\hat{\mathcal{S}}(L)$, $\hat{\mathcal{A}}^\dagger(L)$ and rewrite as

$$\hat{\mathcal{A}}^\dagger(0) = \frac{-\hat{\mathcal{A}}^\dagger(L) - \mathcal{K}_a\Xi(L)\hat{\mathcal{S}}(0) + J_A(L)}{\Pi_s^-(L)}. \tag{89}$$

Replacing Eq. (89) into Eqs. (85) and (86) to eliminate $\hat{\mathcal{A}}^\dagger(0)$ gives the result

$$\hat{\mathcal{S}}(z,\nu) = \left(\Pi_a^+(z) - \frac{\mathcal{K}_s\mathcal{K}_a\Xi(z)\Xi(L)}{\Pi_s^-(L)}\right)\hat{\mathcal{S}}(0) - \frac{\mathcal{K}_s\Xi(z)}{\Pi_s^-(L)}\hat{\mathcal{A}}^\dagger(L) + \frac{\mathcal{K}_s\Xi(z)}{\Pi_s^-(L)}J_A(L) + J_S(z), \tag{90}$$

$$\hat{\mathcal{A}}^\dagger(z,\nu) = \frac{\Pi_s^-(z)}{\Pi_s^-(L)}\hat{\mathcal{A}}^\dagger(L) + \left[\frac{\Pi_s^-(z)}{\Pi_s^-(L)}\Xi(L) - \Xi(z)\right]\mathcal{K}_a\hat{\mathcal{S}}(0) - \frac{\Pi_s^-(z)}{\Pi_s^-(L)}J_A(L) + J_A(z). \tag{91}$$

At $z = L$ we have

$$\hat{\mathcal{S}}(L) = \frac{-e^{-(\mathcal{G}_s-\mathcal{G}_a)L}}{\Pi_s^-(L)}\hat{\mathcal{S}}(0) + \mathcal{K}_s\Xi(L)\frac{-\hat{\mathcal{A}}^\dagger(L) + J_A(L)}{\Pi_s^-(L)} + J_S(L), \tag{92}$$

where we used

$$\Pi_a^+(z)\Pi_s^-(z) - \mathcal{K}_s\mathcal{K}_a\Xi(z)^2 = -e^{-(\mathcal{G}_s-\mathcal{G}_a)z}, \tag{93}$$

$$q_\pm = \frac{1}{2}(\mathcal{G}_s - \mathcal{G}_a) \pm \frac{1}{2}\sqrt{(\mathcal{G}_s-\mathcal{G}_a)^2 + 4(\mathcal{G}_a\mathcal{G}_s - \mathcal{K}_a\mathcal{K}_s)}. \tag{94}$$

In general,

$$\hat{\mathcal{S}}(z_s,\nu) = \Psi_s^s(z_s,\nu)\hat{\mathcal{S}}(0,\nu) + \Psi_a^s(z_s,\nu)\hat{\mathcal{A}}^\dagger(L,\nu) \tag{95}$$

$$+ \int_0^L \left[\psi_s^s(z_s,s,\nu)\hat{\mathcal{F}}_s(s,\nu) + \psi_a^s(z_s,s,\nu)\}\hat{\mathcal{F}}_a^\dagger(s,\nu)\right]ds, \tag{96}$$

$$\hat{\mathcal{A}}^\dagger(z_a,\nu) = \Psi_a^a(z_a,\nu)\hat{\mathcal{A}}^\dagger(L,\nu) + \Psi_s^a(z_a,\nu)\hat{\mathcal{S}}(0,\nu) \tag{97}$$

$$+ \int_0^L \left[\psi_s^a(z_a,s,\nu)\hat{\mathcal{F}}_s(s,\nu) + \psi_a^a(z_a,s,\nu)\}\hat{\mathcal{F}}_a^\dagger(s,\nu)\right]ds, \tag{98}$$

with the coefficients

$$\Psi_s^s(z_s,\nu) = \left(\Pi_a^+(z_s) - \frac{\mathcal{K}_s\mathcal{K}_a\Xi(z_s)\Xi(L)}{\Pi_s^-(L)}\right),$$

$$\Psi_a^s(z_s,\nu) = -\frac{\mathcal{K}_s\Xi(z_s)}{\Pi_s^-(L)}, \tag{99a}$$

$$\Psi_s^a(z_a,\nu) = \mathcal{K}_a\left[\frac{\Pi_s^-(z_a)}{\Pi_s^-(L)}\Xi(L) - \Xi(z_a)\right],$$

$$\Psi_a^a(z_a,\nu) = \frac{\Pi_s^-(z_a)}{\Pi_s^-(L)}, \tag{99b}$$

$$\psi_s^s(z_s,s,\nu) = \Pi_a^+(z_s-s)\Theta(z_s-s) - \left(\frac{\mathcal{K}_s\Xi(z_s)}{\Pi_s^-(L)}\right)\mathcal{K}_a\Xi(L-s)\Theta(L-s), \tag{100a}$$

$$\psi_a^s(z_s,s,\nu) = -\mathcal{K}_s\Xi(z_s-s)\Theta(z_s-s) + \left(\frac{\mathcal{K}_s\Xi(z_s)}{\Pi_s^-(L)}\right)\Pi_s^-(L-s)\Theta(L-s), \tag{100b}$$

$$\psi_s^a(z_a,s,\nu) = -\mathcal{K}_a\Xi(z_a-s)\Theta(z_a-s) + \left(\frac{\Pi_s^-(z_a)}{\Pi_s^-(L)}\right)\mathcal{K}_a\Xi(L-s)\Theta(L-s), \tag{100c}$$

$$\psi_a^a(z_a,s,\nu) = \Pi_s^-(z_a-s)\Theta(z_a-s) - \left(\frac{\Pi_s^-(z_a)}{\Pi_s^-(L)}\right)\Pi_s^-(L-s)\Theta(L-s), \tag{100d}$$

where the Heaviside function Θ ensures that the first term in ψ is integrated up to z_s or z_a while the second term is integrated up to L. The phase-matching condition here is $\Delta k_{2A} = (k_p - k_c - k_s + k_a) = 0$.

E. Case 2B: Backward geometry, Stokes (anti-Stokes) propagating towards −z (+z)

Here, $\hat{n}_s = -\hat{z}$ and $\hat{n}_a = +\hat{z}$ ($\varsigma_s = -1$, $\varsigma_a = 1$) with the fields must be expressed in terms of the fields at boundaries $\hat{\mathcal{S}}(L)$ and $\hat{\mathcal{A}}^\dagger(0)$. The solutions are obtained from Eqs. (90)

and (91) by the changes $\hat{\mathcal{S}}(z) \leftrightarrow \hat{\mathcal{A}}^\dagger(z)$, $\mathcal{G}_a \leftrightarrow \mathcal{G}_s$, $\mathcal{K}_a \leftrightarrow \mathcal{K}_s$, and $\hat{\mathcal{F}}_a^\dagger(z) \leftrightarrow \hat{\mathcal{F}}_s(z)$,

$$\hat{\mathcal{A}}^\dagger(z,\nu) = \left(\Pi_s^+(z) - \frac{\mathcal{K}_s\mathcal{K}_a\Xi(z)\Xi(L)}{\Pi_a^-(L)}\right)\hat{\mathcal{A}}^\dagger(0) - \mathcal{K}_a\Xi(z)\frac{\hat{\mathcal{S}}(L) - J_S(L)}{\Pi_a^-(L)} + J_A(z), \quad (101)$$

$$\hat{\mathcal{S}}(z,\nu) = \Pi_a^-(z)\frac{\hat{\mathcal{S}}(L) - J_S(L)}{\Pi_a^-(L)} + \left[\frac{\Pi_a^-(z)}{\Pi_a^-(L)}\Xi(L) - \Xi(z)\right]\mathcal{K}_s\hat{\mathcal{A}}^\dagger(0) + J_S(z), \quad (102)$$

$$J_A(z) = \int_0^z [\Pi_s^+(z-s)\hat{\mathcal{F}}_a^\dagger(s) - \mathcal{K}_a\Xi(z-s)\hat{\mathcal{F}}_s(s)]ds, \quad (103)$$

$$J_S(z) = \int_0^z [\Pi_a^-(z-s)\hat{\mathcal{F}}_s(s) - \mathcal{K}_s\Xi(z-s)\hat{\mathcal{F}}_a^\dagger(s)]ds. \quad (104)$$

The phase-matching condition here is $\Delta k_{2B} = (k_p - k_c + k_s - k_a) = 0$.

F. Analysis of resonance effect

The resonance conditions for backward Cases 2A and 2B are determined by the denominator of the solutions, i.e.,

$$\Pi_f^- = 0, \quad \frac{\sinh\beta z}{\beta}(\alpha - \mathcal{G}_f) = \cosh\beta z,$$

$$\tanh\beta z = \frac{\beta}{\frac{1}{2}(\mathcal{G}_a/\varsigma_a + \mathcal{G}_s/\varsigma_s) - \mathcal{G}_f},$$

which is the key to enhancement and mirrorless oscillations of the quantum fields. For Case 2A, the resonance condition $\Pi_s^-(L_r) = \mathcal{G}_s\Xi - \Xi_q \simeq 0$ gives

$$\tanh\beta L_r = \frac{\beta}{\frac{1}{2}(-\mathcal{G}_a + \mathcal{G}_s) - \mathcal{G}_s} = -\frac{2\beta}{(\mathcal{G}_a + \mathcal{G}_s)} = -\sqrt{1 - \frac{4\mathcal{K}_a\mathcal{K}_s}{(\mathcal{G}_a + \mathcal{G}_s)^2}}, \quad (105)$$

where $\beta = \frac{1}{2}[(\mathcal{G}_a + \mathcal{G}_s)^2 - 4\mathcal{K}_a\mathcal{K}_s]^{1/2}$. If $(\mathcal{G}_a + \mathcal{G}_s)^2 < 4\mathcal{K}_a\mathcal{K}_s$, β is imaginary, and using $\tanh\beta z + i\tan i\beta z = 0$ we can write the condition for the optimal lengths that give resonant peaks as

$$\tan\frac{L_r}{2}aC = -C, \quad (106)$$

where $[4\mathcal{K}_a\mathcal{K}_s - (\mathcal{G}_s + \mathcal{G}_a)^2]^{1/2} = aC$ and $a = (\mathcal{G}_s + \mathcal{G}_a)$. So there are discrete resonant lengths

$$L_r = 2\frac{\tan^{-1}(-C) + m\pi}{aC}, \quad (107)$$

where $m = 0, 1, 2\ldots$. This formula correctly explains the resonant peaks in Fig. 3(e) with spacing of $2\pi/aC = 4.216 \times 10^4$.

For symmetric scheme, i.e., identical pump and control field parameters $\Delta_c = \Delta_p$, $T_{ad} = T_{bc}$, $I_c = I_p = I$, we may set $w_{bb}^{aa} = w_{cc}^{aa} = w_{cc}^{dd} = w_{bb}^{dd}$, $T_{ac} = T_{ab} = T_{dc}$, $T_{bd}^* = T_{dc}^* = T_{ab}^*$, and $g_a^*\kappa_a^* \simeq g_s\kappa_s$, with the analytical expressions

$$a = (\mathcal{G}_s + \mathcal{G}_a) \simeq -\frac{g\kappa w}{\frac{(\gamma^2+\Delta^2)}{2\gamma} + I\mathcal{V}}, \quad (108)$$

$$C = \sqrt{\frac{4\mathcal{K}_a\mathcal{K}_s}{(\mathcal{G}_s + \mathcal{G}_a)^2} - 1} \simeq \sqrt{\frac{4(I\mathcal{V})^2}{\gamma^2 + \Delta^2} - 1}, \quad (109)$$

$$\mathcal{V} = \left(\frac{1}{T_{bc}} + \frac{1}{T_{ad}}\right) \simeq \frac{1}{\gamma_{bc}} + \frac{1}{\gamma_{ad}}, \quad (110)$$

$$\beta = \frac{1}{2}iaC \simeq \frac{1}{2}\frac{g\kappa w}{\frac{(\gamma^2+\Delta^2)}{2\gamma} + I\mathcal{V}}\sqrt{1 - \frac{4(I\mathcal{V})^2}{(\gamma^2 + \Delta^2)}}. \quad (111)$$

In the above expressions we use the steady-state expressions for $\tilde{\rho}_{ab}$ and $\tilde{\rho}_{dc}$ to obtain simplified expressions for $\mathcal{K}_f$ and $\mathcal{G}_f$:

$$\mathcal{K}_s \simeq \frac{1}{\mathcal{D}}g_s\kappa_s w\Omega_p\Omega_q\left[\frac{T_{ac}}{T_{dc}^*} + 1\right](T_{bc} + T_{ad}) \simeq g_s\kappa_s w\Omega_p\Omega_c(T_{ad} + T_{bc})\frac{2\gamma}{\gamma - i\Delta}, \quad (112)$$

$$\mathcal{K}_a \simeq \frac{1}{\mathcal{D}}g_a^*\kappa_a^* w\Omega_p^*\Omega_q^*\left[\frac{T_{bd}^*}{T_{ab}} + 1\right](T_{bc} + T_{ad}) \simeq g_a^*\kappa_a^* w\Omega_p^*\Omega_c^*(T_{bc} + T_{ad})\frac{2\gamma}{\gamma + i\Delta}, \quad (113)$$

$$\mathcal{K}_a\mathcal{K}_s \simeq \frac{1}{\mathcal{D}^2}g_a^*\kappa_a^* g_s\kappa_s w^2 I_p I_c\frac{4\gamma^2}{\gamma^2 + \Delta^2}(T_{bc} + T_{ad})^2, \quad (114)$$

$$\mathcal{G}_s \simeq -\frac{1}{\mathcal{D}}g_s\kappa_s w(T_{ac}T_{ad}T_{bc}) - \frac{i\nu}{c}, \quad (115)$$

$$\mathcal{G}_a \simeq -\frac{1}{\mathcal{D}}g_a^*\kappa_a^* w(T_{bd}^*T_{ad}T_{bc}) - \frac{i(\nu - \Delta\nu)}{c}, \quad (116)$$

$$(\mathcal{G}_s - \mathcal{G}_a) = \frac{-i2\Delta}{\mathcal{D}}g_s\kappa_s wT_{ad}T_{bc}, \quad (117)$$

$$(\mathcal{G}_s + \mathcal{G}_a) \simeq -\frac{1}{\mathcal{D}}g\kappa wT_{ad}T_{bc}(T_{bd}^* + T_{ac}) \quad (118)$$

$$= -\frac{g\kappa w}{\left(\frac{\gamma^2+\Delta^2}{2\gamma}\right) + I\left(\frac{T_{ad}+T_{bc}}{T_{ad}T_{bc}}\right)}, \quad (119)$$

where we note that

$$\frac{T_{bd}^*T_{ac}}{(T_{bd}^* + T_{ac})} \simeq \frac{(\gamma^2 + \Delta^2)}{2\gamma},$$

and $\mathcal{D} \approx (\gamma^2 + \Delta^2)T_{ad}T_{bc} + 2\gamma I(T_{ad} + T_{bc})$.

V. PAIRED CORRELATIONS

From the solutions $\hat{\mathcal{S}}(z_s,\nu) = \hat{\mathcal{S}}^b + \hat{\mathcal{S}}^n$, $\hat{\mathcal{A}}(z_a,\nu) = \hat{\mathcal{A}}^b + \hat{\mathcal{A}}^n$ we have developed a code to compute all the following pairs: $\langle\hat{\mathcal{S}}^\dagger(z_s,\nu)\hat{\mathcal{S}}(z_s,\nu)\rangle$, $\langle\hat{\mathcal{S}}(z_s,\nu)\hat{\mathcal{S}}^\dagger(z_s,\nu)\rangle$, $\langle\hat{\mathcal{A}}^\dagger(z_a,\nu)\hat{\mathcal{A}}(z_a,\nu)\rangle$, $\langle\hat{\mathcal{A}}(z_a,\nu)\hat{\mathcal{A}}^\dagger(z_a,\nu)\rangle$, $\langle\hat{\mathcal{A}}(z_a,\nu)\hat{\mathcal{S}}(z_s,\nu)\rangle$, $\langle\hat{\mathcal{S}}(z_s,\nu)\hat{\mathcal{A}}(z_a,\nu)\rangle$ needed to obtain correlations

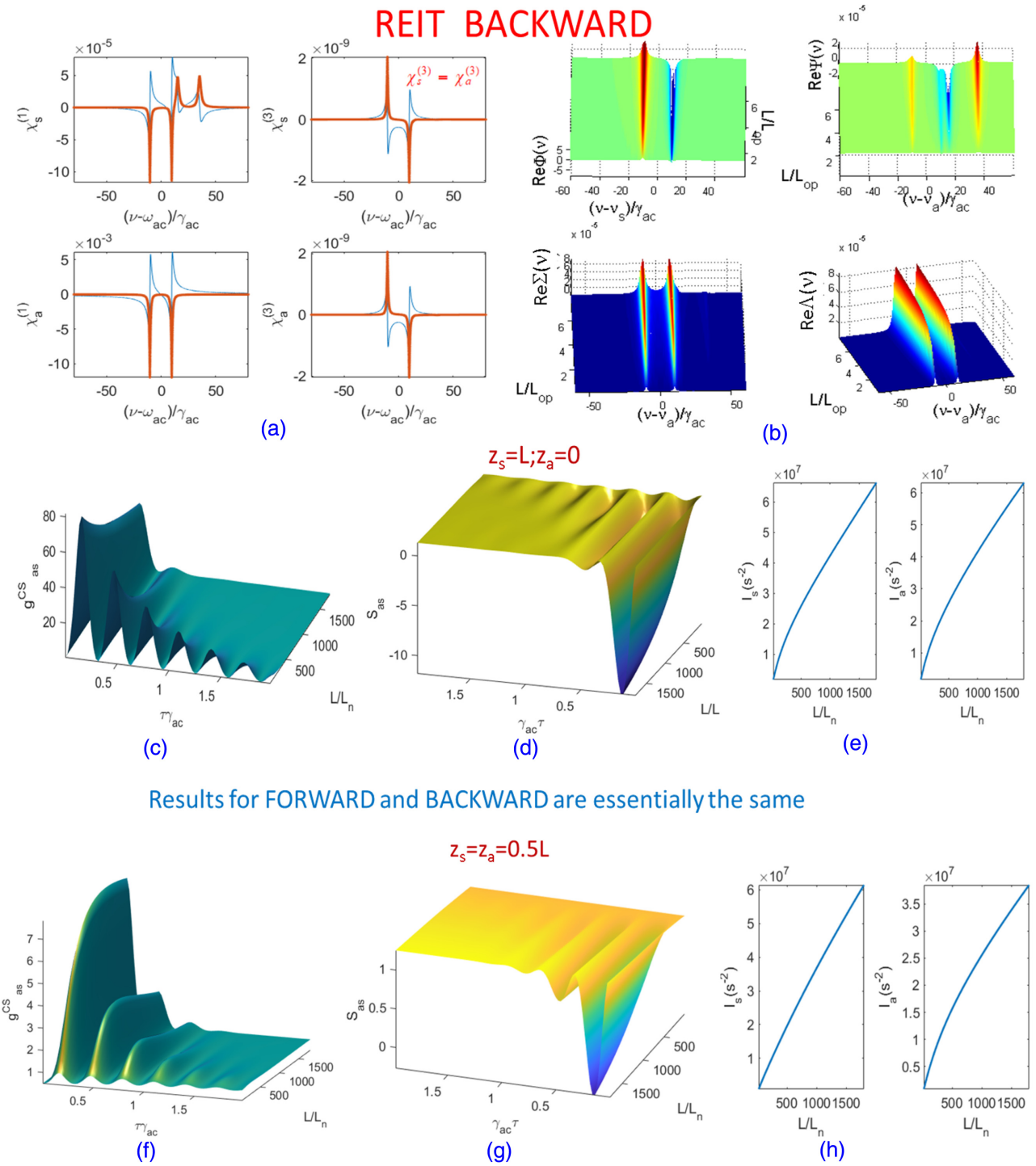

FIG. 2. Effects of propagation length for Raman-EIT scheme: (a) Spectra of linear ($n = 1$) and third-order ($n = 3$) susceptibilities $\chi_f^{(n)}$, (b) correlation spectra $\Phi(\nu)$, $\Psi(\nu)$, $\Sigma(\nu)$, $\Lambda(\nu)$, (c) Cauchy Schwarz correlation of anti-Stokes to Stokes $g_{as}^{CS}(\tau)$, (d) two-mode squeezing S_q, and (e) intensities $I_f(z_f)$ for Stokes ($f = s$) at $z_s = L$ and anti-Stokes ($f = s$) at $z_a = 0$ vs propagation length L. At $z_a = z_s = 0.5L$ [similar to panels (c)–(e)] we plot (f) $g_{as}^{CS}(\tau)$, (g) S_{as}, (h) $I_f(z_f)$ vs propagation length L to show the effect of spatial correlations. For normalization, we use $\Gamma = 2\pi \times 5.89 \times 10^6$, $L_n = c/\omega_{ac}$, $\omega_{ac} = 2\pi c/(795\ \text{nm})$.

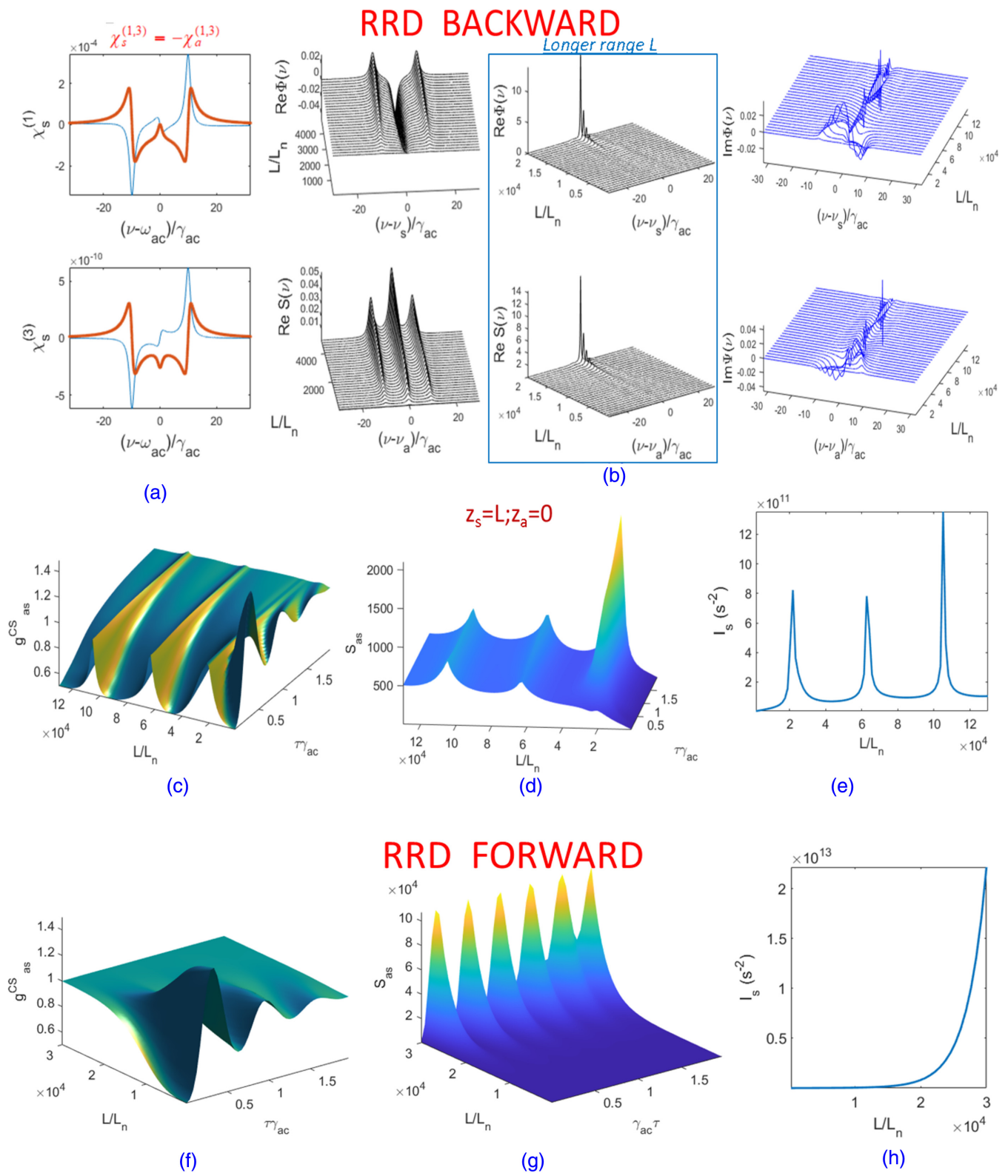

FIG. 3. Effects of propagation length for Raman resonant doublet (RRD) scheme. For backward case: (a) Spectra of linear ($n = 1$) and third order ($n = 3$) susceptibilities $\chi_f^{(n)}$, (b) correlation spectra $\Phi(\nu)$, $\Psi(\nu)$, $\Sigma(\nu)$, $\Lambda(\nu)$, (c) Cauchy Schwarz correlation of anti-Stokes to Stokes $g_{as}^{CS}(\tau)$, (d) two-mode squeezing S_{as}, and (e) intensities $I_f(z_f)$ for Stokes ($f = s$) at $z_s = L$ and anti-Stokes ($f = s$) at $z_a = 0$ vs propagation length L. Similarly, for forward case: (e) Cauchy Schwarz correlation of anti-Stokes to Stokes $g_{as}^{CS}(\tau)$, (f) two-mode squeezing S_{as}, and (g) intensities $I_f(z_f)$.

functions

$$G^{(2)}_{as}(\tau) = \langle \hat{E}^{\dagger}_s(z_s,t)\hat{E}^{\dagger}_a(z_a,t+\tau)\hat{E}_a(z_a,t+\tau)\hat{E}_s(z_s,t)\rangle \tag{120}$$

$$= \frac{1}{|g_s|^2|g_a|^2}\langle \hat{S}^{\dagger}(z_s,t)\hat{A}^{\dagger}(z_a,t+\tau)\hat{A}(z_a,t+\tau)\hat{S}(z_s,t)\rangle$$

$$= \frac{1}{|g_s|^2|g_a|^2} \times \begin{bmatrix} |\langle \hat{A}^b(z_a,\tau)\hat{S}^b(z_s)\rangle + \langle \hat{A}^n(z_a,\tau)\hat{S}^n(z_s)\rangle|^2 \\ +\left[I^b_a(z_a,0)+I^n_a(z_a,0)\right]\left[I^b_s(z_s,0)+I^n_s(z_s,0)\right] \end{bmatrix}, \tag{121}$$

$$G^{(2)}_{ff}(\tau) = \frac{1}{|g_f|^4}\Big[\big|I^b_f(z_f,\tau)+I^n_f(z_f,\tau)\big|^2 + \big[I^b_f(z_f,0)+I^n_f(z_f,0)\big]^2\Big], \tag{122}$$

with $f = s,a$. The expressions (in time domain) $\langle \hat{A}^{\odot}(z_a,\tau)\hat{S}^{\odot}(z_s)\rangle$, $\langle \hat{S}^{\odot}(z_s,\tau)\hat{A}^{\odot}(z_a)\rangle$, $I^{\odot}_s(z_s,\tau) = \langle \hat{S}^{\odot}(z_s,\tau)\hat{S}^{\odot}(z_s)\rangle$, $I^{\odot}_a(z_a,\tau) = \langle \hat{A}^{\odot}(z_a,\tau)\hat{A}^{\odot}(z_a)\rangle$ for $\odot = b$ (boundary terms), n (noise terms) are given in Appendixes E and F, respectively. The terms $\langle \hat{S}(z_s,\nu)\hat{A}^{\dagger}(z_a,\nu)\rangle$, $\langle \hat{A}^{\dagger}(z_a,\nu)\hat{S}(z_s,\nu)\rangle$, $\langle \hat{S}^2(z_s,\nu)\rangle$, $\langle \hat{A}^2(z_a,\nu)\rangle$ are zero due to thermal photons.

We also compute the normalized correlations

$$g^{CS}_{as}(\tau) = \frac{G^{(2)}_{as}(\tau)}{\sqrt{G^{(2)}_{ss}(0)G^{(2)}_{aa}(0)}}, \tag{123}$$

$$g^{(2)}_{as}(\tau) = \frac{G^{(2)}_{as}(\tau)}{G^{(1)}_s(0)G^{(1)}_a(0)} = \frac{\langle \hat{N}_a(\tau)\hat{N}_s\rangle + \langle \hat{N}_s\hat{N}_a(\tau)\rangle}{2\langle \hat{N}_s\rangle\langle \hat{N}_a\rangle}, \tag{124}$$

$$g^{(2)}_f(\tau) = \frac{G^{(2)}_{ff}(\tau)}{G^{(1)}_f(0)G^{(1)}_f(0)} = \frac{\langle a^{\dagger}_f(t)a_f(t+\tau)a^{\dagger}_f(t+\tau)a_f(t)\rangle - \langle a^{\dagger}_f(t)a_f(t)\rangle}{\langle a^{\dagger}_f(t)a_f(t)\rangle^2}, \tag{125}$$

$$g^{(2)}_f(0) = \frac{\langle \hat{N}^2_f\rangle - \langle \hat{N}_f\rangle}{\langle \hat{N}_f\rangle^2} = \frac{Q_f}{\langle \hat{N}_f\rangle} + 1, \tag{126}$$

where $\hat{N}_f(t) = a^{\dagger}_f(t)a_f(t)$, $Q_f = \langle \Delta\hat{N}^2_f\rangle/\langle \hat{N}_f\rangle - 1 = \langle \hat{N}_f\rangle(g^{(2)}_f(0)-1)$, $G^{(2)}_{ff}(\tau) = G^{(2)}_{as}(\tau)|_{s\to f,a\to f}$, $I_f(\tau) = |g_f|^2G^{(1)}_f(\tau)$, and $G^{(1)}_f(0) = \langle \hat{E}^{\dagger}_f(t)\hat{E}_f(t)\rangle$ is assumed to be the same as $\langle \hat{E}^{\dagger}_f(t+\tau)\hat{E}_f(t+\tau)\rangle$ for the steady-state scenario. To relate $\hat{N}_f(t)$ and $\hat{E}^{\dagger}_f(t)\hat{E}_f(t)$ we have used $\frac{1}{2}2\varepsilon_0\langle \hat{E}^{\dagger}_f(t)\hat{E}_f(t)\rangle V = \hbar v_f\langle \hat{N}_f\rangle$. We get the relations $\langle \hat{N}_f\rangle = I_f/c_f$ and

$$G^{(2)}_{as}(\tau) = \left(\frac{\hbar\sqrt{v_sv_a}}{\varepsilon_0 V}\right)^2\langle \hat{N}_a(\tau)\hat{N}_s\rangle,$$

where

$$c_f = |g_f|^2\left(\frac{\hbar v_f}{\varepsilon_0 V}\right) = C_f\Big/\left(\frac{\pi l}{c}\right),$$

and $V = Al$ is the quantization volume. Typically $\hat{N}_f \approx 1$ so $\varepsilon_0 V\langle \hat{E}^{\dagger}_f(t)\hat{E}_f(t)\rangle \sim \hbar v_f$. Using $\langle \hat{E}^{\dagger}_f(t)\hat{E}_f(t)\rangle \sim \gamma C_f/|g_f|^2$, $C_f = \frac{\hbar v_f\pi}{\varepsilon_0 Ac}|g_f|^2$ gives $\varepsilon_0 V\frac{\hbar v_f\pi}{\varepsilon_0 Ac}\gamma \sim \hbar v_f$ and finally $l\frac{\pi}{c}\gamma \approx 1$, $l \sim c/\pi\gamma$.

The power of the quantum field is $P = dU/dt = \varepsilon_0\frac{d}{dt}\int\langle \hat{E}^{\dagger}_f(t)\hat{E}_f(t)\rangle dV = \varepsilon_0 A\langle \hat{E}^{\dagger}_f(t)\hat{E}_f(t)\rangle c$.

The evaluation of the correlation functions make use of the paired correlations of the boundary operators and noise operators as detailed in Appendixes E and F, respectively.

Squeezing

We expect that the noise of the Stokes and anti-Stokes are somewhat correlated, therefore the quantity $(\hat{N}_s - \hat{N}_a)$ would be of interest for noise reduction via relative photon number detection, such as in quantum interferometry. The investigation of squeezing is relevant in the context of the quantum light spectroscopy, as broadly discussed in Ref. [28]. Thus, we analyze the normalized two-mode relative intensity variance to detect any sign of nonclassicality, i.e., two-mode squeezing,

$$S_{as}(\tau) = \frac{Var(\hat{N}_s(t)-\hat{N}_a(t+\tau))}{\langle \hat{N}_s(t)\rangle + \langle \hat{N}_a(t+\tau)\rangle} = \frac{\langle(\hat{N}_s(t)-\hat{N}_a(t+\tau))^2\rangle - \{\langle \hat{N}_s(t)\rangle - \langle \hat{N}_a(t+\tau)\rangle\}^2}{\langle \hat{N}_s(t)\rangle + \langle \hat{N}_a(t+\tau)\rangle} \tag{127a}$$

$$= \frac{\langle \hat{N}^2_s\rangle + \langle \hat{N}^2_a(\tau)\rangle - \langle \hat{N}_s\hat{N}_a(\tau)\rangle - \langle \hat{N}_a(\tau)\hat{N}_s\rangle - \langle \hat{N}_s\rangle^2 - \langle \hat{N}_a(\tau)\rangle^2 + 2\langle \hat{N}_s\rangle\langle \hat{N}_a(\tau)\rangle}{\langle \hat{N}_s\rangle + \langle \hat{N}_a(\tau)\rangle} \tag{127b}$$

$$= \frac{\langle \Delta\hat{N}^2_s\rangle + \langle \Delta\hat{N}^2_a(\tau)\rangle - \langle \hat{N}_s\hat{N}_a(\tau)\rangle - \langle \hat{N}_a(\tau)\hat{N}_s\rangle + 2\langle \hat{N}_s\rangle\langle \hat{N}_a(\tau)\rangle}{\langle \hat{N}_s\rangle + \langle \hat{N}_a(\tau)\rangle}. \tag{127c}$$

Using $[\mathcal{E}^{\dagger}_s(t), \hat{N}_a(\tau)] = c$, $[\hat{N}_a(\tau), \mathcal{E}_s(t)] = c^*$,

$$\langle \hat{N}_s\hat{N}_a(\tau)\rangle = \langle \mathcal{E}^{\dagger}_s(t)\mathcal{E}_s(t)\mathcal{E}^{\dagger}_a(t+\tau)\mathcal{E}_a(t+\tau)\rangle = \langle \mathcal{E}^{\dagger}_s(t)\{\mathcal{E}^{\dagger}_a(t+\tau)\mathcal{E}_a(t+\tau)\mathcal{E}_s(t) - c^*\}\rangle = G^{(2)}_{as} - \langle \mathcal{E}^{\dagger}_s(t)c^*\rangle,$$
$$\langle \hat{N}_a(\tau)\hat{N}_s\rangle = \langle \mathcal{E}^{\dagger}_a(t+\tau)\mathcal{E}_a(t+\tau)\mathcal{E}^{\dagger}_s(t)\mathcal{E}_s(t)\rangle = \langle \{\mathcal{E}^{\dagger}_s(t)\mathcal{E}^{\dagger}_a(t+\tau)\mathcal{E}_a(t+\tau) - c\}\mathcal{E}_s(t)\rangle = G^{(2)}_{as} - \langle c\mathcal{E}_s(t)\rangle,$$

where $\langle c\mathcal{E}_s(t)\rangle + \langle \mathcal{E}_s^\dagger(t)c^*\rangle$ must be a real number and assume to be small in value, so $\langle \hat{N}_s\hat{N}_a(\tau)\rangle$ and $\langle \hat{N}_a(\tau)\hat{N}_s\rangle$ approximate the normal order. We rewrite in terms of the correlations (126) $g_f^{(2)}(0)$ and (124) $g_{as}^{(2)}(\tau)$,

$$S_{as}(\tau) = \frac{\langle \Delta\hat{N}_s^2\rangle + \langle \Delta\hat{N}_a^2\rangle - \langle \hat{N}_s\hat{N}_a(\tau)\rangle - \langle \hat{N}_a(\tau)\hat{N}_s\rangle + 2\langle \hat{N}_s\rangle\langle \hat{N}_a\rangle}{\langle \hat{N}_s\rangle + \langle \hat{N}_a\rangle}, \tag{128}$$

$$= 1 + \frac{\{g_s^{(2)}(0)-1\}\langle \hat{N}_s\rangle^2 + \{g_a^{(2)}(0)-1\}\langle \hat{N}_a\rangle^2 - 2\{g_{as}^{(2)}(\tau)-1\}\langle \hat{N}_s\rangle\langle \hat{N}_a\rangle}{\langle \hat{N}_s\rangle + \langle \hat{N}_a\rangle}, \tag{129}$$

$$= 1 + \frac{\{g_s^{(2)}(0)-1\}\left(\frac{I_s}{c_s}\right)^2 + \{g_a^{(2)}(0)-1\}\left(\frac{I_a}{c_a}\right)^2 - 2\left(g_{as}^{(2)}(\tau)-1\right)\left(\frac{I_s}{c_s}\frac{I_a}{c_a}\right)}{\left(\frac{I_s}{c_s}\right) + \left(\frac{I_a}{c_a}\right)}, \tag{130}$$

which shows nonclassical squeezing when anti-Stokes is correlated to Stokes (i.e., $g_{as}^{(2)}$ is large) and not otherwise. We will see (in Fig. 2) that the REIT scheme that gives large nonclassical correlations also gives large intensity squeezing, particularly at $\tau \simeq \Omega_{p,c}^{-1}$. For the coherent state, $Var(\hat{N}_s(t) - \hat{N}_a(t)) = \langle \Delta\hat{N}_s^2\rangle + \langle \Delta\hat{N}_a^2\rangle = \langle \hat{N}_s\rangle + \langle \hat{N}_a\rangle$ means $S_{as}(\tau) = 1$ and $\langle \hat{N}_s\hat{N}_a\rangle = \langle \hat{N}_s\rangle\langle \hat{N}_a\rangle$ are uncorrelated.

Written in terms of Mandel's parameters $Q_f = \frac{\langle \Delta\hat{N}_f^2\rangle}{\langle \hat{N}_f\rangle} - 1 = \langle \hat{N}_f\rangle[g_f^{(2)}(0)-1]$,

$$S_{as} = 1 + \frac{Q_s\langle \hat{N}_s\rangle + Q_a\langle \hat{N}_a\rangle - (g_{as}^{(2)}(\tau)-1)2\langle \hat{N}_s\rangle\langle \hat{N}_a\rangle}{\langle \hat{N}_s\rangle + \langle \hat{N}_a\rangle}, \tag{131}$$

which shows squeezing, i.e., $S_{as} < 1$ when the photons are sub-Poissonian $Q_{s,a} < 1$ and/or highly correlated $g_{as}^{(2)} \gg 1$. If $\langle \hat{N}_s\rangle = \langle \hat{N}_a\rangle$ we have

$$S_{as} = 1 + \langle \hat{N}\rangle\left(\frac{g_s^{(2)}(0) + g_a^{(2)}(0)}{2} - g_{as}^{(2)}(\tau)\right),$$

so the necessary for nonclassicality or squeezing is $g_{as}^{(2)}(\tau) > g_f^{(2)}(0)$.

Below we discuss the subtle difference between antibunching and sub-Poissonian based on the definitions of $g_f^{(2)}(0)$, Q_f and antibunching

$$\begin{aligned}\langle :\Delta\hat{N}_f^2: \rangle &= \langle a_f^\dagger(t)\{a_f^\dagger(t)a_f(t)\}a_f(t)\rangle - \langle \hat{N}_f\rangle^2 \\ &= \langle \Delta\hat{N}_f^2\rangle - \langle \hat{N}_f\rangle \\ &= \langle \hat{N}_f\rangle^2\{g_f^{(2)}(0)-1\} = \langle \hat{N}_f\rangle Q_f < 0. \end{aligned} \tag{132}$$

Sub-Poissonian means $Q_f < 0$ or $\langle :\Delta\hat{N}_f^2: \rangle < 0$ (negative values) or $g_f^{(2)}(0) < 1$. Although antibunching means, by definition, $g_f^{(2)}(0) < g_f^{(2)}(\tau > 0)$ the situation where $g_f^{(2)}(0) \approx 0$ is considered as antibunching since it is essentially a minimum value and would satisfy $g_f^{(2)}(0) < g_f^{(2)}(\tau > 0)$.

Note that $g_f^{(2)}(0) \approx 0$ (antibunching) obviously also means sub-Poissonian $Q_f \approx -\langle \hat{N}_f\rangle$, although the reverse is not always true, i.e., sub-Poissonian may not necessarily mean antibunching (but can be accompanied by bunching). In any case, one can safely mention sub-Poissonian when $\langle :\Delta\hat{N}_f^2: \rangle$ is negative and only say antibunching when $\langle :\Delta\hat{N}_f^2: \rangle = -\langle \hat{N}_f\rangle^2$.

VI. RESULTS

Based on the semi-analytical expressions above we have computed the spectra of linear $\chi_f^{(1)}(\nu)$ and nonlinear $\chi_f^{(3)}(\nu)$ susceptibilities, spectra of correlations $\Phi(\nu)$, $\Psi(\nu)$, $\Sigma(\nu)$, $\Lambda(\nu)$, power or intensity of Stokes and anti-Stokes $I_f(\tau = 0)$, normalized photon correlations $g_{as}^{(2)}(\tau)$, Cauchy-Schwarz correlation $g_{as}^{CS}(\tau)$, and relative intensity squeezing $S_{as}(\tau)$ versus time delay for several cases of laser fields: Raman-EIT (REIT), Raman resonant doublet (RR, and Raman off-resonant doublet (ROD). The default detunings and Rabi frequencies used in the figures are

(a) REIT: $\Delta_p = -25\gamma_{ac}$, $\Delta_c = 0$, $\Omega_p = 2.5\gamma_{ac}$, $\Omega_c = 10\gamma_{ac}$, with $\tau_p\gamma_{ac} = \frac{\pi}{\Omega_c/\gamma_{ac}} = \frac{\pi}{10}$.

(b) RRD: $\Delta_p = 0$, $\Delta_c = 0$, $\Omega_p = \Omega_c = 5\gamma_{ac}$, with $\tau_p\gamma_{ac} = \frac{\pi}{\Omega_c/\gamma_{ac}} = \frac{\pi}{5}$.

(c) ROD: $\Delta_p = -20\gamma_{ac}$, $\Delta_c = -20\gamma_{ac}$, $\Omega_p = \Omega_c = 5\gamma_{ac}$, with $\tau_p\gamma_{ac} = \pi\gamma_{ac}[(\frac{\Delta_p}{2})^2 + \Omega_c^2]^{-1/2} = \frac{\pi}{5\sqrt{5}}$.

The τ_p refers to the period of oscillations in the $g_{as}^{(2)}(\tau)$. We have used same detuning for each Raman transition $\delta_s = \Delta_p$, $\delta_a = \Delta_c$, number density $N = 8\times10^{17}$ m^{-3} of Rb-87 and radius $r = 100$ μm. To normalize the axes of time, frequency and length, we use $\Gamma = 2\pi \times 5.89 \times 10^6$, $L_n = c/\omega_{ac}$, $\omega_{ac} = 2\pi c/(795\text{ nm})$. To compute the total spectrum, we add the contributions of boundary and noise terms $Z(\nu) = Z^f(\nu) + Z^n(\nu)$, where $Z \in \Phi$, Ψ, Σ, Λ are given in Appendixes E and F.

A. Effects of propagation length

For REIT (Fig. 2), the nonlinear spectra for Stokes and anti-Stokes are surprisingly identical $\chi_s^{(3)} = \chi_a^{(3)}$, as shown in Fig. 2(a). The $\chi_s^{(1)}$ shows four resonances corresponding to loss at $\nu - \omega_{ac} = \pm\Omega_c$ and gain at $|\Delta_p| \pm \Omega_c$. The peaks in the noise correlation spectra Φ of Fig. 2(b) correspond to the two central peaks of $\chi_{s,a}^{(3)}$ in Fig. 2(a). The Ψ noise correlation shows three peaks corresponding to the peaks of $\chi_s^{(1)}$. The two central peaks in spectra $S(\nu)$ and $A(\nu)$ correspond to gain as shown in Fig. 2(b). The correlation spectra tell a lot about the dependency on time delay as they are related by Fourier transform. Note that $\Sigma(\nu)$, $\Lambda(\nu)$ are real.

For backward($z_s = L$ and $z_a = 0$), the photon correlation g_{as}^{CS} shown in Fig. 2(c) between Stokes and anti-Stokes fields oscillate with τ but decays rapidly with L, implying the loss of interference effect and reduced correlation time are due

to the many-particle effect as the size of medium increases. Although the oscillations (side lobes due to interference) in g_{as}^{CS} as well as $g_{as}^{(2)}$ vanish as L increases, the main peak is essentially constant.

Nonclassical squeezing shown by the dip of S_{as} at τ_p in Fig. 2(d), corresponds to indistinguishability and maximum quantum correlations. Since $g_{as}^{(2)}(\tau) \gg g_{ss}^{(2)}(\tau)$ and $g_{aa}^{(2)}(\tau)$ for the REIT case, the shape of $S(\tau)$ is identical to $g_{as}^{(2)}(\tau)$ except that it is inverted. The Stokes and anti-Stokes intensities are essentially the same [Fig. 2(e)], $I_s(L, \tau = 0) = I_a(L, \tau = 0)$ due the cross-coupling nature of the propagation, even though the Stokes is largely detuned while the anti-Stokes is resonant.

For the backward case the correlation g_{as}^{CS} at the same point in the midway $z_s = z_a = 0.5L$ shows a similar qualitative dependence. As L increases, the correlation peaks [Fig. 2(f)] increase with L from maximum peak value of around unity to some saturated values while maintaining the features of complete antibunching and oscillations. In the two-mode squeezing [Fig. 2(g)] there is a significant dip ($S_{as} < 1$) at delay τ_p, which show nonclassicality that coincides with the first peak of $g_{as}^{(2)}(\tau)$. However, quantitatively, the dip is only to 0.88, which can be said to essentially represent classical correlation regime. We therefore noted that quantum correlations is not fully developed in the middle of the sample at $L/2$, i.e., the value for g_{as}^{CS} is smaller than the former case, while $I_s(L, 0)$ and $I_a(L, 0)$ are noticeably different due to asymmetry [Fig. 2(h)].

The situation is differently more interesting for RRD (Fig. 3) where the two lasers are on resonant, specifically in the case of backward geometry. The spectra for Stokes and anti-Stokes show the characteristic $\chi_s^{(1,3)} = -\chi_a^{(1,3)}$ due to symmetry of the two Raman transitions in RRD scheme with three strong resonances composed of a mixture of absorption and gain at $\nu - \omega_{ac} = 0, \pm|\Omega_p + \Omega_c|$, as shown in Fig. 3(a), corresponding to the three (Mollow) peaks in the noise spectra [Fig. 3(b)]. However, for large L the central peak close to $\nu - \omega_{ac} \approx 0$ becomes dominant. The correlation in RRD scheme [Fig. 3(c)] is essentially classical due to the small value of $g_{as}^{CS}(\tau)$ with antibunching and oscillations appearing only for small L. As L increases, $g_{as}^{CS}(0)$ oscillates between 0 (antibunching) and 1 (coherent). The squeezing also varies in a similar fashion as L increases but it is entirely classical [(Fig. 3(d)]. The periodic points L_r where bunching occurs correspond to high-intensity resonant peaks of $I_s(L_r, 0) = I_a(L_r, 0)$ in Fig. 3(e) that satisfy the analytical formula (107) we have obtained, recast as

$$L_r = \left(\frac{\gamma^2 + \Delta^2 + 2\gamma I\mathcal{V}}{\gamma g\kappa|w|}\right)\frac{\tan^{-1}\left(-\sqrt{\frac{4(I\mathcal{V})^2}{\gamma^2+\Delta^2} - 1}\right) + m\pi}{\sqrt{\frac{4(I\mathcal{V})^2}{\gamma^2+\Delta^2} - 1}}.$$

The plot of L_r vs detuning Δ_p (with $\Delta_c = 0$) and Rabi Ω_p (with $\Omega_c = \Omega_p$ or $5\gamma_{ac}$; Fig. 10). shows very small resonance length is needed to achieve resonance with weak fields $\Omega_p \approx \gamma_{ac}$ at discrete values of detuning.

For RRD with forward geometry, the oscillations in the correlation vanish [Fig. 3(f)] and the photons become classical (coherent state) as L increases. However, there is nonclassical squeezing [Fig. 3(g)] where S_{as} reaches a saturation level at moderate negative values as L increases. The contrasting results show that propagation effect can render one quantity classical yet and another quantity nonclassical. This allows for spatial control of quantum correlation given the desired quantity. The intensity $I_{s,a}(L)$ grows exponential-like with L for forward RRD [Fig. 3(h)] due to the large gain but saturation is not shown as it is presently not included in our model.

For ROD, the spectra for Stokes and anti-Stokes for nonlinear and linear susceptibilities are symmetric $\chi_s^{(3)} = \chi_a^{(3)}$ and antisymmetric $\chi_s^{(1)}(\nu - \omega_{ac}) = -\chi_a^{(1)}(\omega_{ac} - \nu)$, respectively, as shown in Fig. 4(a). The linear susceptibilities clearly show a single peak shifted by the large detuning $|\Delta_p|$ but in opposite manner. The noise spectra [Fig. 4(b)] display single dominant peak around $\nu - \omega_{ac} \approx 0$. The correlation is small [Fig. 4(c)], with the oscillations being washed out at larger L for both forward and backward cases. The nonclassical squeezing ($S_{as} < 1$) at delay τ_p increases log-like with L [Fig. 4(d)]. This behavior is much like the case of RRD.

For backward case with $z_s = z_a = 0.5L$, we have different feature in the correlation [Fig. 4(f)], which increases with τ while oscillating (but eroded as L increases), while the squeezing [Fig. 4(g)] is entirely classical for any propagation length. The intensities of quantum fields grow linearly with length [Fig. 4(h)], indicating noncooperative effect of the off-resonant scheme.

B. Effects of pump- and control-laser detunings

The results of both forward and backward geometries are essentially the same for REIT and ROD schemes, even for large L. The effects of backward propagation is only significant for RRD scheme with sufficiently large L, i.e., $5 \times 10^3/k_o$, where interesting resonant features are found. While the spectra vary depending on the sign of Δ_p and Δ_c, the correlations and squeezing depend on just the magnitudes, $|\Delta_p|$ and $|\Delta_c|$. For forward case (not shown), we find the correlation spectra show no qualitative difference (only small quantitative difference) are totally unaffected compared with the backward case. This robustness against laser geometry is an interesting and surprising characteristic of the REIT scheme.

1. Spectra of susceptibilities

We have plotted the susceptibilities versus detunings for different pump and control Rabi frequencies in Fig. 5.

Only at $\Delta_c = 0$ and large Δ_p the spectral lines of the linear susceptibilities [in Figs. 5(a) and 5(d)] show symmetric EIT absorption peaks at around $\omega_{ac} \pm \Omega_c$ as they correspond to the Raman-EIT case, the region that produces highly correlated photon pairs.

The symmetric EIT peaks at resonance $\Delta_c = 0$ in $\chi_a^{(1)}$ [Fig. 5(a)] become increasingly asymmetric, shifted, and separated as Δ_c increases. Figures 5(b), the strong off-resonant anti-Stokes Raman enhances the EIT peaks in $\chi_s^{(1)}$ due to the weak pump laser $\Omega_p = 2.5\gamma_{ac}$ in the resonant Stokes Raman transition. The separation between the EIG (gain) peaks and the EIT (absorption) peaks in $\chi_a^{(1)}$ widens with increasing Δ_c. In Fig. 5(c) shows closely spaced (due to weak pump) EIT peaks in $\chi_s^{(1)}$ when $\Delta_p = 0$ with one of the peaks diminishing while shifted with the pump frequency.

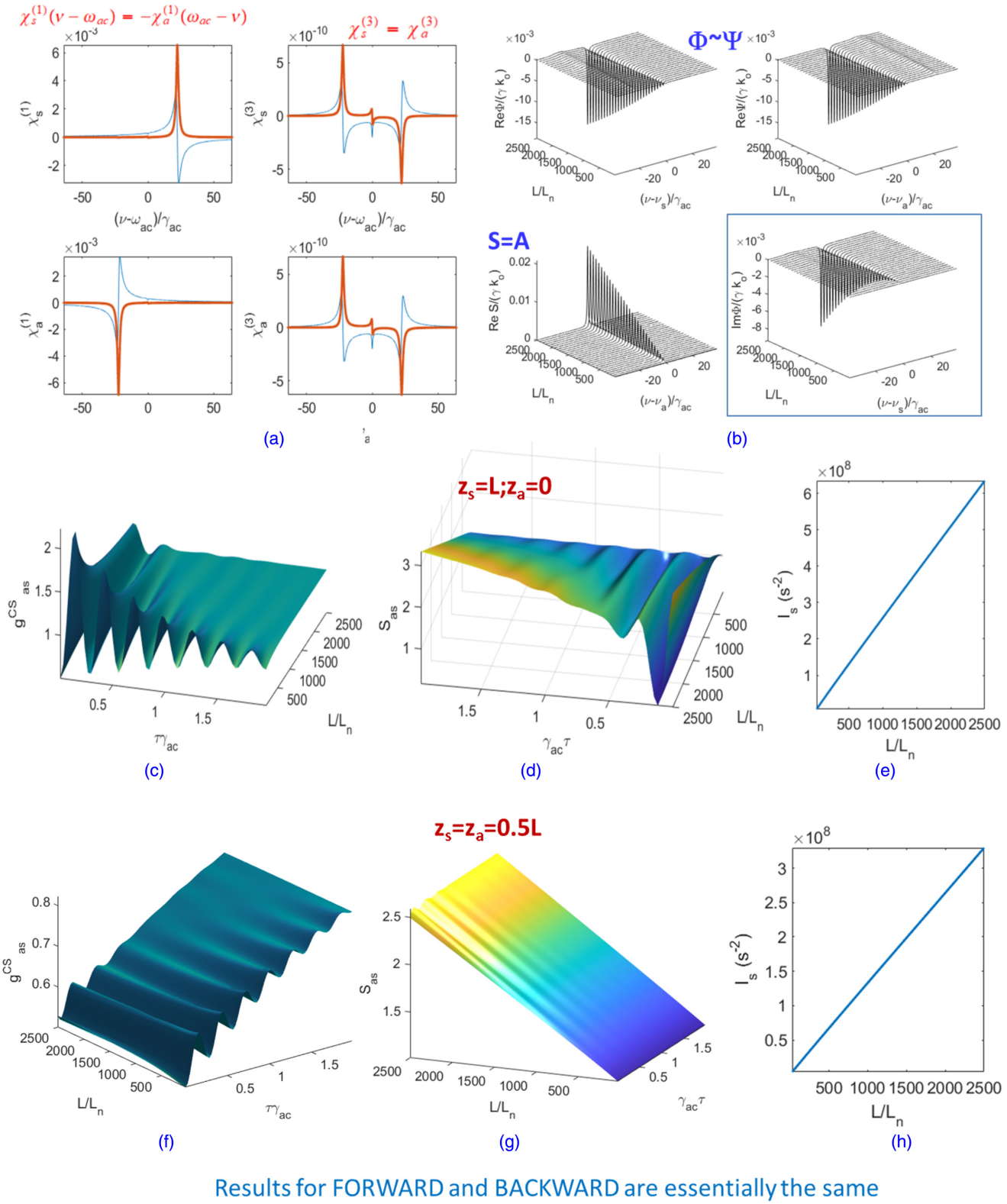

FIG. 4. Effects of propagation length for Raman off-resonant doublet (ROD) scheme: (a) Spectra of linear ($n = 1$) and third-order ($n = 3$) susceptibilities $\chi_f^{(n)}$, (b) correlation spectra $\Phi(\nu)$, $\Psi(\nu)$, $\Sigma(\nu)$, $\Lambda(\nu)$, (c) Cauchy Schwarz correlation of anti-Stokes to Stokes $g_{as}^{CS}(\tau)$, (d) two-mode squeezing S_q and (e) intensities $I_f(z_f)$ for Stokes ($f = s$) at $z_s = L$ and anti-Stokes ($f = s$) at $z_a = 0$ vs propagation length L. Similar to panels (c)–(e) but at $z_a = z_s = 0.5L$ we plot (f) $g_{as}^{CS}(\tau)$, (g) S_q, (h) $I_f(z_f)$ vs propagation length L to show the effect of spatial correlations.

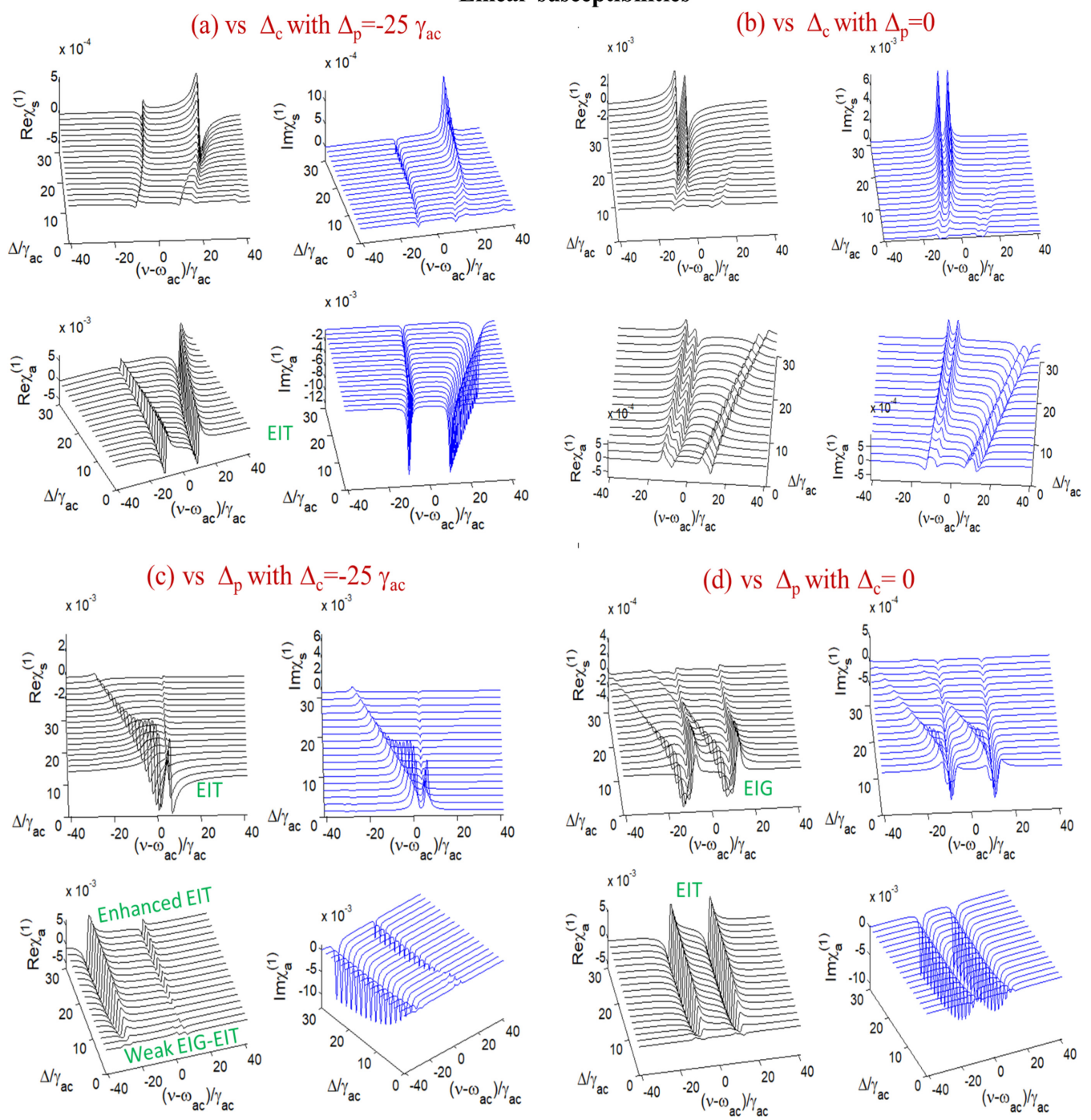

FIG. 5. Linear susceptibilities $\chi_{s,a}^{(1)}$ versus $\Delta_{p(c)}$ with (a), (c) $\Delta_{c(p)} = -25\gamma_{ac}$ and (b), (d) $\Delta_{c(p)} = 0$ for different pump and control Rabi frequencies $\Omega_p = 2.5\gamma_{ac}$, $\Omega_c = 10\gamma_{ac}$.

The off-resonant Stokes Raman enhances the asymmetrical peaks in $\chi_a^{(1)}$ (due to strong off-resonant anti-Stokes transition). In Fig. 5(d) we have gain peaks in $\chi_s^{(1)}$ that are diminishing and transforming into absorption peaks as Δ_p increases.

The spectra of $\chi_s^{(3)}$ and $\chi_a^{(3)}$ are identical for any $|\Delta_{p(c)}|$ if one of the detunings is fixed at $\Delta_{c(p)} = -25\gamma_{ac}$ [Figs. 6(a) and 6(c)], but they are identical only for large $|\Delta_{p(c)}|$ if one of the lasers is resonant $\Delta_{c(p)} = 0$ [Figs. 6(b) and 6(d)]. When Δ_p and Δ_c are close to $0\gamma_{ac}$ the spectra are antisymmetric $\chi_s^{(1,3)} \approx -\chi_a^{(1,3)}$ [Figs. 5(b), 5(d) and 6(b), 6(d)]. These features are the same even if the pump and control Rabi frequencies are the same.

2. *Correlations and squeezing*

While the reverse correlation g_{sa}^{CS} remains essentially classical, below unity [Fig. 7(a)], the correlation g_{as}^{CS} is still nonclassical but the (side lobes) oscillations are washed out

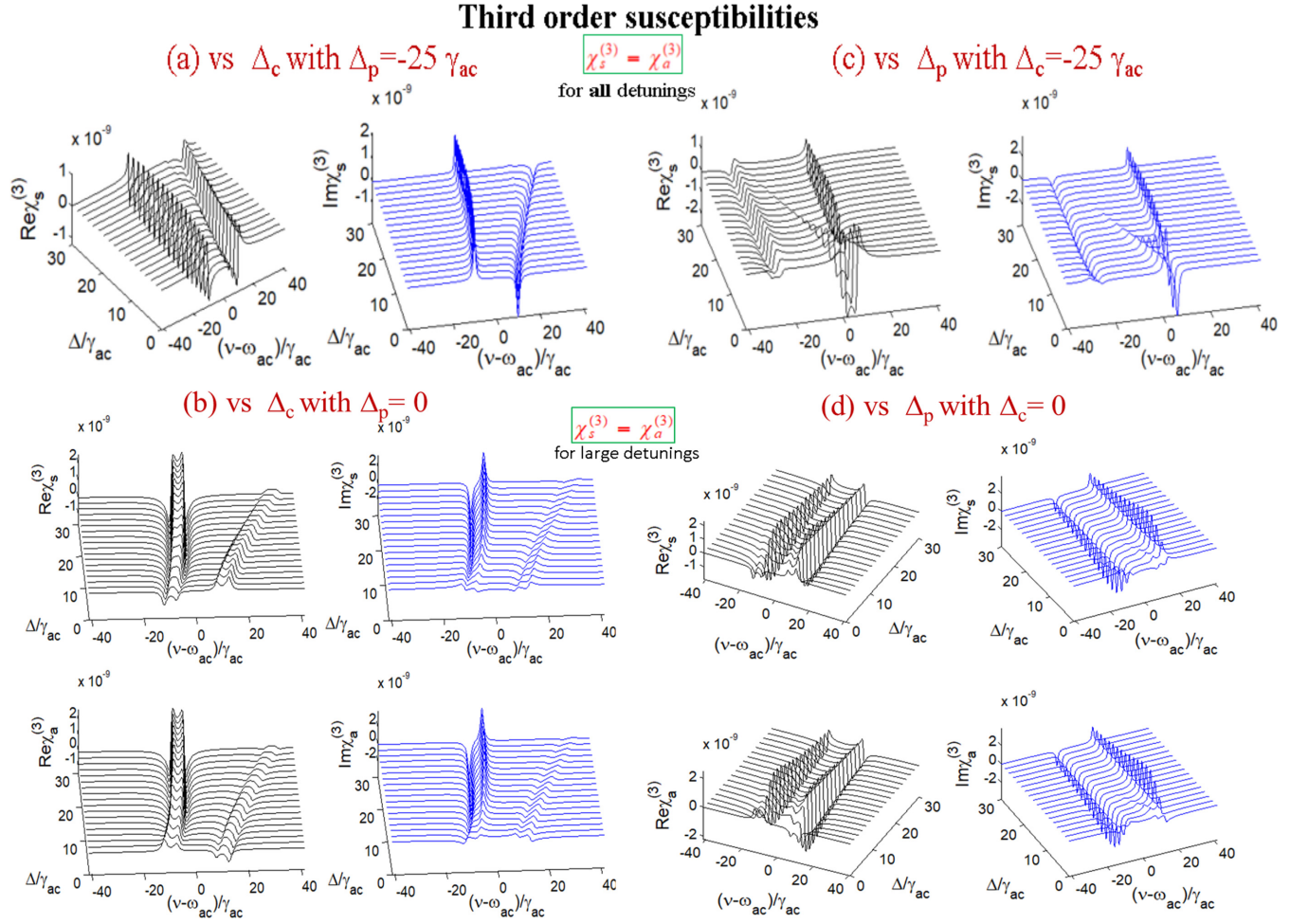

FIG. 6. Third-order susceptibilities $\chi^{(3)}_{s,a}$ versus $\Delta_{p(c)}$ with (a), (c) $\Delta_{c(p)} = -25\gamma_{ac}$ and (b), (d) $\Delta_{c(p)} = 0$ for different pump and control Rabi frequencies $\Omega_p = 2.5\gamma_{ac}$, $\Omega_c = 10\gamma_{ac}$.

[Fig. 7(b)] after a finite propagation length. These correlations and the two mode squeezing S_{as} [Fig. 7(c)] are not much affected by Δ_c. This is consistent with the corresponding correlation spectra, $\Phi(\nu)$, $\Psi(\nu)$, $\Sigma(\nu)$, $\Lambda(\nu)$ that vary more significantly with detunings Δ_p than Δ_c(not shown). Surprisingly, the intensities $I_f(\tau = 0)$ increase [Fig. 7(d)] as $|\Delta_c|$ increases. This can be explained as matching of the value of detuning with $|\Delta_p| = 25\gamma_{ac}$. However, if we increase $|\Delta_p|$ instead, the oscillations in g^{CS}_{sa} and g^{CS}_{as} for small $|\Delta_p|$ would disappear [Fig. 7(e)] and the nonclassicality in g^{CS}_{as} continues to increase (typical Raman-EIT characteristic) [Fig. 7(f)] although the photon numbers $I_f(\tau = 0)$ for the Stokes and anti-Stokes drop, as expected.

Two mode squeezing S_{as} is classical for $S_{as}(0) > 1$ and shows nonclassical squeezing mainly at time delay $\tau_p < 1/2.5\gamma_{ac}$ when $|\Delta_p| \gtrsim 2\gamma_{ac}$ [Fig. 7(g)]. Here, the intensities $I_f(\tau = 0)$ are still large [Fig. 7(h)] as the detuning is close to the matching value of $|\Delta_c| = 0$, but drop as $|\Delta_p|$ increases. The lack of nonclassical squeezing here is because the length here is $k_oL = 5 \times 10^3$, much greater than the small resonant length ($k_oL_r \approx 10^2$) for the Raman EIT regime (large Δ_p, small Ω_p), according to Fig. 10.

In Fig. 8, we use RRD parameters $\Omega_p = \Omega_c = 5\gamma_{ac}$ with resonant Δ_p, $\Delta_c = 0$ by default. Specifically, first, we vary $|\Delta_p|$. The correlations g^{CS}_{sa} [Fig. 8(a)(i)] and g^{CS}_{as} [Fig. 8(b)(i)] are small, they are equal due to symmetry only when $\Delta_p = 0$. The normalized correlations $g^{(2)}_{sa}$, $g^{(2)}_{as}$ [Figs. 8(a)(ii) and 8(b)(ii)] only show a quantitative difference from the Cauchy-Schwarz correlations. We have large nonclassical S_{as} [Fig. 8(c)], but only for backward case, at around $\Delta_p = \Omega_p + \Omega_c = 10\gamma_{ac}$ ($\Delta_c = 0$) we have the double-resonance dips (down to negative values) with the corresponding peak output power of anti-Stokes (I_a) at 50% of the Stokes (I_s) [Fig. 8(d)]. Similar single resonance occurs at $\Delta_p = 13.4\gamma_{ac}$ and the peaks agree exactly with Fig. 10(b)(iii). The "zoom-in panels" (with red borders) reveal more details at $\Delta_p \sim 10\gamma_{ac}$ and $\sim 13.4\gamma_{ac}$, each of the narrow peaks has a hole-burning effect. At these detunings, we have interesting effects, i.e., the ridges in g^{CS}_{sa}, g^{CS}_{as} show persistent photon correlations for any time delay τ and the oscillations across τ are suppressed. The separation between the resonant peaks in Δ_p increases from $3.3\gamma_{ac}$ to $12.75\gamma_{ac}$ as we reduce the Rabi frequency from $5\gamma_{ac}$ to $4\gamma_{ac}$.

However, if we vary Δ_c instead of Δ_p, we find that the dips in S_{as} become large positive peaks while the correlations and intensities g^{CS}_{sa}, g^{CS}_{as}, I_a, I_s remain identical, with the Stokes and anti-Stokes indices interchanged.

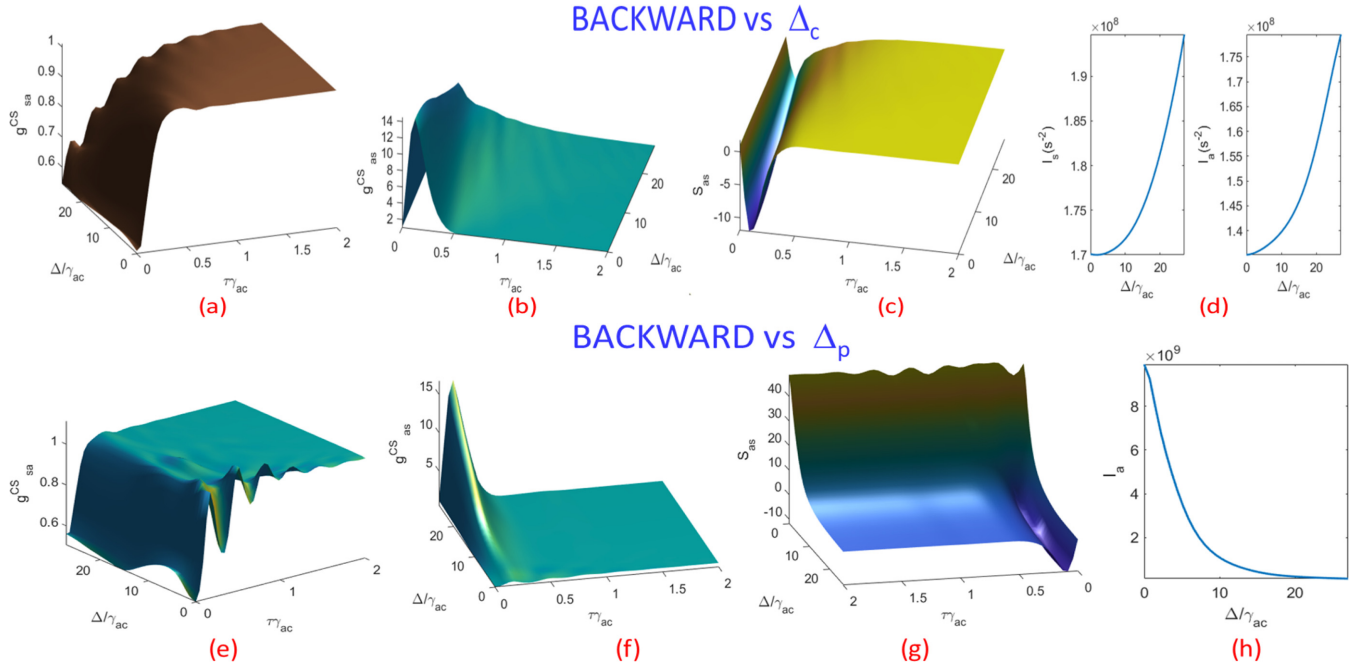

FIG. 7. Effects of laser detuning for asymmetric Raman scheme (different Rabi frequencies, default parameters follow Raman-EIT $\Delta_p = -25\gamma_{ac}$, $\Delta_c = 0$, $\Omega_p = 2.5\gamma_{ac}$, $\Omega_c = 10\gamma_{ac}$) for backward geometry with $L/L_n = 5 \times 10^3$. We only show backward case since results for the forward case are essentially the same. Effects of control laser detuning Δ_c on: (a) Cauchy Schwarz correlation of Stokes to anti-Stokes $g_{sa}^{CS}(\tau)$, (b) anti-Stokes to Stokes $g_{as}^{CS}(\tau)$, (c) two-mode squeezing S_{as}, and (d) intensities $I_f(z_f)$ for Stokes ($f = s$) and anti-Stokes ($f = a$). Similarly we plot the effects of pump-laser detuning Δ_p for backward geometry in panels (e)–(h).

When dips become peaks in S_{as} (which is like a noise figure), the noise above the shot noise limit can be another state which is nonsqueezed, just like the antibunching (dip) can become a bunching (peak) in $g_{as}^{(2)}$. While both $g_{as}^{(2)}$ and S_{as} represent fourth-order correlations, their normalization and their physics are different. The statistics of S_{as} can change dramatically while $g_{as}^{(2)}$ remains the same with the change of the detuning from Δ_p to Δ_c. This is because S_{as} is very sensitive to this resonance structure than $g_{as}^{(2)}$.

For the forward case, those resonances do not appear and we have squeezing (very small) only when Δ_p is close to zero. The plots for S_{as} vs Δ_p are generally different from S_{as} vs Δ_c but they are only identical around zero detunings. For forward case, g_{as}^{CS} shows increasing nonclassicality [Figs. 8(e) and 8(f)] but S_{as} becomes more classical [Fig. 8(g)] and the intensities drop [Fig. 8(h)] as the detuning $|\Delta_p|$ goes to a larger value (or $|\Delta_c|$ goes to zero). This behavior is essentially towards the REIT scheme.

Our analysis reveal the symmetric properties: g_{as}^{CS}, g_{sa}^{CS}, $I_s(\tau = 0)$, $I_a(\tau = 0)$, $\Phi(\nu)$, $\Psi(\nu)$, $\Sigma(\nu)$, $\Lambda(\nu)$ versus Δ_p for forward (backward) geometry are identical to g_{sa}^{CS}, g_{as}^{CS}, $I_a(\tau = 0)$, $I_s(\tau = 0)$, $\Psi(\nu)$, $\Phi(\nu)$, $\Lambda(\nu)$, $\Sigma(\nu)$ versus Δ_c for forward (backward) geometry, respectively.

For ROD parameters $\Omega_p = \Omega_c = 5\gamma_{ac}$ with large detuning $\Delta_p = -20\gamma_{ac}$ and varying $|\Delta_c|$, or $\Delta_c = -20\gamma_{ac}$ varying $|\Delta_p|$ (Fig. 9), the spectra of $\chi_s^{(3)}$ and $\chi_a^{(3)}$ are identical as we vary both Δ_p and Δ_c. However, $\chi_s^{(1)} \approx -\chi_a^{(1)}$ when Δ_p and Δ_c are close to each other (i.e., around $-20\gamma_{ac}$) since ROD is symmetric for Stokes and anti-Stokes. The above observations are similar to the RRD case.

The g_{sa}^{CS} [Figs. 9(a) and 9(e)], g_{as}^{CS} [Figs. 9(b) and 9(f)] and S_{as} [Figs. 9(c) and 9(g)] are different for forward and backward cases. They show classicality for all values of detuning $|\Delta_p|$ and time delay τ. However, g_{as}^{CS} and S_{as} show some nonclassicality as the detuning $|\Delta_c|$ goes to zero, which is essentially towards the REIT characteristics. The time delay of nonclassicality for g_{as}^{CS} (large peak) and $S_{as} < 1$ always coincide. Similar to RRD, g_{as}^{CS}, g_{sa}^{CS}, $I_s(\tau = 0)$, $I_a(\tau = 0)$, $\Phi(\nu)$, $\Psi(\nu)$, $\Sigma(\nu)$, $\Lambda(\nu)$ versus Δ_p for forward (backward) geometry are identical to g_{sa}^{CS}, g_{as}^{CS}, $I_a(\tau = 0)$, $I_s(\tau = 0)$, $\Psi(\nu)$, $\Phi(\nu)$, $\Lambda(\nu)$, $\Sigma(\nu)$ versus Δ_c for forward (backward) geometry, respectively. This is due to the symmetry of the ROD scheme. However, the squeezing S_{as} vs Δ_p, Δ_c, forward [Figs. 9(e)–9(h)] and backward are all different. While both Stokes and anti-Stokes intensities drop with Δ_c [Fig. 9(d)] in the backward case, the anti-Stokes intensity rises with Δ_c after reaching a minimum value at $\Delta_c = 7.5\gamma_{ac}$ [Fig. 9(h)].

C. Resonances vs laser parameters

For a set of laser parameters there exists a resonant length L_r that gives large Stokes and anti-Stokes photons and nonclassical intensity squeezing. Based on Eq. (107) we can now know how the resonant length changes with detuning $\Delta_{p,c}$ and Rabi frequency $\Omega_{p,c}$. Figure 10(a) shows that, in general, for large Ω_p or Ω_c and small Δ_p ($\Delta_c = 0$) we need larger L_r but the situation is different otherwise ($\Delta_p = \Delta_c$). Very small L_r is needed for small $\Omega_p \simeq 2\gamma_{ac}$ with certain discrete detunings Δ_p only if the control laser is resonant($\Delta_c = 0$).

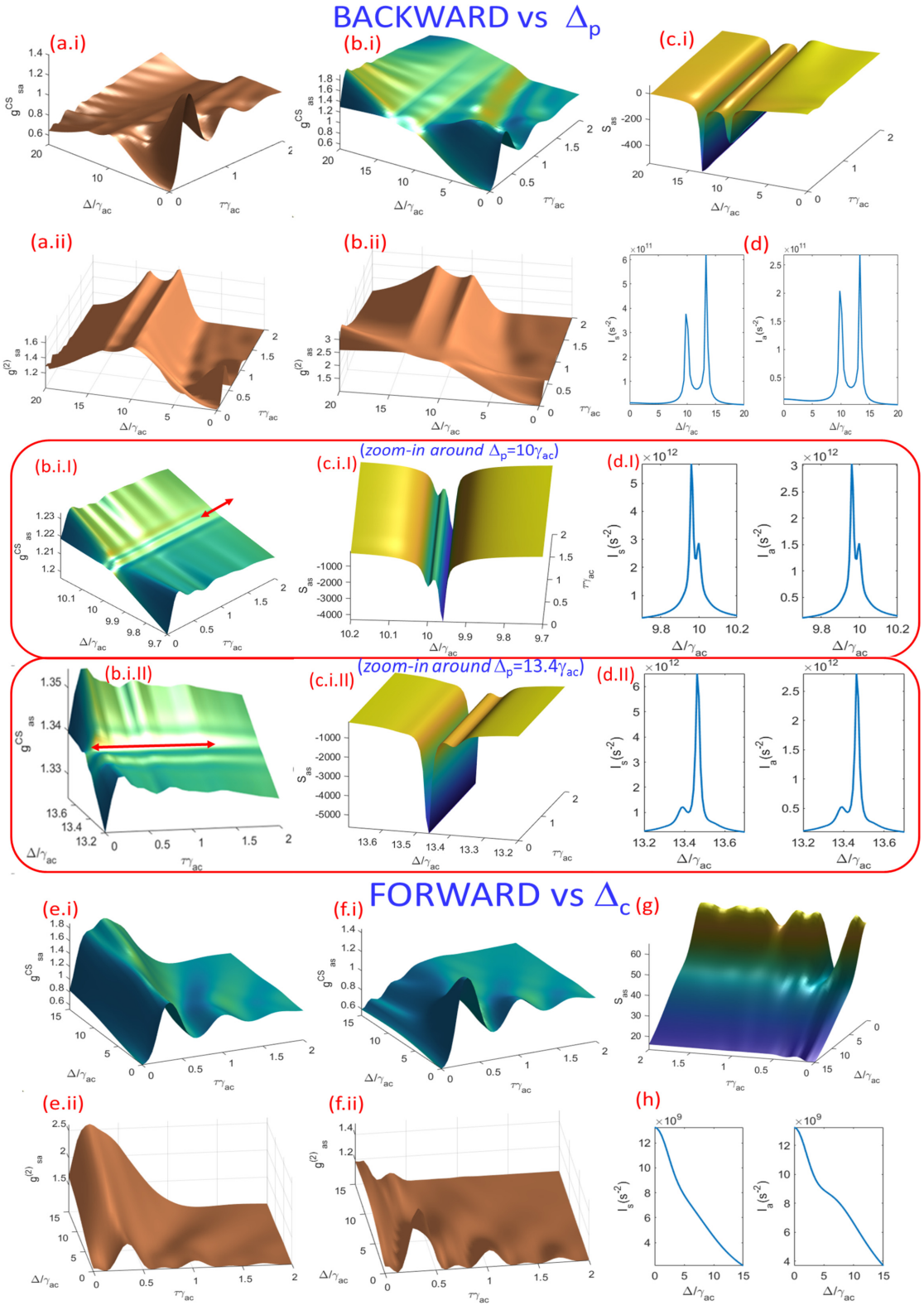

FIG. 8. Effects of varying pump-laser detuning Δ_p with symmetric default parameters of Raman resonant doublet (RRD) scheme $\Delta_p = \Delta_c = 0$, $\Omega_p = \Omega_c = 5\gamma_{ac}$. For backward geometry: (a) Cauchy Schwarz and normalized correlations of Stokes to anti-Stokes $g^{CS}_{sa}(\tau)$, $g^{(2)}_{sa}(\tau)$, (b) anti-Stokes to Stokes $g^{CS}_{as}(\tau)$, $g^{(2)}_{as}(\tau)$, (c) two-mode squeezing S_{as}, and (d) intensities $I_f(z_f)$ for Stokes ($f = s$) and anti-Stokes ($f = a$) for $L/L_n = 5 \times 10^3$. The plots within red borders (b.i.I), (c.i.I), (d.i.I), (b.i.II), (c.i.II), (d.i.II) are zoom-in around the resonant peaks. Similar plots vs Δ_p for forward geometry in panels (e)–(h). The results are the same as varying Δ_c and setting $\Delta_p = 0$ due to symmetry of the RRD scheme.

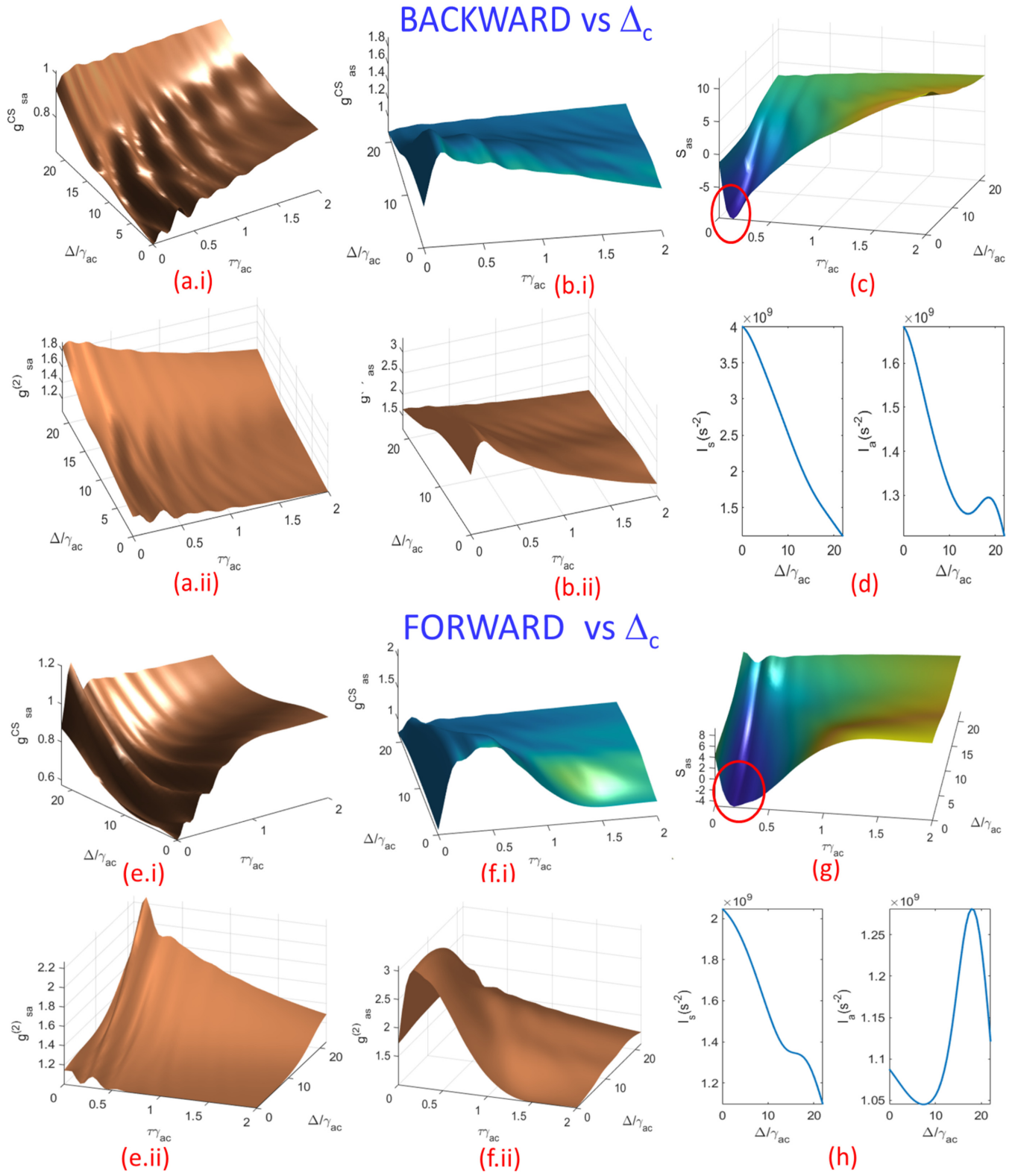

FIG. 9. Effects of varying laser detuning Δ_c for symmetric default parameters of Raman off-resonant double (ROD) scheme $\Delta_p = \Delta_c = -20\gamma_{ac}$, $\Omega_p = \Omega_c = 5\gamma_{ac}$. For backward geometry: (a) Cauchy Schwarz and normalized correlations of Stokes to anti-Stokes $g^{CS}_{sa}(\tau)$, $g^{(2)}_{sa}(\tau)$, (b) anti-Stokes to Stokes $g^{CS}_{as}(\tau)$, $g^{(2)}_{as}(\tau)$, (c) two-mode squeezing S_{as}, and (d) intensities $I_f(z_f)$ for Stokes ($f = s$) and anti-Stokes ($f = a$) with $L/L_n = 5 \times 10^3$. Similarly, for forward geometry in (e)–(h). The results are the same as varying Δ_p (with $\Delta_c = -20\gamma_{ac}$) instead, due to symmetry of ROD scheme.

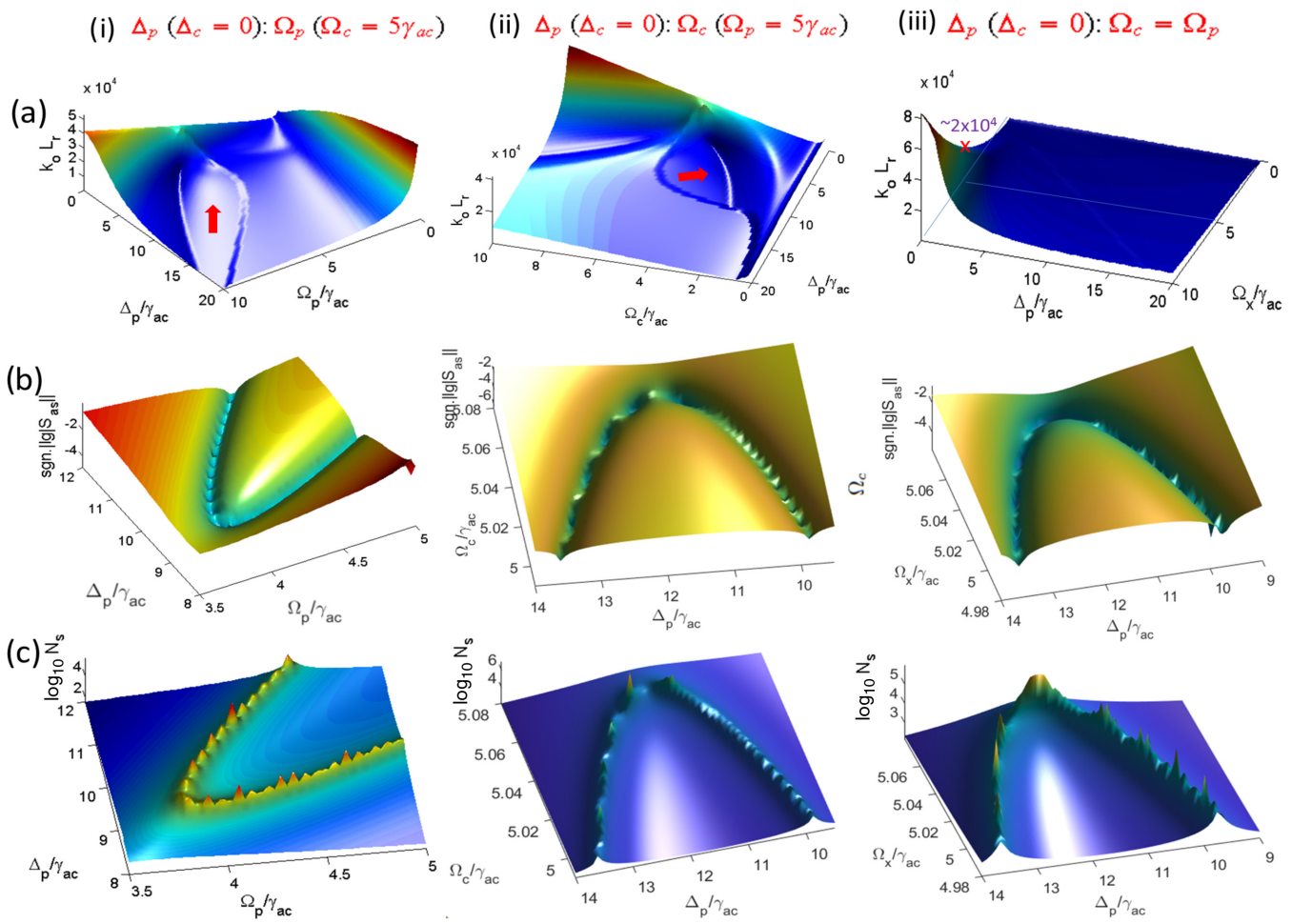

FIG. 10. Resonant effects of quantities versus pump detunings Δ_p ($\Delta_c = 0$) and Rabi frequency: (i) Ω_p ($\Omega_c = 5\gamma_{ac}$), (ii) Ω_c ($\Omega_p = 5\gamma_{ac}$), and (iii) $\Omega_c = \Omega_p$, (a) Resonant propagation length L_r according to Eq. (107) for zeroth order, $m = 0$ ($k_o = \omega_{ac}/c$) [red arrows plateau without resonance, red cross in (iii) corresponds to the first peak in Fig. 3(e)], (b) log of relative squeezing, $\log_{10} S_{as}$ showing nonclassical regions (negative values) corresponding to the resonant peaks in panel, (c) log of Stokes photon number, $\log_{10} N_s$.

We have also plotted [in Fig. 10(b)] sgn ln $|S_{as}|$ (where sgn is the sign of $S_{as} - 1$ that determines nonclassicality) and $I_{s,a}(L, \tau = 0)$ vs Δ_p ($\Delta_c = 0$) and vs (i) Ω_p ($\Omega_c = 5\gamma_{ac}$), (ii) Ω_c ($\Omega_p = 5\gamma_{ac}$), and (iii) $\Omega_c = \Omega_p$. We have nonclassical squeezing ($S_{as} < 1$) only when Δ_p varies ($\Delta_c = 0$). Parabolic contour indicates that squeezing happens at two values Δ_p only when $\Omega_c \lesssim 5\gamma_{ac}$, i.e., for both $\Omega_p = 5\gamma_{ac}$ and $\Omega_c = \Omega_p$. The red line intersects the nonclassical (dip) region exactly at $\Delta_p = 10\gamma_{ac}$ and $13.4\gamma_{ac}$ as depicted in Fig. 8(d).

We have computed the possible nine scenarios below.

(a)

(i) Δ_p ($\Delta_c = 0$): Ω_p ($\Omega_c = 5\gamma_{ac}$), Raman EIT for large Δ_p, small Ω_p;

(ii) Δ_p ($\Delta_c = 0$): Ω_c ($\Omega_p = 5\gamma_{ac}$), Raman EIT for large Δ_p, Ω_c;

(iii) Δ_p ($\Delta_c = 0$): $\Omega_c = \Omega_p$, RRD for $\Delta_c = 0$;

(b)

(i) Δ_c ($\Delta_p = 0$): Ω_p ($\Omega_c = 5\gamma_{ac}$), reverse Raman EIT for large Δ_c, large Ω_p;

(ii) Δ_c ($\Delta_p = 0$): Ω_c ($\Omega_p = 5\gamma_{ac}$), opp a i) reverse Raman EIT for large Δ_c, small Ω_c;

(iii) Δ_c ($\Delta_p = 0$): $\Omega_c = \Omega_p$, RRD for $\Delta_c = 0$;

(c)

(i) $\Delta_c = \Delta_p$: Ω_p ($\Omega_c = 5\gamma_{ac}$), asymmetric Raman;

(ii) $\Delta_c = \Delta_p$: Ω_c ($\Omega_p = 5\gamma_{ac}$), asymmetric Raman;

(iii) $\Delta_c = \Delta_p$: $\Omega_c = \Omega_p$, ROD for large $\Delta_c = \Delta_p$ and RRD for $\Delta_c = \Delta_p = 0$.

Only cases in (a) show nonclassical squeezing. We verify that (b)(i), (b)(ii), and (b)(iii) are the same as (a)(ii), (a)(i), and (a)(iii), respectively, due to symmetry except their S_{as} are positive (classical).

VII. DISCUSSIONS

A. Main findings

The results here go beyond the nontrivial general analytical solutions of the quantum fields at any point inside the coherent medium with noise operators self-consistently and properly included. Analytical solutions of all four possible cases of co- and counterpropagating geometries are presented in an elegant and holistic manner, not available in previous publications. Our full quantum formalism with analytical results lead to three-dimensional (3D) plots of various limiting Raman schemes that provide more comprehensive picture and insightful illustration of the effects of co- and counterpropagating geometries and laser parameters on the quantities of

interest, especially the nonclassical properties. Results for Cases 2A and 2B are qualitatively the same for backward geometry. We learn that quantum correlations between photons at any two points inside the coherent medium are smaller than between the ends of the medium, as shown in Figs. 2(f) and 4(f).

Thorough critical analysis and observations lead to discovery of many new features. Most striking are the resonant length condition and laser parameters (detuning) that give large quantum fields, nonclassical correlations and relative intensity squeezing for backward geometry, as shown in Figs. 3, 8, 10. The backward geometry has significant effects on the nonclassicality of two-photon correlations and the intensity squeezing properties particularly when the lasers are resonant. One important finding is that persistent correlation over very long delay τ exists only under certain conditions associated with resonance.

Detuning either the pump or the control laser determines whether we have classical or nonclassical intensity difference squeezing S_{as} in the case of backward propagation, since it determines whether anti-Stokes is correlated to Stokes or otherwise. The results of intensity difference squeezing are useful and relevant to future works involving noise-free detection of Raman photons.

When one of the lasers makes resonant Raman transition with certain propagation lengths the backward-propagating photons show interesting new resonant features as very high intensity $I_{s,a}$ and large nonclassical squeezing S_{as} (provided $\Omega_p, \Omega_c \lesssim 5\gamma_{ac}$) at two detunings whose separation decreases with Ω_p, as shown in Fig. 10. This analysis is operationally useful, providing the optimal laser parameters and optimal propagation length to generate nonclassical squeezing.

The complex susceptibilities (Fig. 5) of double Raman scheme show the rich physics in the aspects of symmetries and laser control parameters. Clearer symmetrical properties can be seen in the spectra of the susceptibilities (Figs. 2–4), i.e., $\chi_s^{(3)} = \chi_a^{(3)}$ for REIT and ROD, $\chi_s^{(1,3)} = -\chi_a^{(1,3)}$ antisymmetric for RRD.

B. Quantum memory

Although our theory and solutions are not valid for pulses typically used in quantum memory, the cw pump and control lasers scenario (that serves as a clean reference case) makes extensive analytical solutions possible. The analytical solutions of the field operators obtained here provide insights on the structure of the solutions for the controllable quantum fields and the simulated results have helped in understanding the effects of counterpropagating geometry on the photon correlations and the spectral content of the quantum fields. This serves as an important reference and foundation for further understanding of nonclassical properties of correlated photons in transient studies of quantum fields when extending to pulsed lasers and pulsed input in actual quantum memory.

Our present Heisenberg-Langevin formulation is fully quantum that includes quantum noise in a correct and self-consistent manner that would be the appropriate theory to describe the quantum noise performance of the time-dependent quantum fields in quantum memory. The present formulation can also compute other performance parameters of quantum memory such as efficiency and fidelity by combining numerical approach with analytical solutions under certain approximations. The theory can be adopted to study enhanced counterpropagating fields inside a cavity [33] and atomic motion averaging technique [34] that were able to circumvent atomic motion problem at room temperature for achieving scalable and broadband Raman quantum memory with higher efficiency.

C. Phase matching in higher dimensions

A spatial propagation in higher dimensions [two dimensions (2D) or 3D] is needed to fully account for phase matching of the FWM wave vectors, i.e., to include the transverse directions (x and y). This is beyond the present scope where we consider only 1D propagation, i.e., all wave vectors are along z direction. The phase-matching condition arises because of the different refractive indexes or linear dispersions for the nondegenerate FWM where the two lasers and the two quantum fields have different carrier frequencies. While perfect phase matching condition is needed to obtain maximum FWM signal, this is not always critically necessary while it is possible to adjust the transitions such that the refractive indexes do not change much across the frequencies of all the four fields.

For noncollinear lasers, such as lasers crossed at a small angle [35], the transverse components ($\epsilon = x, y$) of the wave vectors are finite and give rise to transverse phase matching condition $(\Delta\mathbf{k}_{1A})_\epsilon = (\mathbf{k}_p + \mathbf{k}_c - \mathbf{k}_s - \mathbf{k}_a)_\epsilon$, in addition to the (axial) phase matching of the z-component wave vectors: $(\Delta k_{1A}) = (k_p + k_c - k_s - k_a) = 0$, $(\Delta k_{1B}) = (-k_p - k_c + k_s + k_a) = 0$, $(\Delta k_{2A}) = (k_p - k_c - k_s + k_a) = 0$, $(\Delta k_{2B}) = (k_p - k_c + k_s - k_a) = 0$ as given in earlier section for our 1D propagation.

The small angle between the lasers is used in seeded experiment for convenience, where phase matching can be controlled by the input fields. It does not change our results of propagation length dependence too much as the z-component wave vectors are only slightly less than the wave vectors of perfectly collinear case while the radial and transverse component wave vectors are much smaller. The interaction length can be adjusted by balancing the laser beam width and the small angle between the two lasers. Alternatively one can adopt the fully collinear geometry and use prisms to separate different wavelengths. For nonseeded (spontaneously generated FWM) this is not a problem as we can place the detectors anywhere.

D. Doppler effect

The atomic center of mass motion effect is related to the "velocity-selective coherent population trapping" effect and requires the inclusion of Doppler and recoil shifts. Perfect phase matching is achieved only at certain velocity class of atoms. The Doppler effect can be included by adding the Doppler frequency shift $\mathbf{k}_j \cdot \mathbf{u} = k_j u$ (for the jth field in 1D case) to the photon frequencies $v_j - \mathbf{k}_j \cdot \mathbf{u}$ in the detunings $\Delta_c = v_c - \omega_{ab}$, $\delta_a = v_a - \omega_{ac}$, $\Delta_p = v_p - \omega_{dc}$, $\delta_s = v_s - \omega_{db}$ and the quantized electric fields is the sum over all velocities $\mathbf{u}$ in the Maxwell-Boltzmann distribution. For 1D,

the polarization has to be averaged over all velocities with a normalized weight function $P(u) = \sqrt{m/(\pi k_B T)} e^{-mu^2/k_B T}$ that depends on temperature T. For example,

$$\left(\frac{1}{c}\frac{\partial}{\partial t} + \frac{\partial}{\partial z}\right)\hat{S}(z,t) = ig_s\kappa_s \int_{-\infty}^{\infty} P(u)\hat{p}_{bd}(z,t;u)du. \quad (133)$$

Due to the integral, the numerous analytical expressions obtained above would not be possible unless we regard $S(z,t)$ as $S(u,z,t)$ the field associated with a particular value of u, where the total field is $\hat{S}(z,t) = \int_{-\infty}^{\infty} P(u)\hat{S}(u,z,t)du$.

The spectra of the parameters in the parametric equation are expected to be smeared out by the Doppler effect depending on the width of $P(u)$ and this would cause the efficiency to drop, physically the resonant peaks are randomized or dispersed by Doppler broadening of the atomic gas.

Zhou *et al.* [35] obtained higher efficiency FWM by using counterpropagating control lasers. The scheme is different from our double Raman. Their phase-matching condition $k_p - 2k_c + k_r = 0$ ($\mathbf{k}_r = -zk_r$ due to reflection) can be connected to our counterpropagating double Raman [Case 2A $(\Delta k_{2A}) = k_p - k_c - k_s + k_a$] where their control lasers can take the roles of both our control laser and Stokes photon that are always antiparallel ($k_c = k_s$), which is known to be more efficient than the copropagating case. Further elaboration requires proper formulation and careful analysis (to be reported in subsequent submission) of the Doppler (and recoil) shift in phase-matching effects on Raman and FWM efficiency.

E. Hyperfine sublevels

In actual experiments the presence of relevant hyperfine sublevels depends on the laser polarizations, may extend the pumping cycle beyond few-level (three or four levels) scheme in optical pumping, EIT and also influence the efficiency of Raman parametric oscillations. The polarization of lasers is important when taking account of the multiplets. Right-circularly (left-circularly) polarized laser would couple the diagonal transitions between m_F at lower level to $m_F \pm 1$ ($\Delta m_F = \pm 1$) at higher level. Similarly, linearly polarized laser connects the vertical transitions with $\Delta m_F = 0$. So there are several simultaneous Raman transitions during the interactions. Populations can move outside the four levels by spontaneous emissions into other multiplets (via $\Delta m_F = 0$ transitions) with some branching ratios depending on the dipole transition matrix element and the laser interaction cycle is not strictly closed. Hence, the efficiency of Raman process would be lower. In degenerate hyperfine magnetic sublevels of the states [36] (e.g., $F = 1$ and $F = 2$ in ^{87}Rb) several pairs of transitions that are (vertically) diagonally coupled simultaneously by (linearly) circular polarized laser fields can have effect on spatial localization through interaction time. However, the effects of multi-Zeeman-sublevel atoms on EIT and coherent population trapping (CPT) [37] can be minimized by using strong pumping scheme to maintain close to ideal three states lambda system. In our case of quasisteady state only the few sublevels need to be considered that are coupled in an (almost) closed cycle by the circularly polarized lasers in lambda configuration.

F. Proposed experiments

For standard forward propagating geometries we propose an experimental setup similar to those used in Refs. [38]. Furthermore, the theoretical results in Ref. [27] which are based on a simplified nonpropagating model, while using the same limiting conditions as in our present work as shown in Figs. 3(d) and 3(e). These results are confirmed experimentally in Ref. [23] in the hot Rb vapor cell irradiated by a 100 mW Ti:sapphire pump power and weak 20 μW probe beam mixed in a copropagating geometry at 7 mrad angle inside a 12 mm long vapor cell containing ^{85}Rb gas at 113 °C temperature. We therefore propose to use similar setup for the $D1$ line in a counterpropagating geometry with small angle of the mrad range for the phase-matching control.

Several advantageous properties of counterpropagating geometry have been mentioned in the introduction, including intrinsic high efficiency due to internal auto-feedback [39]. However, for thermal atoms, counterpropagating Raman fields geometry may yield a lower efficiency (depending on atomic density) since only the fraction of atoms with zero axial velocity component (along laser direction) with nearly no Doppler effect are resonantly coupled. In other words, counterpropagating Raman fields are able to selectively excite only atoms with zero axial velocity into resonances.

One practical advantage of the counterpropagating geometry is the greater spatial overlapping of the counterpropagating fields. The counterpropagating collinear laser beams (need not cross at an angle) can completely overlapped and discernible by using polarization control. Thus, the situation of backward geometry is closer to our theory and the results for forward geometry are shown for comparison.

G. Laser phase

We emphasize that the pump and control lasers need to be phase locked, especially when we have Raman transition involving the lasers and with the quantum fields. Generally our scheme would have two-photon effective Rabi frequency $\Omega_{\text{eff}} = \Omega_1\Omega_2^*/\Delta$ that may be averaged out to zero if the phases φ_j of the two fields or lasers are random ($j = 1, 2$). Here, Ω_j is the complex single-photon Rabi frequency that includes the phase $e^{i\varphi_j}$ and Δ finite single-photon detuning. There are terms like $g_f^{(*)}\Omega_p\Omega_c$, $g_f^{(*)}\Omega_p$, or $g_f^{(*)}\Omega_c$ in the coefficients $\mathcal{K}_f$, $\mathcal{G}_f$ and the $\hat{\mathcal{F}}_f$ noise operators of the parametric equations (38) and (39) that require stable relative phase between the lasers and with the fields. The phase locking is also necessary when phase-sensitive detection is used, such as the case of interferometric (home-heterodyne) detection, especially in the measurement of squeezing effect.

H. Relevance

Our work has high relevance to the existing theoretical and experimental works. The population dynamics in Rb vapor and susceptibility plotted in Figs. 8 and 10 in Ref. [37] and also Ref. [40] resembles our susceptibilities shown in Figs. 3 and 4, while using similar method for calculation of propagation in the context of EIT in Λ scheme based on Rb levels.

In Ref. [35] a Doppler-free propagation is demonstrated experimentally in the counterpropagating geometry enhanced

by the EIT effect in the similar way our result indicate the propagation effects in the squeezing and gain of the four-wave mixing. A noise reduction in the spectra of the noise due to squeezing has been shown in $D1$ and $D2$ lines in Rb vapor [26], where operation has been in the similar parameter regime as shown in our Figs. 3 and 4.

Most experiments are performed in copropagating geometry. The counterpropagating we study here has several important advantages. First, it allows us to control and reduce the inhomogeneous broadening caused by Doppler effect [41] enabling detection using counterpropagating geometries in oxygen lasing. Second, the counterpropagating geometry is highly relevant for stand-off detection and sensing and air lasing, which became an important topic over the last decades in a context of remote sensing applications [42]. Further discussion of these applications and relevant calculations could be done in the upcoming works as it is outside of the scope of the present work.

VIII. CONCLUSIONS

We have studied all possible forward- and backward-propagating geometries of quantum parametric oscillators medium with finite length composed of four-level double Raman system, driven by arbitrary detuning and strength of the pump and control lasers using the full quantum Heisenberg-Langevin framework with noise operators. The coupled parametric oscillator equations yield analytical solutions for the quantum fields that depend on the propagation length, frequency, and strength of the lasers. Systematic and comprehensive analysis show how the nonclassical photon correlations and intensity difference squeezing are affected by the propagation length, the parameters of the lasers and interaction geometry (forward or backward). Systematic analysis of limiting Raman schemes with different detuning and Rabi frequencies provided useful insight on the conditions for enhancing and controlling nonclassicality. We have discussed practical aspects that connect our work well with recent development in low-noise nonclassical light and quantum spectroscopy through the analysis of squeezing. We have laid out a proper full quantum framework that can be extended to pulsed regime, particularly useful for the study of quantum memory with backward geometry. The promising findings of this study, especially the resonant effects and nonclassicality of two-mode relative intensity squeezing are useful for quantum metrology and spectroscopy, especially in the unprecedented levels of high precision, spatial and temporal resolution through new modes of measurements.

ACKNOWLEDGMENTS

This work is supported by Ministry of Higher Education Malaysia (MOHE), under Long-Term Research Grant Scheme, LRGS/1/2020/UM/01/5/1 and Fundamental Research Grant Scheme, FRGS/1/2020/STG07/UM/01/1. R.O. thanks Marlan Scully for kind hospitality at TAMU, Prof. Philip Hemmer and Prof. M. Suhail Zubairy for discussions. K.E.D. is supported by the National Science Foundation of China (Grant No. 11934011), the Zijiang Endowed Young Scholar Fund, the East China Normal University, and the Overseas Expertise Introduction Project for Discipline Innovation (111 Project, Grant No. B12024).

APPENDIX A: HEISENBERG-LANGEVIN EQUATIONS

The Heisenberg equation of motion $\frac{d}{dt}\hat{O} = \frac{1}{i\hbar}[\hat{O}, \hat{H}]$ gives

$$\frac{d}{dt}\hat{\sigma}_{aa} = i(g_a\hat{E}_a e^{ik_a z}\hat{p}_{ac} + \Omega_c e^{ik_c z}\hat{p}_{ab} - g_a^*\hat{E}_a^\dagger e^{-ik_a z}\hat{p}_{ca} - \Omega_c^* e^{-ik_c z}\hat{p}_{ba}) - (\Gamma_{ab} + \Gamma_{ac})\hat{\sigma}_{aa} + \hat{F}_{aa}, \tag{A1a}$$

$$\frac{d}{dt}\hat{\sigma}_{bb} = i(\Omega_c^* e^{-ik_c z}\hat{p}_{ba} + g_s^*\hat{E}_s^\dagger e^{-ik_s z}\hat{p}_{bd} - \Omega_c e^{ik_c z}\hat{p}_{ab} - g_s\hat{E}_s e^{ik_s z}\hat{p}_{db}) + \Gamma_{ab}\hat{\sigma}_{aa} + \Gamma_{db}\hat{\sigma}_{dd} + \hat{F}_{bb}, \tag{A1b}$$

$$\frac{d}{dt}\hat{\sigma}_{cc} = -i(\Omega_p e^{ik_p z}\hat{p}_{dc} + g_a\hat{E}_a e^{ik_a z}\hat{p}_{ac} - \Omega_p^* e^{-ik_p z}\hat{p}_{cd} - g_a^*\hat{E}_a^\dagger e^{-ik_a z}\hat{p}_{ca}) + \Gamma_{ac}\hat{\sigma}_{aa} + \Gamma_{dc}\hat{\sigma}_{dd} + \hat{F}_{cc}, \tag{A1c}$$

$$\frac{d}{dt}\hat{\sigma}_{dd} = i(\Omega_p e^{ik_p z}\hat{p}_{dc} + g_s\hat{E}_s e^{ik_s z}\hat{p}_{db} - \Omega_p^* e^{-ik_p z}\hat{p}_{cd} - g_s^*\hat{E}_s^\dagger e^{-ik_s z}\hat{p}_{bd}) - (\Gamma_{db} + \Gamma_{dc})\hat{\sigma}_{dd} + \hat{F}_{dd}, \tag{A1d}$$

$$\frac{d}{dt}\hat{p}_{ba} = -T_{ab}^*\hat{p}_{ba} + i(g_a\hat{E}_a e^{ik_a z}\hat{p}_{bc} + \Omega_c e^{ik_c z}(\hat{\sigma}_{bb} - \hat{\sigma}_{aa}) - g_s\hat{E}_s e^{ik_s z}\hat{p}_{da}) + e^{iv_c t}\hat{F},_{ab}^{+} \tag{A2a}$$

$$\frac{d}{dt}\hat{p}_{ca} = -T_{ac}^*\hat{p}_{ca} + i((\hat{\sigma}_{cc} - \hat{\sigma}_{aa})g_a\hat{E}_a e^{ik_a z} + \Omega_c e^{ik_c z}\hat{p}_{cb} - \Omega_p e^{ik_p z}e^{-i\Delta vt}\hat{p}_{da}) + e^{iv_a t}\hat{F}_{ac}^{+}, \tag{A2b}$$

$$\frac{d}{dt}\hat{p}_{cb} = -T_{bc}^*\hat{p}_{cb} + i(\Omega_c^* e^{-ik_c z}\hat{p}_{ca} + g_s^*\hat{E}_s^\dagger e^{-ik_s z}e^{-i\Delta vt}\hat{p}_{cd} - g_a\hat{E}_a e^{ik_a z}\hat{p}_{ab} - \Omega_p e^{ik_p z}e^{-i\Delta vt}\hat{p}_{db}) + e^{-iv_{qa}t}\hat{F}_{bc}^{+}, \tag{A2c}$$

$$\frac{d}{dt}\hat{p}_{ad} = -T_{ad}\hat{p}_{ad} + i(\Omega_p e^{ik_p z}\hat{p}_{ac}e^{-i\Delta vt} + g_s\hat{E}_s e^{ik_s z}\hat{p}_{ab} - g_a^*\hat{E}_a^\dagger e^{-ik_a z}e^{-i\Delta vt}\hat{p}_{cd} - \Omega_c^* e^{-ik_c z}\hat{p}_{bd}) + e^{-iv_{qs}t}\hat{F}_{ad}, \tag{A2d}$$

$$\frac{d}{dt}\hat{p}_{bd} = -T_{db}^*\hat{p}_{bd} + i(\Omega_p e^{ik_p z}e^{-i\Delta vt}\hat{p}_{bc} + g_s\hat{E}_s e^{ik_s z}(\hat{\sigma}_{bb} - \hat{\sigma}_{dd}) - \Omega_c e^{ik_c z}\hat{p}_{ad}) + e^{iv_s t}\hat{F}_{db}^{+}, \tag{A2e}$$

$$\frac{d}{dt}\hat{p}_{cd} = -T_{dc}^*\hat{p}_{cd} + i(\Omega_p e^{ik_p z}(\hat{\sigma}_{cc} - \hat{\sigma}_{dd}) + g_s\hat{E}_s e^{ik_s z}e^{i\Delta vt}\hat{p}_{cb} - g_a\hat{E}_a e^{ik_a z}\hat{p}_{ad}) + e^{iv_p t}\hat{F}_{dc}^{+}, \tag{A2f}$$

where $\nu_{\alpha\beta} = \nu_\alpha - \nu_\beta$ with $\alpha, \beta = p, s, c, a$ and the complex decoherences

$$T_{ac} = i\delta_a + \gamma_{ac}, \tag{A3a}$$
$$T_{ad} = i(\Delta_c - \delta_s) + \gamma_{ad}, \tag{A3b}$$
$$T_{bc} = i(\delta_a - \Delta_c) + \gamma_{bc}, \tag{A3c}$$
$$T_{db} = i\delta_s + \gamma_{db}, \tag{A3d}$$
$$T_{ab} = i\Delta_c + \gamma_{ab}, \tag{A3e}$$
$$T_{dc} = i\Delta_p + \gamma_{dc}, \tag{A3f}$$

effective decoherence rates γ_{uv}

$$\gamma_{ac} \doteq \tfrac{1}{2}\{\Gamma_{ac}(2\bar{n}_{ac}+1) + \Gamma_{ab}(\bar{n}_{ab}+1)\} + \gamma_{ac}^{\rm dep}, \tag{A4a}$$
$$\gamma_{ad} = \tfrac{1}{2}\{\Gamma_{db}(\bar{n}_{db}+1) + \Gamma_{dc}(\bar{n}_{dc}+1) + \Gamma_{ab}(\bar{n}_{ab}+1) + \Gamma_{ac}(\bar{n}_{ac}+1)\} + \gamma_{ad}^{\rm dep}, \tag{A4b}$$
$$\gamma_{bc} = \tfrac{1}{2}\{\Gamma_{ab}\bar{n}_{ab} + \Gamma_{db}\bar{n}_{db} + \Gamma_{ac}\bar{n}_{ac} + \Gamma_{dc}\bar{n}_{dc}\} + \gamma_{bc}^{\rm dep}, \tag{A4c}$$
$$\gamma_{db} \doteq \tfrac{1}{2}\{\Gamma_{db}(2\bar{n}_{db}+1) + \Gamma_{dc}(\bar{n}_{dc}+1)\} + \gamma_{db}^{\rm dep}, \tag{A4d}$$

where $\Gamma_{\alpha\beta}$ are the spontaneous emission rates, $\bar{n}_{\alpha\beta} = (e^{\hbar\omega_{\alpha\beta}/k_BT} - 1)^{-1}$ and $\gamma_{\alpha\beta}^{\rm dep}$ are the dephasings due to phonons in condensed phase or atomic collisions in gas. Here, the noise operators $\hat{F}_{uv}$, $u, v = a, b, c, d$ appear self-consistently, whose full expressions are obtained from quantized radiation fields [32].

APPENDIX B: COEFFICIENTS IN FOURIER FREQUENCY

To include two-photon detuning $\Delta\nu = \nu_p + \nu_c - \nu_s - \nu_a$ (assuming $\Delta_c = \delta_a$, $\Delta\nu = \nu_p - \nu_s - \omega_{bc}$)

$$e^{-i\Delta\nu t}\left(\frac{d}{dt} + T_{ac}\right)\hat{p}_{ac} = \left(\frac{d}{dt} + T_{ac} + i\Delta\nu\right)\left(\hat{p}_{ac}e^{-i\Delta\nu t}\right), \tag{B1}$$
$$e^{-i\Delta\nu t}\left(\frac{d}{dt} + T_{bc}\right)\hat{p}_{bc} = \left(\frac{d}{dt} + T_{bc} + i\Delta\nu\right)\left(\hat{p}_{bc}e^{-i\Delta\nu t}\right), \tag{B2}$$

gives $T_{ac}(\nu') = T_{ac} - i(\nu - \Delta\nu)$, $T_{bc}(\nu') = T_{bc} - i(\nu - \Delta\nu)$, where $\nu' = \nu - \Delta\nu$ and we use $\frac{d}{dt}(Ae^{-i\Delta t}) = -i\Delta A e^{-i\Delta t} + e^{-i\Delta t}\frac{d}{dt}A$. The main coefficients in the susceptibilities are

$$\mathcal{W}_s' = \mathcal{N}_2'\tilde{\rho}_{ba} - \mathcal{N}_3'\tilde{\rho}_{cd} - \mathcal{N}_4' w_{bb}^{dd}, \tag{B3a}$$
$$\mathcal{W}_a' = \mathcal{N}_2'\tilde{\rho}_{dc} - \mathcal{N}_3'\tilde{\rho}_{ab} - \mathcal{N}_1' w_{cc}^{aa}, \tag{B3b}$$
$$\mathcal{W}_s = \mathcal{N}_2\tilde{\rho}_{ba} - \mathcal{N}_3\tilde{\rho}_{cd} - \mathcal{N}_4 w_{bb}^{dd}, \tag{B3c}$$
$$\mathcal{W}_a = \mathcal{N}_2\tilde{\rho}_{dc} - \mathcal{N}_3\tilde{\rho}_{ab} - \mathcal{N}_1 w_{cc}^{aa}, \tag{B3d}$$
$$\mathcal{W}_{as} = \{\mathcal{W}_s'\mathcal{W}_a - \mathcal{W}_s\mathcal{W}_a'\}/\mathcal{D}, \tag{B3e}$$

where

$$\mathcal{N}' = \begin{Bmatrix} \Omega_p\Omega_c[T_{ad}(\nu) + T_{bc}(\nu')] \\ i\Omega_c[I_{pc} - T_{ac}(\nu')T_{bc}(\nu')] \\ i\Omega_p[I_{pc} + T_{ac}(\nu')T_{ad}(\nu)] \\ T_{ac}(\nu')T_{ad}(\nu)T_{bc}(\nu') + I_pT_{bc}(\nu') + I_cT_{ad}(\nu) \end{Bmatrix}, \tag{B4}$$

$$\mathcal{N} = \begin{Bmatrix} I_pT_{ad}(\nu) + I_cT_{bc}(\nu') + T_{bd}^*(\nu)T_{ad}(\nu)T_{bc}(\nu') \\ i\Omega_p^*[I_{pc} + T_{bd}^*(\nu)T_{bc}(\nu')] \\ i\Omega_c^*[I_{pc} - T_{bd}^*(\nu)T_{ad}(\nu)] \\ \Omega_p^*\Omega_c^*[T_{bc}(\nu') + T_{ad}(\nu)] \end{Bmatrix}, \tag{B5}$$

where $T_{xy}(\nu) = T_{xy} - i\nu$ and $I_p = \Omega_p\Omega_p^*$, $I_c = \Omega_c\Omega_c^*$, $I_{pc} = I_p - I_c$.

$$D_q = \mathcal{D} + \frac{\kappa_s g_s}{Q(\nu)}\mathcal{W}_s' + \frac{\kappa_a^* g_a^*}{Q_\varphi(\nu)}\mathcal{W}_a + \frac{\kappa_a^* g_a^*}{Q_\varphi(\nu)}\frac{\kappa_s g_s}{Q(\nu)}\mathcal{W}_{as} \tag{B6}$$

$$= \mathcal{D}\left(1 + \frac{\kappa_s g_s}{Q(\nu)\mathcal{D}}\mathcal{W}_s' + \frac{\kappa_a^* g_a^*}{Q_\varphi(\nu)\mathcal{D}}\mathcal{W}_a + \frac{\kappa_a^* g_a^*}{Q_\varphi(\nu)\mathcal{D}}\frac{\kappa_s g_s}{Q(\nu)\mathcal{D}}\{\mathcal{W}_s'\mathcal{W}_a - \mathcal{W}_s\mathcal{W}_a'\}\right), \tag{B7}$$

$$\mathcal{D} = T_{db}^*(\nu)T_{ac}(\nu')T_{ad}(\nu)T_{bc}(\nu') + (I_p - I_c)^2 + I_p\{T_{ac}(\nu')T_{ad}(\nu) + T_{db}^*(\nu)T_{bc}(\nu')\} + I_c\{T_{ac}(\nu')T_{bc}(\nu') + T_{db}^*(\nu)T_{ad}(\nu)\}$$

$$= T_{ad}(\nu)T_{bc}(\nu')\{T_{db}^*(\nu) + \delta_s\}\{T_{ac}(\nu') + \delta_a\}[1 - \beta_s\beta_a]. \tag{B8}$$

The coefficients associated with the noise are

$$\mathcal{G}' = \mathcal{N}' + \frac{\kappa_a^* g_a^*}{Q_\varphi(\nu)}\begin{Bmatrix} i\tilde{\rho}_{ab}\Omega_p T_{ad}(\nu) + i\tilde{\rho}_{dc}\Omega_c T_{bc}(\nu) \\ -I_{pc}\tilde{\rho}_{ab} + iw_{cc}^{aa}\Omega_c T_{bc}(\nu) \\ -I_{pc}\tilde{\rho}_{dc} - iw_{cc}^{aa}\Omega_p T_{ad}(\nu) \\ i\tilde{\rho}_{dc}\Omega_p^* T_{bc}(\nu) + i\tilde{\rho}_{ab}\Omega_c^* T_{ad}(\nu) - w_{cc}^{aa}T_{ad}(\nu)T_{bc}(\nu) \end{Bmatrix}, \tag{B9}$$

$$\mathcal{G} = \mathcal{N} + \frac{\kappa_s g_s}{Q(\nu)}\begin{Bmatrix} -\{i\tilde{\rho}_{cd}\Omega_p T_{ad}(\nu) + i\tilde{\rho}_{ba}\Omega_c T_{bc}(\nu) + w_{bb}^{dd}T_{ad}(\nu)T_{bc}(\nu)\} \\ I_{pc}\tilde{\rho}_{cd} - iw_{bb}^{dd}\Omega_p^* T_{bc}(\nu) \\ I_{pc}\tilde{\rho}_{ba} + iw_{bb}^{dd}\Omega_c^* T_{ad}(\nu) \\ -\left\{i\tilde{\rho}_{ba}\Omega_p^* T_{bc}(\nu) + i\tilde{\rho}_{cd}\Omega_c^* T_{ad}(\nu)\right\} \end{Bmatrix}, \tag{B10}$$

and the noise operators

$$\begin{pmatrix} \hat{\mathcal{F}}_{ac}(q,\nu) \\ \hat{\mathcal{F}}_{ad}(q,\nu) \\ \hat{\mathcal{F}}_{bc}(q,\nu) \\ \hat{\mathcal{F}}_{bd}(q,\nu) \end{pmatrix} = \mathcal{L}\mathcal{F}\begin{pmatrix} e^{i\Delta kz}e^{ik_a z}e^{-i\Delta\nu t}e^{-i(\nu_a t)}\hat{F}_{ac} \\ e^{ik_{cs}z}e^{i(-\nu_{cs}t)}\hat{F}_{ad} \\ e^{i\Delta kz}e^{-ik_{ca}z}e^{-i\Delta\nu t}e^{i(\nu_{ca}t)}\hat{F}_{bc} \\ e^{-ik_s z}e^{i(\nu_s t)}\hat{F}_{db}^+ \end{pmatrix}. \tag{B11}$$

APPENDIX C: ROOTS OF PARAMETRIC EQUATIONS

To find roots of D_q we factorize

$$Q(\nu) = \varsigma_s q - i\nu/c + \varsigma_s q_\pm + i\nu/c = \varsigma_s(q + q_\pm), \tag{C1}$$

$$Q_\varphi(\nu)Q(\nu) + \mathcal{P}_s Q_\varphi(\nu) + \mathcal{P}_a Q(\nu) + \mathcal{R} = \varsigma_a\varsigma_s[q^2 + qX + Y] = \varsigma_a\varsigma_s(q + q_+)(q + q_-) = \frac{\varsigma_a}{\varsigma_s}(Q + Q_+)(Q + Q_-) \tag{C2}$$

$$= \varsigma_a\varsigma_s\left(q + \frac{Q_+ - i\nu/c}{\varsigma_s}\right)\left(q + \frac{Q_- - i\nu/c}{\varsigma_s}\right), \tag{C3}$$

$$Q_\pm = \varsigma_s q_\pm + i\nu/c, \tag{C4}$$

$$X = \theta + \alpha + \mathcal{P}_s/\varsigma_s + \mathcal{P}_a/\varsigma_a, \tag{C5a}$$

$$Y = \alpha\theta + \mathcal{P}_s\theta/\varsigma_s + \mathcal{P}_a\alpha/\varsigma_a + \mathcal{R}/\varsigma_a\varsigma_s, \tag{C5b}$$

$$\theta = -i(\nu - \Delta\nu)/\varsigma_a c - i\Delta k, \tag{C5c}$$

$$\alpha = -i\nu/\varsigma_s c, \tag{C5d}$$

$$q_\pm = \frac{1}{2}(\theta + \alpha + \mathcal{P}_s/\varsigma_s + \mathcal{P}_a/\varsigma_a) \pm \sqrt{\left(\frac{-\theta + \alpha + \mathcal{P}_s/\varsigma_s - \mathcal{P}_a/\varsigma_a}{2}\right)^2 + \frac{\varsigma_s}{\varsigma_a}\mathcal{K}_a\mathcal{K}_s} \tag{C6}$$

$$= \frac{1}{2}(-i\Delta k + \mathcal{G}_a/\varsigma_a + \mathcal{G}_s/\varsigma_s) \pm \sqrt{\left(\frac{i\Delta k + \mathcal{G}_s/\varsigma_s - \mathcal{G}_a/\varsigma_a}{2}\right)^2 + \frac{\varsigma_s}{\varsigma_a}\mathcal{K}_a\mathcal{K}_s}. \tag{C7}$$

For forward,

$$Q_\pm = q_\pm + i\nu/c = \frac{1}{2}(\mathcal{P}_a + \mathcal{P}_s + i\varphi) \pm \sqrt{\left(\frac{\mathcal{P}_a + \mathcal{P}_s + i\varphi}{2}\right)^2 - (\mathcal{R} + i\varphi\mathcal{P}_s)}$$

$$= \frac{1}{2}(\mathcal{G}_s + \mathcal{G}_a) + \frac{i\nu}{c} - \frac{i\Delta k}{2} \pm \sqrt{\left(\frac{1}{2}(\mathcal{G}_s + \mathcal{G}_a) + \frac{i\nu}{c} - \frac{i\Delta k}{2}\right)^2 - \left\{\left(\mathcal{G}_s + \frac{i\nu}{c}\right)\left(\mathcal{G}_a + \frac{i\nu}{c} - i\Delta k\right) - \mathcal{K}_a\mathcal{K}_s\right\}}$$

$$= \frac{1}{2}(\mathcal{G}_s + \mathcal{G}_a) + \frac{i\nu}{c} - \frac{i\Delta k}{2} \pm \sqrt{\left(\frac{1}{2}(\mathcal{G}_s - \mathcal{G}_a + i\Delta k)\right)^2 + \mathcal{K}_a\mathcal{K}_s}. \tag{C8}$$

For $\Delta k = 0$ we have

$$q_\pm = \frac{1}{2}(\mathcal{G}_a + \mathcal{G}_s) \pm \frac{1}{2}\sqrt{(\mathcal{G}_a + \mathcal{G}_s)^2 - 4(\mathcal{G}_a\mathcal{G}_s - \mathcal{K}_a\mathcal{K}_s)}. \tag{C9}$$

APPENDIX D: SPATIALLY DEPENDENT RELATIONS

To check the validity of the solutions, the definitions of the spatial factors $\Pi_f^\pm$ and their relations have been useful:

$$\Pi_f^\pm = (\mathcal{G}_f \Xi \pm \Xi_q), \tag{D1}$$

$$\frac{\partial}{\partial z}\Pi_f^\pm = \left(-\mathcal{G}_f \pm \frac{\partial}{\partial z}\right)\Xi_q(z) \tag{D2}$$

$$= -\mathcal{G}_f \Xi_q(z) \mp \left(\frac{\mathcal{G}_a}{\varsigma_a} + \frac{\mathcal{G}_s}{\varsigma_s}\right)\Xi_q(z) \mp (\mathcal{K}_s\mathcal{K}_a - \mathcal{G}_s\mathcal{G}_a)\frac{\Xi(z)}{\varsigma_s\varsigma_a}. \tag{D3}$$

Thus we have the identity

$$\left[\frac{\partial}{\partial z} + \left(\frac{\mathcal{G}_a}{\varsigma_a} + \frac{\mathcal{G}_s}{\varsigma_s}\right)\right]\Xi_q(z) = (\mathcal{G}_s\mathcal{G}_a - \mathcal{K}_s\mathcal{K}_a)\frac{\Xi(z)}{\varsigma_s\varsigma_a}, \tag{D4}$$

$$\left(\frac{\partial}{\partial z} + q_+ + q_-\right)\Xi_q(z) = q_+q_-\,\Xi(z). \tag{D5}$$

We also found the following identities that are used to verify the correctness of the solutions:

$$\frac{\partial\,\Xi(z)}{\partial z} = -\Xi_q(z), \quad \frac{\partial\,\Xi_q(z)}{\partial z} = -\frac{\partial^2\Xi(z)}{\partial z^2}. \tag{D6}$$

APPENDIX E: BOUNDARY-BOUNDARY CORRELATIONS (FOR BACKWARD GEOMETRY)

$\langle\hat{N}_a(z_a,\tau)\hat{N}_s(z_s)\rangle$, $\langle\hat{N}_s(z_s,\tau)\hat{N}_a(z_a)\rangle$, $I_s^n(z_s,\tau) = \langle\hat{S}^n(z_s,\tau)\hat{S}^n(z_s)\rangle$, $I_a^n(z_a,\tau)$
To obtain $\langle\hat{\mathcal{A}}(z_a,t+\tau)\hat{\mathcal{S}}(z_s,t)\rangle$ we need

$$\left[\Psi_a^{a*}(z_a,\nu)\hat{\mathcal{A}}(0,\nu) + \Psi_s^{a*}(z_a,\nu)\hat{\mathcal{S}}^\dagger(L,\nu)\right]\left[\Psi_s^s(z_s,\nu)\hat{\mathcal{S}}(L,\nu) + \Psi_a^s(z_s,\nu)\hat{\mathcal{A}}^\dagger(0,\nu)\right],$$

$$\langle\hat{A}^b(z_a,\tau)\hat{S}^b(z_s,0)\rangle = \int_{-\infty}^{\infty}\Phi^b(z_s,z_a,\nu)e^{i\nu\tau}\frac{d\nu}{2\pi}\,. \tag{E1}$$

To obtain $\langle\hat{\mathcal{S}}(z_s,t+\tau)\hat{\mathcal{A}}(z_a,t)\rangle$ we reverse the order:

$$\left[\Psi_s^s(z_s,\nu)\hat{\mathcal{S}}(L,\nu) + \Psi_a^s(z_s,\nu)\hat{\mathcal{A}}^\dagger(0,\nu)\right]\left[\Psi_a^{a*}(z_a,\nu)\hat{\mathcal{A}}(0,\nu) + \Psi_s^{a*}(z_a,\nu)\hat{\mathcal{S}}^\dagger(L,\nu)\right],$$

$$\langle\hat{S}^b(z_s,\tau)\hat{A}^b(z_a,0)\rangle = \int_{-\infty}^{\infty}\Psi^b(z_s,z_a,\nu)e^{-i\nu\tau}\frac{d\nu}{2\pi}, \tag{E2}$$

For the boundary contributions to $\langle\hat{\mathcal{S}}^\dagger(z_s,t+\tau)\hat{\mathcal{S}}(z_s,t)\rangle$ we need

$$\left[\Psi_s^{s*}(z_s,\nu)\hat{\mathcal{S}}^\dagger(L,\nu) + \Psi_a^{s*}(z_s,\nu)\hat{\mathcal{A}}(0,\nu)\right]\left[\Psi_s^s(z_s,\nu)\hat{\mathcal{S}}(L,\nu) + \Psi_a^s(z_s,\nu)\hat{\mathcal{A}}^\dagger(0,\nu)\right],$$

$$I_s^b(z_s,\tau) = \langle\hat{S}^{b\dagger}(z_s,\tau)\hat{S}^b(z_s)\rangle = \int_{-\infty}^{\infty}\Sigma^b(z_s,\nu)e^{i\nu\tau}\frac{d\nu}{2\pi}. \tag{E3}$$

For the boundary contributions to $\langle\hat{\mathcal{A}}^\dagger(z_a,t+\tau)\hat{\mathcal{A}}(z_a,t)\rangle$ we need

$$\big\{\Psi_a^a(z_a,\nu)\hat{\mathcal{A}}^\dagger(0,\nu)+\Psi_s^a(z_a,\nu)\hat{\mathcal{S}}(L,\nu)\big\}\big\{\Psi_a^{a*}(z_a,\nu)\hat{\mathcal{A}}(0,\nu)+\Psi_s^{a*}(z_a,\nu)\hat{\mathcal{S}}^\dagger(L,\nu)\big\},$$

$$I_a^b(0,\tau)=\langle\hat{A}^{b\dagger}(0,\tau)\hat{A}^b(0)\rangle=\int_{-\infty}^{\infty}\Lambda^b(z_a,\nu)e^{-i\nu\tau}\frac{d\nu}{2\pi}, \tag{E4}$$

where

$$\Phi^b(z_s,z_a,\nu)=\big[C_a(\bar{n}_a+1)\Psi_a^{a*}(z_a,\nu)\Psi_a^s(z_s,\nu)+C_s\bar{n}_s\Psi_s^{a*}(z_a,\nu)\Psi_s^s(z_s,\nu)\big], \tag{E5}$$

$$\Psi^b(z_s,z_a,\nu)=\big[C_a\bar{n}_a\Psi_a^s(z_s,\nu)\Psi_a^{a*}(0,\nu)+C_s(\bar{n}_s+1)\Psi_s^s(z_s,\nu)\Psi_s^{a*}(0,\nu)\big], \tag{E6}$$

$$\Sigma^b(z_s,\nu)=\big[C_a(\bar{n}_a+1)\big|\Psi_a^s(z_s,\nu)\big|^2+C_s\bar{n}_s\big|\Psi_s^s(z_s,\nu)\big|^2\big], \tag{E7}$$

$$\Lambda^b(z_a,\nu)=\big[C_s(\bar{n}_s+1)\big|\Psi_s^a(0,\nu)\big|^2+C_a\bar{n}_a\big|\Psi_a^a(0,\nu)\big|^2\big]. \tag{E8}$$

where $C_f=\frac{\hbar\nu_f\pi}{\varepsilon_0 Ac}|g_f|^2$, $A=\pi r^2$ is the cross section, and $\bar{n}_f=(e^{\hbar\nu_f/k_BT}-1)^{-1}$ the mean photon number.

We have used the quantum field at the boundary:

$$\hat{E}_f(\mathbf{r},t)=i\sum_{\mathbf{k}_f}\sqrt{\frac{\hbar\nu_f}{2\varepsilon_o V}}\hat{a}_{\mathbf{k}_f}e^{i(\mathbf{k}_f\cdot\mathbf{r}-\nu_f t)}, \tag{E9}$$

$$\hat{E}_f(\mathbf{r},\nu)=\int e^{i\nu t}\hat{E}_f(\mathbf{r},t)dt=i\sum_{\mathbf{k}_f}\sqrt{\frac{\hbar\nu_f}{2\varepsilon_o V}}\hat{a}_{\mathbf{k}_f}e^{i\mathbf{k}_f\cdot\mathbf{r}}\int e^{i(\nu-\nu_f)t}dt \tag{E10}$$

$$=i\sum_{\mathbf{k}_f}\sqrt{\frac{\hbar\nu_f}{2\varepsilon_o V}}\hat{a}_{\mathbf{k}_f}e^{i\mathbf{k}_f\cdot\mathbf{r}}2\pi\delta(\nu-\nu_f)\to i\sum_{\mathbf{k}_f}\sqrt{\frac{\hbar\nu_f}{2\varepsilon_o V}}\hat{a}_{\mathbf{k}_f}e^{i\mathbf{k}_f\cdot\mathbf{r}}2\pi\delta(\nu-\nu_f), \tag{E11}$$

with $\delta(\nu-\nu_f)=\frac{1}{2\pi}\int e^{i(\nu-\nu_f)t}dt$, the convention $X(t)=\frac{1}{2\pi}\int\mathcal{X}(\nu)e^{-i\nu t}dt$ and the commutation

$$[\hat{E}_f(0,\nu),\hat{E}_f^\dagger(0,\nu')]=\sum_{\mathbf{k}_f,\mathbf{k}'_f}\frac{\hbar\sqrt{\nu_f\nu'_f}}{2\varepsilon_o V}e^{i(\mathbf{k}_f-\mathbf{k}'_f)\cdot\mathbf{r}}(2\pi)^2\delta(\nu-\nu_f)(\nu'-\nu_f) \tag{E12}$$

$$\simeq(2\pi)^2\sum_{\mathbf{k}_f}\frac{\hbar\nu_f}{2\varepsilon_o V}\delta(\nu-\nu_f)(\nu'-\nu_f) \tag{E13}$$

$$=\frac{(2\pi)^2\hbar}{2\varepsilon_o AL}\frac{L}{2\pi c}\int\nu_f\delta(\nu-\nu_f)\delta(\nu'-\nu_f)d\nu_f \tag{E14}$$

$$=\frac{\pi\hbar\nu}{\varepsilon_o Ac}\delta(\nu-\nu'). \tag{E15}$$

APPENDIX F: NOISE-NOISE CORRELATIONS

The noise correlations are expressed as

$$\langle\hat{A}^n(z_a,\tau)\hat{S}^n(z_s)\rangle=e^{i\Delta kz}\int_{-\infty}^{\infty}e^{i\nu\tau}\Phi^n(z_s,z_a,\nu)\frac{d\nu}{2\pi}, \tag{F1}$$

$$\langle\hat{S}^n(z_s,\tau)\hat{A}^n(z_a)\rangle=e^{i\Delta kz}\int_{-\infty}^{\infty}e^{-i\nu\tau}\Psi^n(z_s,z_a,\nu)\frac{d\nu}{2\pi}, \tag{F2}$$

with the phase mismatch Δk and the intensities $I_f^n(z)=I_f^n(z,\tau=0)$ are obtained from the self-correlation amplitudes

$$I_s^n(z_s,\tau)=\langle\hat{S}^{n\dagger}(z_s,\tau)\hat{S}^n(z_s)\rangle=\int_{-\infty}^{\infty}e^{i\nu\tau}\Sigma^n(z_s,\nu)\frac{d\nu}{2\pi}, \tag{F3}$$

$$I_a^n(z_a,\tau)=\langle\hat{A}^{n\dagger}(z_a,\tau)\hat{A}^n(z_a)\rangle=\int_{-\infty}^{\infty}e^{-i\nu\tau}\Lambda^n(z_a,\nu)\frac{d\nu}{2\pi}. \tag{F4}$$

The contributions of noise terms become important for significant propagation length [43]. This is because the correlation amplitudes are the Fourier transforms of the spectral functions that depend on propagation length L,

$$\Phi^n(z_s, z_a, \nu) = \frac{(2\pi)^2}{AN} \sum_{x,x'} \int_0^L 2\tilde{D}^n_{x,x'}(z) K^{a*}_x(z_a, s, \nu) K^s_{x'}(z_s, s, \nu) ds, \tag{F5}$$

$$\Psi^n(z_s, z_a, \nu) = \frac{(2\pi)^2}{AN} \sum_{x,x'} \int_0^L 2\tilde{D}^{an}_{x,x'}(z) K^s_x(z_s, s, \nu) K^{a*}_{x'}(z_a, s, \nu) ds, \tag{F6}$$

$$\Sigma^n(z_s, \nu) = \frac{(2\pi)^2}{AN} \sum_{x,x'} \int_0^L 2\tilde{D}^n_{x,x'}(z) K^{s*}_x(z_s, s, \nu) K^s_{x'}(z_s, s, \nu) ds, \tag{F7}$$

$$\Lambda^n(z_a, \nu) = \frac{(2\pi)^2}{AN} \sum_{x,x'} \int_0^L 2\tilde{D}^{an}_{x,x'}(z) K^a_x(z_a, s, \nu) K^{a*}_{x'}(z_a, s, \nu) ds, \tag{F8}$$

where s represents dependency on z, z_s, z_a and L and $x, x' = ac, ad, bc, bd$, and

$$K^s_i(z_s, s, \nu) = ig_s\kappa_s \mathcal{C}'_i(\nu)\psi^s_s(z_s, s, \nu) - ig^*_a\kappa^*_a \mathcal{C}_i(\nu)\psi^s_a(z_s, s, \nu), \tag{F9}$$

$$K^a_j(z_a, s, \nu) = ig_s\kappa_s \mathcal{C}'_j(\nu)\psi^a_s(z_a, s, \nu) - ig^*_a\kappa^*_a \mathcal{C}_j(\nu)\psi^a_a(z_a, s, \nu). \tag{F10}$$

We have evaluated $\langle \hat{\mathcal{F}}^\dagger_s(z'', \nu)\hat{\mathcal{F}}_s(z', \nu)\rangle$, $\langle \hat{\mathcal{F}}^\dagger_s(z'', \nu)\hat{\mathcal{F}}^\dagger_a(z', \nu)\rangle$, $\langle \hat{\mathcal{F}}_a(z'', \nu)\hat{\mathcal{F}}_s(z', \nu)\rangle$, $\langle \hat{\mathcal{F}}_a(z'', \nu)\hat{\mathcal{F}}^\dagger_a(z', \nu)\rangle$ using Eqs. (40) and (41):

$$\left\langle \hat{\mathcal{F}}^\dagger_j(s', \nu')\hat{\mathcal{F}}_i(s, \nu)\right\rangle = \frac{2\pi}{AN} D^n_{ji}\delta(s' - s)\delta(\nu' - \nu), \tag{F11}$$

which follows from

$$\langle \hat{F}_{\beta\alpha}(z, t)\hat{F}_{\delta\gamma}(z', t')\rangle \simeq D_{\beta\alpha,\delta\gamma}(z, t)\delta(z' - z)\delta(t - t')\frac{(2\pi)^2}{(AN)}, \tag{F12}$$

$$\left\langle \hat{F}^\dagger_{x_j}(z_j, t_j)\hat{F}_{x_i}(z_i, t_i)\right\rangle = D^n_{x_j x_i}\delta(z_j - z_i)\delta(t_j - t_i)\frac{(2\pi)^2}{AN}, \tag{F13}$$

$$\left\langle \hat{F}_{x_j}(z_j, t_j)\hat{F}^\dagger_{x_i}(z_i, t_i)\right\rangle = D^a_{x_j x_i}\delta(z_j - z_i)\delta(t_j - t_i)\frac{(2\pi)^2}{AN}. \tag{F14}$$

Hence, we obtain the commutations

$$[\hat{\mathcal{F}}_i(z', \nu'), \hat{\mathcal{F}}^\dagger_j(z'', \nu'')] = \frac{2\pi}{AN}\left\{D^a_{ij} - D^n_{ji}\right\}\delta(z' - z'')\delta(\nu' - \nu''), \tag{F15a}$$

$$[\hat{\mathcal{F}}_s(z', \nu'), \hat{\mathcal{F}}^\dagger_s(z'', \nu'')] = \frac{2\pi}{AN}\delta(z' - z'')\delta(\nu' - \nu'')\sum_{i,j=1}^{4} \mathcal{C}'_i\mathcal{C}'^*_j\left\{D^a_{ij} - D^n_{ji}\right\}, \tag{F15b}$$

$$[\hat{\mathcal{F}}^\dagger_a(z', \nu'), \hat{\mathcal{F}}_a(z'', \nu'')] = \frac{2\pi}{AN}\delta(z' - z'')\delta(\nu' - \nu'')\sum_{i,j=1}^{4} \mathcal{C}_i\mathcal{C}^*_j\left\{D^a_{ij} - D^n_{ji}\right\}. \tag{F15c}$$

All terms due to the boundary-noise correlations vanish as the initial fields are uncorrelated to the noise for the case of thermal radiation. To compute the total spectrum, $Z(\nu) = Z^f(\nu) + Z^n(\nu)$, where $Z \in \Phi, \Psi, \Sigma, \Lambda$. Note that the inverse transform of $I_f(\tau)$ is essentially the spectrum, for example $\Sigma(z_s, \nu) = \int_0^\infty e^{-i\nu\tau} I_s(z_s, \tau) d\tau$.

[1] A. Yariv and D. M. Pepper, Amplified reflection, phase conjugation, and oscillation in degenerate four-wave mixing, Opt. Lett. **1**, 16 (1977).

[2] M. Fleischhauer, M. D. Lukin, A. B. Matsko, and M. O. Scully, Threshold and Linewidth of a Mirrorless Parametric Oscillator, Phys. Rev. Lett. **84**, 3558 (2000).

[3] C. Canalias and V. Pasiskevicius, Mirrorless optical parametric oscillator, Nat. Photonics **1**, 459 (2007).

[4] S. Zibrov, M. D. Lukin, and M. O. Scully, Nondegenerate Parametric Self-Oscillation via Multiwave Mixing in Coherent Atomic Media, Phys. Rev. Lett. **83**, 4049 (1999).

[5] M. D. Lukin, A. B. Matsko, M. Fleischhauer, and M. O. Scully, Quantum Noise and Correlations in Resonantly Enhanced Wave Mixing Based on Atomic Coherence, Phys. Rev. Lett. **82**, 1847 (1999).

[6] K. Nawata, Y. Tokizane, Y. Takida and H. Minamide, Tunable terahertz-wave parametric oscillation, Sci. Rep. **9**, 726 (2019).

[7] Dominik S. Wild, Ephraim Shahmoon, Susanne F. Yelin, and Mikhail D. Lukin, Quantum Nonlinear Optics in Atomically Thin Materials, Phys. Rev. Lett. **121**, 123606 (2018).

[8] V. Balić, D. A. Braje, P. Kolchin, G. Y. Yin, and S. E. Harris, Generation of Paired Photons with Controllable Waveforms, Phys. Rev. Lett. **94**, 183601 (2005).

[9] D. A. Braje, V. Balic, S. Goda, G. Y. Yin, and S. E. Harris, Frequency Mixing Using Electromagnetically Induced Transparency in Cold Atoms, Phys. Rev. Lett. **93**, 183601 (2004).

[10] Y. Mei, X. Guo, L. Zhao, and S. Du, Mirrorless Optical Parametric Oscillation with Tunable Threshold in Cold Atoms, Phys. Rev. Lett. **119**, 150406 (2017).

[11] S. A. Moiseev and S. Kröll, Complete Reconstruction of the Quantum State of a Single-Photon Wave Packet Absorbed by a Doppler-Broadened Transition, Phys. Rev. Lett. **87**, 173601 (2001).

[12] K. Tikhonov, T. Golubeva, and Y. Golubev, Complete reconstruction of the quantum state of a single-photon wave packet absorbed by a doppler-broadened transition, Eur. Phys. J. D **69**, 252 (2015).

[13] P. Vernaz-Gris, A. D. Tranter, J. L. Everett, A. C. Leung, K. V. Paul, G. T. Campbell, P. K. Lam, and B. C. Buchler, High-performance Raman memory with spatio-temporal reversal, Opt. Express **26**, 12424 (2018).

[14] J. L. Everett, P. Vernaz-Gris, G. T. Campbell, A. D. Tranter, K. V. Paul, A. C. Leung, P. K. Lam, and B. C. Buchler, Time-reversed and coherently enhanced memory: A single-mode quantum atom-optic memory without a cavity, Phys. Rev. A **98**, 063846 (2018).

[15] J.-L. Le Gouët and P. R. Berman, Raman scheme for adjustable-bandwidth quantum memory, Phys. Rev. A **80**, 012320 (2009).

[16] Y. Jiang, J. Rui, X. H. Bao, and J. W. Pan, Dynamical zeroing of spin-wave momentum to suppress motional dephasing in an atomic-ensemble quantum memory, Phys. Rev. A **93**, 063819 (2016).

[17] Z. Qin, L. Cao, H. Wang, A. M. Marino, W. Zhang, and J. Jing, Experimental Generation of Multiple Quantum Correlated Beams from Hot Rubidium Vapo, Phys. Rev. Lett. **113**, 023602 (2014); H. Wang, L. Cao, and J. Jing, Characterization of pairwise correlations from multiple quantum correlated beams generated from cascaded four-wave mixing processes, Sci. Rep. **7**, 40410 (2017).

[18] Y. Fang and J. Jing, Quantum squeezing and entanglement from a two-mode phase-sensitive amplifier via four-wave mixing in rubidium vapor, New J. Phys. **17**, 023027 (2015); S. Liu, Y. Lou, and J. Jing, Interference-Induced Quantum Squeezing Enhancement in a Two-beam Phase-Sensitive Amplifier, Phys. Rev. Lett. **123**, 113602 (2019).

[19] Zukauskas, A. L. Viotti, C. Liljestrand, V. Pasiskevicius, and C. Canalias, Cascaded counter-propagating nonlinear interactions in highly-efficient sub-μm periodically poled crystals, Sci. Rep. **7**, 8037 (2017).

[20] Y. C. Liu, D. J. Guo, R. Yang, C. W. Sun, J. C. Duan, Z. Xie, Y. X. Gong, and S. N. Zhu, Narrow-band photonic quantum entanglement with counterpropagating domain engineering, Photonics Res. **9**, 1998 (2021).

[21] S. Chen, Y.-A. Chen, B. Zhao, Z.-S. Yuan, J. Schmiedmayer, and J.-W. Pan, Demonstration of a Stable Atom-Photon Entanglement Source for Quantum Repeaters, Phys. Rev. Lett. **99**, 180505 (2007); J. Wen, S. Du, and M. H. Rubin, Spontaneous parametric down-conversion in a three-level system, Phys. Rev. A **76**, 013825 (2007).

[22] D. M. Bloom and G. C. Bjorklund, Conjugate wave-front generation and image reconstruction by four-wave mixing, Appl. Phys. Lett. **31**, 592 (1977).

[23] K. Dorfman, S. Liu, Y. Lou, T. Wei, J. Jing, F. Schlawin, and S. Mukamel, Multidimensional four-wave mixing signals detected by quantum squeezed light, Proc. Natl. Acad. Sci. U. S. A. **118**, e2105601118 (2021).

[24] J. Appel, E. Figueroa, D. Korystov, M. Lobino, and A. I. Lvovsky, Quantum Memory for Squeezed Light, Phys. Rev. Lett. **100**, 093602 (2008)

[25] A. B. Matsko, I. Novikova, and G. R. Welch, D. Budker, D. F. Kimball, and S. M. Rochester, Vacuum squeezing in atomic media via self-rotation, Phys. Rev. A **66**, 043815 (2002).

[26] I. H. Agha, G. Messin, and P. Grangier, Generation of pulsed and continuous-wave squeezed light with ^{87}Rb vapor, Opt. Express **18**, 4198 (2010).

[27] Z. Yang, P. Saurabh, F. Schlawin, S. Mukamel, and K. E. Dorfman, Multidimensional four-wave-mixing spectroscopy with squeezed light, Appl. Phys. Lett. **116**, 244001 (2020).

[28] K. E. Dorfman, F. Schlawin, and S. Mukamel, Nonlinear optical signals and spectroscopy with quantum light, Rev. Mod. Phys. **88**, 045008 (2016).

[29] C. H. Raymond Ooi, Q. Sun, M. S. Zubairy, and M. O. Scully, Correlation of photon pairs from the double Raman amplifier: Generalized analytical quantum Langevin theory, Phys. Rev. A **75**, 013820 (2007).

[30] D. Zhang, C. Li, Z. Zhang, Y. Zhang, Y. Zhang, and M. Xiao, Enhanced intensity-difference squeezing via energy-level modulations in hot atomic media, Phys. Rev. A **96**, 043847 (2017).

[31] M. O. Scully and M. S. Zubairy, *Quantum Optics* (Cambridge University Press, Cambridge, England, 1997).

[32] C. H. Raymond Ooi and P. R. Berman, Preservation of bosonic commutation relation: Explicit evaluation of quantum Langevin operator products, Phys. E (Amsterdam, Neth.) **42**, 407 (2010).

[33] D. J. Saunders, J. H. D. Munns, T. F. M. Champion, C. Qiu, K. T. Kaczmarek, E. Poem, P. M. Ledingham, I. A. Walmsley, and J. Nunn, Cavity-Enhanced Room-Temperature Broadband Raman Memory, Phys. Rev. Lett. **116**, 090501 (2016).

[34] J. Borregaard, M. Zugenmaier, J. M. Petersen, H. Shen, G. Vasilakis, K. Jensen, E. S. Polzik, and A. S. Sorensen, Scalable photonic network architecture based on motional averaging in room temperature gas, Nat. Commun. **7**, 11356 (2016).

[35] H.-T. Zhou, D.-W. Wang, D. Wang, J.-X. Zhang, and S.-Y. Zhu, Efficient reflection via four-wave mixing in a Doppler-free electromagnetically-induced-transparency gas system, Phys. Rev. A **84**, 053835 (2011).

[36] J. Choi and D. S. Elliott, Influence of interaction time and population redistribution on the localization of atomic excitation through electromagnetically induced transparency, Phys. Rev. A **89**, 013414 (2014).

[37] Ling, H. Yuan, Y.-Q. Li, and M. Xiao, Coherent population trapping and electromagnetically induced transparency in multi-Zeeman-sublevel atoms, Phys. Rev. A **53**, 1014 (1996).

[38] C. F. McCormick, V. Boyer, E. Arimondo, and P. D. Lett, Strong relative intensity squeezing by four-wave mixing in rubidium vapor, Opt. Lett. **32**, 178 (2007); J. Jing, C. Liu, Z. Zhou, Z. Ou,

and W. Zhang, Realization of a nonlinear interferometer with parametric amplifiers, Appl. Phys. Lett. **99**, 011110 (2011); F. Hudelist, J. Kong, C. Liu, J. Jing, Z. Y. Ou, and W. Zhang, Quantum metrology with parametric amplifier-based photon correlation interferometers, Nat. Commun. **5**, 3049 (2014); S. Liu, Y. Lou, J. Xin, J. Jing, Quantum Enhancement of Phase Sensitivity for the Brightseeded SU(1, 1) Interferometer with Direct Intensity Detection, Phys. Rev. Appl. **10**, 064046 (2018).

[39] S. E. Harris, Proposed backward wave oscillation in the infrared, Appl. Phys. Lett. **9**, 114 (1966); H. Hsu and C. Yu, Complete photon conversion in backward-travelling-wave parametric amplification and oscillation, Electron. Lett. **9**, 442 (1973).

[40] M. D. Lukin, P. R. Hemmer, M. Löffler, and M. O. Scully, Resonant Enhancement of Parametric Processes via Radiative Interference and Induced Coherence, Phys. Rev. Lett. **81**, 2675 (1998).

[41] B. H. Hokr, J. N. Bixler, G. D. Noojin, R. J. Thomas, B. A. Rockwell, V. V. Yakovlev, and M. O. Scully, Single-shot stand-off chemical identification of powders using random Raman lasing, Proc. Natl. Acad. Sci. U.S.A. **111**, 12320 (2014).

[42] A. Dogariu, J. B. Michael, M. O. Scully, and R. B. Miles, High-gain backward lasing in air, Science **331**, 442 (2011); P. R. Hemmer, R. B. Miles, P. Polynkin, T. Siebert, A. V. Sokolov, P. Sprangle, and M. O. Scully, Standoff spectroscopy via remote generation of a backward-propagating laser beam, Proc. Natl. Acad. Sci. U.S.A. **108**, 3130 (2011).

[43] C. H. Raymond Ooi and M. S. Zubairy, Role of noise operators on two-photon correlations in an extended coherent Raman medium, Phys. Rev. A **75**, 053822 (2007).

Correction: The previously published Figure 1 contained labeling errors introduced during the production cycle and has been replaced. The captions to Figures 1 and 8 contained minor errors and have been fixed. δ_s was erroneously presented as Δ_s in an inline equation below Eq. (2) and in Eqs. (18b) and (18d) and has been fixed.